2023

Interrogation and Manipulation of the IGG FC Glycan

Aaron Keshav Gupta

INTERROGATION AND MANIPULATION OF THE IGG FC GLYCAN

A Dissertation

Presented to the Faculty of the David Rockefeller Graduate Program

in Biosciences

in Partial Fulfillment of the Requirements for the Degree of

Doctor of Philosophy

by

Aaron Keshav Gupta

November 2022

INTERROGATION AND MANIPULATION OF THE IGG FC GLYCAN

Aaron Keshav Gupta

The Rockefeller University 2022

Antibody signaling is a cardinal feature of successful adaptive immune responses. The magnitude and direction of this signaling is determined by the structure of a given antibody's fragment crystallizable (Fc) domain, which interfaces with cells of the immune system. Often considered a constant region, the immunoglobulin G (IgG) Fc protein backbone and conserved N-linked glycan combine to introduce structural diversity in IgG molecules that in turn, triggers divergent humoral responses. These N-glycans are variably constructed, ultimately leading to families of highly related, but non-equivalent glycoproteins known as glycoforms. Despite burgeoning interest in understanding the complexities of IgG Fc glycoforms and their functions, there is an evident scarcity of tools available to distinguish and target them. In addition, the highly conserved nature of the glycan and its presence on the B cell receptor (BCR) provokes questions of its possible role in the generation of antibody responses.

In the first part of this thesis, I identify a novel class of synthetic nanobodies that can distinguish glycoforms without reactivity to off-target glycoproteins or glycans. Applying this technology to Fc glycoforms defines nanobodies that specifically recognize either IgG lacking its core-fucose or IgG bearing terminal sialic acid residues. Solving the structure of a nanobody-Fc complex via x-ray crystallography reveals a unique mode of recognition of IgG glycoforms. By adapting nanobodies to standard biochemical methods, I clinically stratify dengue virus and SARS-CoV-2 infected individuals based on their Fc glycan profile, selectively disrupt IgG-Fcγ receptor (FcγR) binding both *in vitro* and *in vivo*, and interrogate BCR glycan structure on living cells.

In the second part of this thesis, I develop mouse models and biochemical tools to help define the role of the IgG Fc glycan in developing antibody responses. Preliminary studies show that following immunization, mice lacking the N-glycan acceptor residue, Asn 297, exhibit deficiencies in germinal center (GC) responses. In this model, B cells with an aglycosylated BCR participate less frequently in the GC reaction, bind antigen less avidly, and show signaling deficits downstream of BCR engagement. Development of an aglycosylated mouse IgG1-specific nanobody shows that in allelic competition experiments, B cells with glycosylated BCRs are favored. To aid future studies, an additional mouse model null for endogenous Fc-FcγR binding is generated. Finally, a mouse expressing human IgG1 in the heavy chain locus proves useful for chronic administration of human antibodies.

To all those finding a sense of purpose

and to my family, friends, and mentors who are helping me find mine

Acknowledgements

First and foremost, I'd like to thank my PhD advisor, Dr. Jeffrey Ravetch. Not only is Jeff a world-renowned immunologist with incredible scientific intuition, but he is also a present and patient mentor. He has without a doubt shaped me into the scientist I am today. I'll admit I was surprised (and maybe a bit intimidated!) to be the first PhD student in the lab in more than 30 years, but Jeff's consistent encouragement and scientific guidance quickly dissolved any anxieties I may have had. I will always look fondly upon our daily chats and weekly meetings both for helpful discussions and laughs. I can truly think of no better advocate for his trainees.

In the Ravetch lab, I've been fortunate to have outstanding colleagues and friends. Back in 2018 during our rotation, Kevin Kao and I first conceived of nanobodies as reagents to identify IgG glycoforms, but it wasn't until the depths of the pandemic in Summer 2020 that we really tackled the project. It has always been inspiring to watch Kevin's wild dedication to science, sometimes coming into lab at 3 AM to check on an exciting result or just to inoculate bacteria as a time-saving measure. We spent a large part of the PhD working side-by-side on difficult problems, sometimes painfully discouraged, sometimes overstimulated with excitement. But through it all, we remained understanding and accommodating towards each other and the data eventually rolled in. I am confident that our friendship and scientific collaboration will extend far into the future. In addition to Jeff, Stylianos Bournazos was my day-to-day mentor, providing key advice ranging from big-picture experimental design to manuscript formatting. I'd like

to thank Rachel Yamin, Andrew Jones, Sara Borghi, and the rest of the infectious disease side for helpful discussions, cathartic complaining, and sharing materials and time. In addition, I want to recognize the rest of the Ravetch lab for their help in supporting me during this journey and for providing an inspiring example of what postgraduate training is supposed to look like. I know I will continue to rely on you all throughout my career.

This work would not have been possible without research collaborators near and far: Deena Oren of the Rockefeller Structural Biology Research Core for her work on nanobody crystal structures and late nights on the beamline; Lai-Xi Wang and his lab for developing critical IgG glycoform reagents; Eric Sundberg and Jonathan Du of Emory University for advice on nanobody engineering strategies; Yehuda Golgur of MSKCC for work on structure refinement; and Jacqueline Achkar of Albert Einstein COM for patient samples and clinical insight.

Thank you to my committee members, Dr. Gabriel Victora, Dr. Michel Nussenzweig, Dr. Randy Longman, and Dr. Jayanta Chauduri for their guidance over the years. I have always looked up to Gabriel for his fearlessness in tackling high-level questions with elegant genetic models and innovative tools. Since day one of the MD-PhD program, Randy has served as a personal mentor for me, providing the most cogent example of a physician-scientist who truly engages in and bridges both disciplines. In the last year of my PhD, Michel became a collaborator and I was a firsthand witness to the productive research empire he's created. A special thanks to Jayanta for serving as the external member for my defense. Thank you to Dr. Olaf Andersen, Dr. Katherine Hsu, Dr. Ruth Gotian, Dr. Catharine Boothroyd, Renee Horton, Hanna Silvast, Dr. Ben Levitt for their personal and professional support over the years.

I'd like to thank my friends all across NYC and beyond, and particularly those in the Tri-I MD-PhD program. 7-8 years of training is no easy feat and requires reliance on those

who understand the process most. In particular, I'd like to thank Jesse Novak, Andrew Toader, Nicky Blobel, and Alexandru Barbulescu for daily lunches, updates, and supportive friendship throughout the PhD. To my family, you have been a source of unwavering support over the past 6 years and I cannot thank you enough. Your love and sacrifice for me has brought me to this big moment.

Finally, my PhD spanned a difficult period for academic trainees. Only six months into my training, COVID-19 swept across the world and the university and our lab quickly closed. But in the face of this global catastrophe, immunologists everywhere rose up to fight against it, developing vaccines, antibodies, and antivirals to save lives. I am grateful for those who worked tirelessly to spread truth, technology, and care to those who need it most and for giving our field newfound relevance. This PhD, and the context in which I experienced it, will be imprinted on me forever.

Table of Contents

List of Figures

List of Tables

Chapter 1

INTRODUCTION

1.1 IgG Fc structural diversity dictates Fc-Fcγ receptor interactions

Antibodies are fundamental components of the adaptive immune system that exhibit both exquisite specificity for their cognate antigens and harbor powerful signaling capability to trigger downstream effector functions. In particular, antibodies are unique in that they are able to adapt to their targets, cycling through multiple iterations of hypermutation and selection in pursuit of superior variants. This property endows antibodies with the ability to target an almost unconstrained number of antigens with strength and precision, while also directing cells of the immune system toward those antigens. This concept is fundamental to the technology and efficacy of vaccines, which are meant to elicit high-affinity, long-lasting, and effective antibodies.

A key attribute of the antibody response is its polyclonality. Individual antibody

clones contain highly variable antigen-binding Fab domains that allow for differential targeting of epitopes on a variety of antigens. On the opposite end of the molecule, antibodies possess an Fc domain responsible for communicating effector signals to the cells of the immune system. Though the Fc domain is often thought to be a constant region that simply serves as an adapter to the effector leukocytes of the immune system, it also harbors considerable structural diversity that serves as an additional layer of regulation in both protective and pathogenic humoral responses. In this thesis, I will focus on the Fc of immunoglobulin G (IgG) antibodies, which can be derived from one of four subclasses and a variety of heavy chain allotypes with distinct amino acid sequences. In addition, the IgG Fc domain is also decorated with a single N-linked complex biantennary glycan that introduces additional Fc glycovariants, thereby combining with sequence diversity to provide hundreds of Fc structural permutations[1].

Fundamentally, these variable structures result in selective binding to Fc receptors (FcγRs), cellular receptors for IgG that initiate a wide array of downstream protective and pathogenic effector functions including tumor and pathogen clearance, removal of infected or cancerous cells, modulation of B cell responses, and the initiation of anti-inflammatory pathways that restrain the immune response. The specific type and magnitude of effector functions critically rely on both the structural composition of the signaling antibody and the FcγR expression of the effector leukocyte, in particular the ratio of occupied activating to inhibitory FcγRs on the surface of a cell. Disruption or modulation of this carefully balanced ratio results in significant in vivo effects, sometimes reflecting overactivation or excess inhibition of the immune response[2,3,4,5]. Indeed, selective engagement of FcγRs with monoclonal antibodies has been a successful strategy to attain desired effector functions both in clinical settings and in several disease models[6,7,8,9].

Here, I review the major components of the Fc-FcγR signaling axis, paying special

attention to the IgG Fc glycan. This structural motif has recently emerged as a major determinant of IgG function, though the complex processes and cell types which regulate its structure are largely unknown. In recent years, researchers have sought to better understand the Fc glycan's endogenous mechanisms of regulation during vaccination or infection, to carefully fine-tune its structure while engineering antibody therapeutics, and to develop more broadly applicable tools to study its diverse structures. My thesis work is a direct response to help overcome these challenges, providing both tools and insights into IgG Fc glycan structure to better serve the research community at large.

1.2 The Fcγ receptor family

FcγRs are central mediators of antibody-triggered responses, coupling the innate and adaptive immune responses in effector cell activation[10]. Canonical, type I FcγRs are broadly classified as activating or inhibitory, depending on the signaling properties of their intracellular domains. In humans, activating FcγRs include FcγRI, FcγRIIa, FcγRIIc, and FcγRIIIa, which contain immunoreceptor tyrosine activating motifs (ITAMs), either in the ligand-binding receptor chain in the case of FcγRIIa and FcγRIIc or in the associated FcγR γ-chain for FcγRI and FcγRIIIa. ITAMs are necessary for receptor expression, surface assembly, and signaling. In contrast, FcγRIIb represents the sole inhibitory FcγR, mediating signaling activity through an immunoreceptor tyrosine inhibitory motif (ITIM) present in its cytoplasmic region. In contrast to activating or inhibitory FcγRs, FcγRIIIb is expressed as a GPI-anchored protein and is therefore incapable of signal transduction; however, FcγRIIIb still has the capacity to transduce activation signals following receptor crosslinking, mainly by associating and acting synergistically with activating receptors such as FcγRIIa[11,12,13,14].

FcγRs are broadly expressed on the surface of both lymphoid and myeloid cells, although the distribution of different FcγRs is unique to each cell type; for example, B cells express FcγRIIb as their sole FcγR, whereas NK cells exclusively express the activating receptor FcγRIIIa. Most other immune cells express a combination of different FcγRs, pairing activating and inhibitory receptors to achieve balanced cellular responses. Perturbations in either arm of the response have been shown to lead to pathological consequences and have been taken as a paradigm of how these systems are likely to work for those paired immunoreceptors with unknown ligand-binding functions. FcγR surface expression is modulated by cytokines in a manner where pro-inflammatory cytokines generally increase expression of activating FcγRs over their inhibitory counterparts, whereas anti-inflammatory signals downregulate activating FcγRs and enhance FcγRIIb expression[15]. Promoter polymorphisms and copy number variation (CNVs) in FcγR genes can also influence the expression levels of FcγRs on the surface of effector leukocytes, acting as an additional determinant for IgG-mediated signaling[16].

The crystal structures of FcγRIIA, FcγRIIB, FcγRIIIA, and FcϵRI have been solved, as have the cocrystals of FcγRIIIA–IgG1 Fc, FcϵRI–IgE Fc, and CD23-IgE Fc[17,18]. These studies demonstrate that the Type I receptors have a common structure in which the two extracellular immunoglobulin domains form a bend, arranged into a heart-shaped domain structure. A 1:1 stoichiometry between the receptor and ligand is observed, with the receptor inserted into the cleft formed between the two Cγ2 domains of the Fc fragment. The asymmetrical interaction of the two Fc chains with a single FcγR prevents a single antibody molecule from triggering dimerization of receptors and initiating signaling. Instead, dimerization is initiated by the interaction of antigen with the Fab arms, thus linking adaptive responses to effector cell triggering. The binding regions of FcγR to Fc fragments consists of rather flexible loops that rearrange upon complex formation. Only domain 2 and the linker region connecting domains 1 and 2 interact in the complex with

different regions of both Fc chains. Conserved tryptophans located on the FcγRs interact with proline to form a "proline sandwich." A solvent-exposed hydrophobic residue at position 155 is conserved among all FcγRs and represents a binding site for the important IgG1 residue Leu 235. Specificity is generated among the receptor–ligand pairs in a variable region connecting the two extracellular domains that is in contact with the lower hinge region of the Fc fragment (residues 234 to 238).

Despite the structural differences between FcγR family members, all activating FcγRs are characterized by the same sequence of signal transduction events. Except for FcγRI, which can engage monomeric IgG with high-affinity, FcγRs exhibit low affinity for IgGs and can only interact with multimeric IgG immune complexes or opsonized cells, generated during an infectious challenge. Despite the high concentration of circulating IgG in serum, FcγRs on immune cells are incapable of crosslinking in the absence of a pathogenic trigger, thereby preventing inappropriate effector cell activation. Such interactions cause receptor clustering and aggregation, which in turn leads to the phosphorylation of ITAM domains[19,20,21,22] – tandem YxxI/L motifs – by Src family kinases such as Lyn, Lck, Hck, and Fgr and the recruitment and activation of Syk family kinases[20,23,24,25,26,27,28]. A crucial step in this phosphorylation cascade is the activation of the PI3K by Syk, which in turn recruits pleckstrin homology (PH) domain–expressing proteins such as Btk, Gab2, and phosphoinositide-specific phospholipase Cγ (PLCγ). These proteins help to generate inositol triphosphate (IP3) for the mobilization of intracellular Ca2+ from the endoplasmic reticulum and diacylglycerol (DAG) for the activation of protein kinase C (PKC)[29]. Taken together, these intracellular biochemical changes, including the subsequent activation of the Rho GTPases Cdc2, Rac1, and Rac2 and actin polymerization mediated by Arp2/3 and WASP proteins leads to phagocytosis of IgG complexes and receptor internalization[21,30]. In addition to these early events, several signaling pathways, including the MEK and MAP family kinases and the Ras pathway, also become activated, leading

to the expression of pro-inflammatory cytokines and chemokines with direct and indirect effects on cellular survival and differentiation[31,32,33]. All these signaling events are counter-balanced by the regulatory activity of FcγRIIb, which is mediated by the recruitment of phosphatases to its ITIM domain following receptor crosslinking and phosphorylation by Src family kinases[34,35,36]. ITIM-recruited phosphatases such as SHIP-1 and SHP-2 promote the hydrolysis of phosphatidylinositol 3,4,5-triphosphate (PIP3) on the inner leaflet of the plasma membrane to phosphatidylinositol 4,5-biphosphate (PIP2), which in turn inhibits the recruitment and activation of PLC-γ and the tyrosine kinase BTK[34,37,38]. Because the majority of effector leukocytes co-express activating FcγRs and FcγRIIb, the outcome of FcγR-mediated signaling represents a fine-balance between the opposing functions of these receptors.

In contrast to Type I receptors, C-type lectins such as DC-SIGN (CD209) and CD23 (FcϵRII), which bind the sialylated form of IgG Fc, and, in the case of CD23, bind IgE with low affinity, represent the Type II Fcγ receptors. These Fcγ receptors do not belong to the immunoglobulin superfamily and therefore have a distinct subunit composition from canonical FcγRs. CD23, a low-affinity receptor for IgE and sialylated IgG, is a type II membrane glycoprotein in the C-type lectin family. It is comprised of three C-type lectin head domains connected to the membrane by a trimeric α-helical coiled-coil stalk, a transmembrane domain, and a short N-terminal cytoplasmic domain. Membrane-bound CD23 can be cleaved from the surface by endogenous proteases to yield soluble CD23 which helps regulate IgE synthesis by B cells. Recent studies have shown that engagement of the Type II FcγR CD23 on germinal center B cells by sialylated IgG Fc in immune complexes can upregulate FcγRIIB on those cells, resulting in selection of higher affinity IgG clones. The contribution of CD23 to the afferent immune response is summarized in the last section of this chapter.

Like CD23, DC-SIGN is a type II membrane glycoprotein belonging to the C-type lectin family. Its long extracellular domain is divided into two structurally and functionally distinct portions: the neck domain responsible for receptor tetramerization, and a calcium-dependent carbohydrate recognition domain responsible for binding heavily glycosylated pathogens such as HIV-1 and Ebola virus. Engagement of DC-SIGN (or its mouse orthologue SIGN-R1) by sialylated IgG results in an intrinsic T_H2 pathway signaling, ultimately leading to the expression of IL-4 which induces FcγRIIB expression on inflammatory macrophages and thus immunosuppression[39,40,41,42]. Other immunoglobulin receptors with specialized functions in the transport of immunoglobulins, such as FcRn[43] and poly-Ig FcR[44], are outside the scope of this introduction.

1.3 Protein structure of the IgG Fc

The structural determinants of IgG function are paramount to understanding the humoral immune response. IgG is composed of four polypeptide chains: two identical heavy chains belonging to one of four subclasses (IgG1-4) and two identical κ or λ light chains. These four polypeptides are linked, resulting in a bent "Y-shaped" symmetric homodimer. The arms of the "Y" represent the Fab, whose specificity is dependent on both heavy and light chain sequence, while the base of the "Y" is the Fc and entirely composed of the two heavy chains.

Each heavy chain consists of three constant domains Cγ1-3 and a hinge region between Cγ1and Cγ2 The two heavy chains are linked by disulfide bonds in the hinge region and non-covalent interactions between the Cγ3domains. Cγ1pairs with the constant region of the light chain, while Cγ2 and Cγ3 interface with FcγRs, FcRn, and other IgG-binding proteins such as protein G. Most pertinent to my thesis work, the lower hinge and up-

per Cγ2 are the binding location for Type I FcγRs. This is also the major site of heavy chain sequence divergence between the four IgG subclasses, which otherwise share 90 percent in amino acid sequence. In the Cγ2domain, the three main sites that interact with a given FcγR are known as the BC, C'E, and FG loops. Sequence variants of IgG engineered for specific FcγR binding generally have mutations in these regions. For example, the FcγR-null variant G236R/L328R has mutations in the BC and FG loop that completely abrogate FcγR interactions, while the A330L/I332E variant has mutations in the FG loop that enhance FcγRIIIA binding. On the contrary, little variation exists between subclasses in the Cγ2/Cγ3 interface, which is important for FcRn binding and thus serum half-life of IgG. The hinge region also harbors remarkable diversity between subclasses. This region provides flexibility between the Fab and Fc and determines the relative conformations between these two antibody fragments. While the IgG1, IgG2, and IgG4 hinges are relatively short (12-15 amino acids), the IgG3 hinge is 62 amino acids long and contains 21 prolines and 11 cysteines, which dramatically alters its flexibility.

In addition to subclass variation, IgG sequence diversity results from allotype differences between individuals and ethnic groups. These are small polymorphisms in IgG that can impact protein structure. In some cases, patients administered IgG of a different allotype from their own will develop an anti-allotype response, reflecting structural differences between donor and recipient. Allotypes typically have limited functional relevance, though some IgG3 variants have extended half-life, and in general, serum Ig titers correlate with allotype differences[45,46].

The Fc domain is a crucial part of surface IgG, the antigen-specific portion of the B cell receptor (BCR). Recently, structures of intact resting human IgG and IgM BCRs were solved by cryo electron microscopy[47,48]. For IgG, this includes the extracellular IgG homodimer complexed with the transmembrane CD79α/CD79β heterodimeric signaling

adaptor. IgG Fc interacts with CD79α/CD79β in a head-to-tail manner, while IgM Fc interacts side-by-side, thereby distinguishing BCR assembly of these two isotypes. The subtleties of these subunit interactions may shed light on the precise mechanisms of BCR signaling, which are unsupported by key structural evidence. Based on *in vitro* bifluorescence complementation assays of IgD^+ B cell lines, in one model, BCRs are proposed to exist as oligomers on the resting B cell surface, but in the presence of antigen, are thought to cluster as monomers[49]. In another model, most BCRs are thought to exist as monomers that then form large clusters upon antigen stimulation[50]. In these studies, IgG BCRs form larger clusters than those composed of IgM, further demonstrating isotype differences in BCR signaling pathways. These recently published structures in combination with biochemical data on BCR clustering are widely expected to aid our understanding of BCR oligomerization and to pinpoint the precise contacts between relevant domains.

In summary, IgG protein structure informs IgG effector and B cell function and is an important contributor to antibody diversity.

1.4 Fc glycosylation

The past few decades of research have shed light on the structural diversity of IgG introduced by Fc glycosylation and the significant impact it has on FcγR binding and resulting IgG effector functions[51]. The IgG Fc harbors a single, complex, biantennary N-linked glycan at Asn 297 in the D-E loop of the Cγ2domain. The core heptasaccharide of this glycan consists of two proximal N-acetyl glucosamine (GlcNAc) residues and one mannose residue connected by β-1,4 linkages; two branching mannose residues (one α-1,3, one α-1,6); and two additional terminal GlcNAc residues connected by β-1,4 linkages (Fig. 1.1). This core $Man_3GlcNAc_4$ motif is present on every IgG molecule regardless of subclass, is

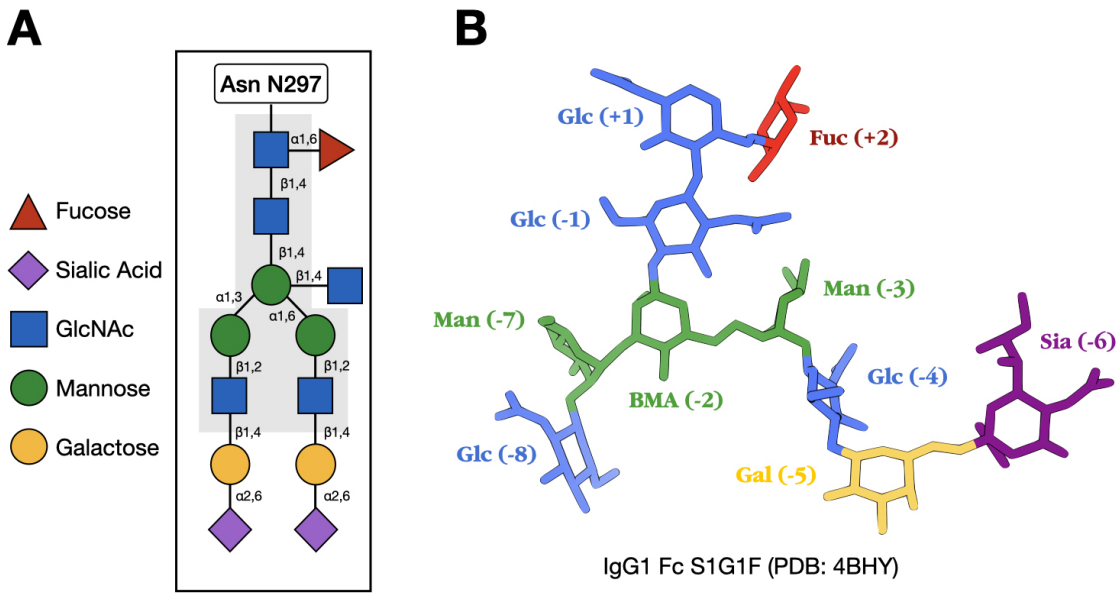

Figure 1.1 | **The highly conserved IgG Fc N-glycan.** (A) Schematic of the complex, biantennary N-glycan at Asn 297. Residues colored according to SNFG standards. Grey shaded area represents the core $Man_3GlcNAc_4$ motif. Residue linkages indicated next to bonds. (B) Structure of the a S1G1F Fc glycan in 3-dimensional space as in a published crystal structure (PDB: 4BHY). Residue numbers according to SNFG standards.

highly conserved across species, and importantly, is critical for FcγR binding. Further, the core heptasaccharide can be extended with core fucose, bisecting GlcNAc, terminal galactose, and terminal sialic acid. Together, these secondary glycan modifications have been observed to modulate Fc-FcγR binding and add an extra layer of regulation to IgG effector function[52,53]. It is important to note that because IgG exists as a homodimer linked by disulfide bonds, each IgG molecule contains two copies of the Fc glycan.

Other Ig isotypes are dependent on Fc glycosylation as well. For instance, IgE glycosylation at Asn 394 has been demonstrated to be essential for FcϵRI binding, mast cell degranulation, and the ensuing anaphylactic response[54,55]. Similarly, IgM glycosylation is important for secretion, presentation on the B cell surface, and pseudo-light chain assembly[56,57,58]. Finally, the Fab can be glycosylated and play a role in antigen recognition, though this only occurs in 10-20 percent of serum antibodies.

The IgG Fc glycan is assembled and attached co-translationally in the endoplasmic reticulum (ER) and further modified in the Golgi apparatus. Initially in the ER, an intact $Glc_3Man_9GlcNAc_2$ precursor is attached to Asn 297 by oligosaccharyltransferases[59]. After transport to the Golgi, a defined set of glycosidases trims this precursor to eventually yield the $Man_3GlcNAc_4$ core heptasaccharide. As the IgG molecule continues to pass through the Golgi, it is further edited by four glycosyltransferases that may add the secondary modifications discussed above, depending on the context: FUT8 adds core fucose, B4GALT1 adds one or two terminal galactoses, MGAT3 adds a bisecting GlcNAc, and ST6GAL1 adds one or two terminal sialic acids. These secondary modifications in Fc glycan composition are dynamically regulated in homeostasis and disease. Some examples are given below, though the precise mechanisms require further study. Ultimately, this additional layer of regulation can lead to 36 theoretical permutations of IgG glycan structure, some of which exhibit differential functions.

The first IgG-FcγR cocrystal structure with differentially glycosylated IgG variants demonstrated that carbohydrate-carbohydrate interactions between IgG and FcγR are essential for intermediate affinity recognition of afucosylated IgG glycovariants byFcγRIIb[60]. In contrast, low affinity binding of FcγRIIb to fucosylated IgG is independent of these carbohydrate interactions. Similarly, the structural impact of IgG Fc sialylation was found to be the primary determinant of Type I FcγR versus Type II FcγR binding. Due to the biantennary nature of the Fc glycan, the two arms have distinct roles in determining IgG conformation. The α-1,6 arm follows the protein backbone of the Cγ2 domain, while the α-1,3 arm occupies the space between Cγ2 domains and interacts with the glycan on the opposing chain[61,62]. Occupying this cavity is what restrains the interdomain flexibility of the Cγ2 domains and stabilizes the "open" conformation of IgG Fc. However, sialylation triggers a destabilization of the Cγ2 domain, converting IgG Fc from its "open" to "closed" conformation. It achieves this by occupying a pocket

formed by Lys 340 and Glu 318, transitioning the Fc fragment to the "closed" conformation. This shift introduces stabilizing interactions between the Fc glycan and Asn 370 of DC-SIGN, additional salt bridge contacts in the Fc-Cγ3 domain, and hydrogen bonds in the Cγ2 domain[63]. This conformational change, by analogy to the CD23-IgE structure, simultaneously allows for Type II FcγR engagement and occludes the Type I FcγR binding site[18,63,64]. In contrast to Type I FcγRs that bind the "open" form of IgG Fc at the hinge-proximal region, the Type II FcγRs CD23 and DC-SIGN bind at the Cγ2-Cγ3 interface of IgG with a 2:1 (receptor:antibody) stoichiometry. This newfound structural principle of IgG sialylation is reminiscent of IgE's inherent C3 domain flexibility, which permits it to bind both Type I (FϵRI) and Type II (CD23) FcγRs in two mutually exclusive conformations, mediating diverse effector functions. These structural insights offer new ways of understanding disease pathogenesis and optimizing IgG-FcγR interactions for enhanced therapeutic activity of IgG.

As discussed, terminal sialylation and core fucosylation of the IgG Fc glycan determine IgG Fc function: sialylation permits DC-SIGN engagement and constitutes a major mechanism of intravenous immunoglobulin (IVIg) therapy[39,40,42,41]; it also allows for engagement of CD23 on B cells, resulting in an enhanced vaccinal response after immunization with sialylated IgG-antigen immune complexes[65,66]. Likewise, afucosylation results in enhanced FcγRIIIA-mediated effector functions such as antibody-dependent cellular cytotoxicity (ADCC) antibody-dependent cellular phagocytosis (ADCP). Afucosylated monoclonal antibodies against neoplastic and infectious diseases are commonly used in the clinic or in clinical testing[9].

While each subclass and Gm allotype are hard coded into the IgG heavy chain locus and are reliably elicited by well-defined cytokine signals to trigger class switch recombination, very little is known about regulation of the glycan. Dozens of Fc glycoforms can

be found in human serum, though the most dominant forms are fucosylated and variably galactosylated[67]. However, several studies have characterized the FcγR binding affinities of some IgG glycoforms and their abundances in various disease contexts[68,69,70,71]. For example, vaccination of mice with model antigens like ovalbumin reliably elicits specific Fc glycoforms dependent on the adjuvant administered[72]. In secondary dengue infection, the Fc glycan may contribute to pathology, where titers of afucosylated IgG1 – and therefore degree of FcγRIIIA engagement – correlates with disease severity[68]. This may be due to enhanced aberrant platelet consumption by phagocytes and resulting thrombocytopenia. In some cases of secondary dengue infection, titers of afucosylated IgG1 at the time of hospital admission predict severe disease later in the clinical course, making Fc glycan structure a valuable prognostic[73]. Similarly, enveloped virus such as SARS-CoV-2 and CMV induce afucosylated IgG1 that is correlated with and may predict severe clinical course[74,75,76]. Studies have also shown that anti-platelet antibodies in neonatal alloimmune thrombocytopenia are significantly afucosylated compared to total IgG and are correlated with disease severity[77].

With regard to sialylation, trivalent influenza vaccination in human subjects reliably causes a spike in sialylated anti-hemagglutinin (HA) IgG1 antibodies seven days after vaccination, with a subsequent increase in afucosylated glycoforms 21 days after vaccination compared to total IgG[65]. Furthermore, the magnitude of the peak in sialylated glycoforms on day 7 was shown to predict the affinity of vaccine-elicited anti-HA IgG, and immunization with sialylated immune complexes was shown to trigger a higher affinity anti-HA IgG response and broader protection against heterologous influenza strains[66]. This tightly regulated control of Fc glycoforms on antigen-specific IgG and its feedback into shaping antibody affinity implies a coordinated mechanism of selection whereby Fc structure may help determine the affinity of the Fab.

Despite their importance, glycans have been difficult to study. This is partly due to a scarcity of analytical tools and the inherent complexity of their structures, which may greatly exceed that of DNA, RNA, and proteins. The need for new technologies in this field has been highlighted recently[78,79,80]. The current gold standard for analyzing protein glycoforms is high-performance liquid chromatography in conjunction with mass spectrometry (LC-MS). Though these methods are highly accurate, they are time-intensive, require purified protein material, and cannot be used *in vivo* to study living cells or organisms. As an alternative, lectins and glycan-binding antibodies have been pursued due to their adaptability to standard molecular biology techniques and potential for use *in vivo*. However, these agents are often promiscuous, binding multiple glycans/glycoproteins. Furthermore, antibodies successfully targeting glycan epitopes are typically only specific for the carbohydrate motif, but non-specific for the particular glycoprotein displaying that motif. In this thesis, I will present the development of IgG glycoform-specific nanobodies that overcome some of the challenges unmet by current technologies.

1.5 The role of Fc-Fcγ receptor interactions in the generation of antibody responses

FcγRs are thought to play a role in processes of antibody production, affinity maturation, and selection. During an adaptive immune response, the affinities of antibodies progressively increase in a process known as affinity maturation. This process occurs in the germinal center (GC), a specialized microanatomical compartment found in lymphoid tissues. Here, B cells diversify their surface Ig – the antigen-specific portion of the (BCR) – and are tested and retested for their ability to bind antigen[81,82,83,84,85]. Only clones with sufficient affinity survive, proliferate, and differentiate into memory B cells and/or

antibody-secreting cells such as plasmablasts and plasma cells. These high-affinity clones are critical to adaptive immune responses, ensuring that secondary exposure to antigen elicits a rapid and specific response. In the GC, antigen exists in the form of immune complexes (ICs), which are retained by follicular dendritic cells (FDCs) via complement receptor (CD21/CD35) and FcγRIIb[86,87,88,89]. The magnitude of IC binding drives the selection of B cells that have undergone Ig variable (V) region hypermutation[83]. Because V region mutation is random, the most likely outcome hypermutation is surface Ig with reduced affinity for antigen. To account for this, B cells with favorable high affinity V region mutations are preferentially stimulated by antigen, which they can more efficiently uptake and present to cognate T helper cells[90,91]. In low affinity clones, the relative absence of these stimulatory signals results in apoptotic cell death and removal by GC macrophages[92]. This constitutes the basic mechanism of affinity-based selection in the GC.

Throughout their development, B cells express the sole inhibitory FcγRIIb which can be bound by ICs. Thus, B cells integrate negative signals from the ITIM-containing FcγRIIb and positive signals from the ITAM-containing BCR to make decisions. Co-engagement of the BCR and FcγRIIb leads to tyrosine phosphorylation of the ITIM[36] and recruitment of SHIP[93,37,94,95]. SHIP hydrolyzes PIP_3[96] and leads to the dissociation of Btk from the membrane and the inhibition of calcium influx into the cell[97,98]. Through this mechanism, FcRIIB can effectively blunt B cell activation and antigen internalization through the recruitment of SHIP. At the extreme, unopposed engagement of FcγRIIb results in membrane disorganization of the BCR and apoptosis of B cells, though this process is not dependent on SHIP[34]. This implies that Fc engagement of FcγRIIb can modulate BCR signaling, the magnitude of which is determined by Fab sequence, providing an important link between these two domains.

Several studies have assessed the impact of FcγRIIb signaling on antibody production

and selection: mice deficient in FcγRIIb have higher IgG titers following immunization and develop spontaneous lupus-like disease due to IgG2a and IgG2b autoantibodies, a reflection of higher tolerance for anti-self clones[2,99]. Follow-up studies using mice with selective deletion of FcγRIIb in B cells showed that this phenotype was due to B cell intrinsic signaling[3]. Moreover, FcγRIIb engagement has been shown to be a key regulator of plasma cell apoptosis, directly controlling the quantity of antibody-secreting cells[100]. In this vein, exposure of plasma cells to cross-linking anti-FcγRIIb antibodies induces cell death. At present, the mechanisms for enhanced IgG titers in FcγRIIb$^{-/-}$ mice are unknown. While it is established that FcγRIIb serves to gate ITAM signaling, whether this process requires bona fide FcγRIIb engagement is unclear. Certainly, BCR is known to tonically signal at a low level in the absence of stimulus[101], though it is not known whether FcγRIIb also recruits SHIP at basal levels. In keep with this, two models of FcγRIIb are theoretically possible: *trans* binding as discussed for soluble ICs, or *cis* binding between the BCR and FcγRIIb, as they are co-expressed. FcγRIIb$^{-/-}$ mice would be absent both modes of binding, so alternate models are required for further investigation.

Finally, as mentioned above, engagement of the Type II FcR CD23 by sialylated IgG immune complexes can also modulate BCR affinity. CD23 binding increases FcγRIIb expression on B cells, thereby raising the threshold of inhibitory signaling that must be overcome for B cells to survive. This biases responses toward higher affinity clones and thus more potent IgG responses. This was validated in an influenza challenge model, where mice immunized with sialylated anti-hemagglutinin IgG-hemagglutinin immune complexes of one strain provided greater protection against subsequent challenges with heterologous strains than asialylated immune complexes did[65,66].

B lineage cells also express several other inhibitory receptors that modulate BCR signaling, such as PD-1, CD72, CD22, and Siglec G/10. Each of these receptors has one or

multiple copies of an ITIM that similar to FcγRIIb, can gate ITAM signaling. Engagement of CD72 and CD22 is known to negatively regulate BCR signaling, though the structural mechanisms are not clear[102,103,104]. Especially of interest in the genetic models presented in Chapter 3 are *cis* interactions with inhibitory receptors that may be altered by Fc glycosylation. This is certainly the case for some Ig binding partners such as CD22, whose association with sialic acid on the IgM BCR in *cis* and *trans* limits B cell activation[105,106].

Despite these discoveries, the full scope of how FcγR signaling contributes to antibody selection is unresolved, but it is likely that the IgG Fc structure plays a role in determining this mechanism. In this thesis, I will present a mouse model of endogenously aglycosylated antibodies and assess responses to immunization and B cell stimulation, showcasing new biochemical tools that will aid our understanding of these processes.

Chapter 2

SYNTHETIC NANOBODIES AS TOOLS TO DISTINGUISH IGG FC GLYCOFORMS

2.1 Introduction

Glycosylation is one of the most common post-translational modifications and is a critical modulator of biological processes. Many proteins can adopt a wide array of glycosylation states—referred to as glycoforms—which can have varying composition, structure, and physiological functions. Despite the importance of protein glycoforms, there is a scarcity of tools to study them. Over the years, there have been numerous attempts to generate glycan-binding reagents, such as lectins or antibodies[80,107,101,108]. However, the majority are suboptimal due to cross-reactivity, poor affinity, and/or promiscuity for multiple glycoproteins. Furthermore, antibodies successfully targeting glycan epitopes are typically only specific for the carbohydrate motif, but non-specific for the particular glycoprotein displaying that motif[109,110,111].

At present, the most accurate and comprehensive method for studying protein glycosylation is mass spectrometry in conjunction with high-performance liquid chromatography (LC-MS)[112,113,114]. Though additional methods, such as capillary electrophoresis or lectin arrays are sometimes used[115,116,117], they also present methodological barriers that limit adaptability to molecular biology techniques such as enzyme-linked immunosorbent assay (ELISA) and flow cytometry and do not allow for *in vivo* manipulation of glycoproteins. This necessitates an alternative approach.

To address this problem, we chose to target one of the most abundant glycoproteins in human serum, immunoglobulin G (IgG). This was an attractive target as all four subclasses of IgG possess a single complex, biantennary N-linked glycan on Asn 297. The presence of this glycan allows for 36 theoretical glycoforms, of which over 30 have been observed by mass spectrometry[118]. These glycoforms have varying affinity and selectivity for Fc gamma receptor (FcγR) binding[119,120], thereby dictating their protective or pathogenic activity[64]. More specifically, IgG lacking its core fucose residue has 10-20-fold higher affinity for the activating FcγRIIIA[121], while terminal sialylation allows for engagement of Type II FcγRs[42,65]. Though it is well established that IgG Fc glycan modifications are dynamically regulated both in health and disease, recent reports have provided support for the role of these modifications as prognostic indicators of disease progression in viral illness[73,75]. In dengue virus-positive patients, levels of afucosylated IgG1 antibodies at admission predict whether a patient will progress to severe disease, namely dengue hemorrhagic fever (DHF) or dengue shock syndrome (DSS)[68]. This same modification also stratifies and serves as a prognostic indicator of clinical severity in PCR-positive COVID-19 patients[74,76]. Further, because the abundance of afucosylated IgG has predictive power in dengue virus and SARS-CoV-2 infection, a probe for this glycoform would open the door for rapid point-of-care tools that could be used to stratify patient risk based on disease-related changes to the IgG glycome. In addition, recent studies have suggested

that afucosylated IgG glycoforms may enhance pathogenesis in some viral illnesses, indicating a potential avenue for therapeutics that target these complex structures. Finally, no methods to date can interrogate IgG glycosylation of the membrane-bound B cell receptor (BCR) of living cells, and thus cannot be used to study cellular regulation of this essential post-translational modification.

Nanobodies are used as therapeutic agents and diagnostic probes due to their small size, ease of production, and excellent specificity and affinity[122,123,124]. Derived from camelid species, they share a similar molecular architecture with human and mouse immunoglobulin variable-heavy chain (VH) domains, with four conserved framework regions surrounding three hypervariable complementarity determining regions (CDRs). However, the CDR3 in most camelids is substantially longer than that of mouse or human variable regions, enabling greater structural flexibility for recognition of recessed or otherwise inaccessible epitopes[125], as may be the case with the N-linked IgG glycan. To capitalize on these advantages and circumvent the challenges of animal immunization, we utilized a purely synthetic yeast nanobody display library that approximates camelid nanobody diversity *in vitro*[126]. Further, because proteins produced by standard recombinant methods generally exist as a heterogeneous pool of glycoforms[62,127], screening for glycoform-specific antibodies has previously been difficult and largely unsuccessful. To overcome this limitation, we chemoenzymatically glycoengineered IgG to adopt a single glycoform of interest, which we hypothesized would allow for selection of nanobodies with high degrees of specificity.

Using this approach, we successfully identified IgG glycoform-specific nanobodies. These molecules demonstrate exquisite specificity for both the complex, biantennary N-linked glycan as well as the protein backbone of IgG Fc. One such nanobody recognizing afucosylated IgG, B7, and its affinity matured progeny, were adapted to standard bio-

chemical assays such as ELISA, Luminex, and flow cytometry. This allowed for rapid quantification of afucosylated IgG in patient sera. In addition, we utilized higher affinity variants to selectively disrupt interactions between FcγRs and specific IgG glycoforms both in vitro and in vivo. X-ray crystallographic studies revealed the structure of the complex of a nanobody clone B7 and its target, afucosylated IgG1, shedding light on this nanobody's unique mode of recognition. Finally, we demonstrated specific nanobody binding to afucosylated BCR on both a lymphoblastic cell line and primary human B cells. These findings constitute the first discovery of broadly applicable tools that can distinguish complex protein glycoforms and provide a rational approach for the generation of additional glycoform specific reagents.

2.2 Results

2.2.1 Discovery and characterization of IgG glycoform specific nanobodies

To precisely select for nanobodies specific for afucosylated and sialylated IgG, we chemoenzymatically engineered clinical grade rituximab into its galactosylated afucosylated (G2), galactosylated fucosylated (G2F), or a galactosylated sialylated fucosylated (S2G2F) glycoforms, as previously described[128,129]. The identity and homogeneity of the glycoengineered glycoforms of rituximab were confirmed by LC-ESI-MS analysis of the Fc domains released by IdeS treatment of the respective rituximab glycoforms. While the commercial rituximab consisted of three major Fc glycoforms, glycoengineered rituximab showed a single Fc glycoform (Fig. 2.1).

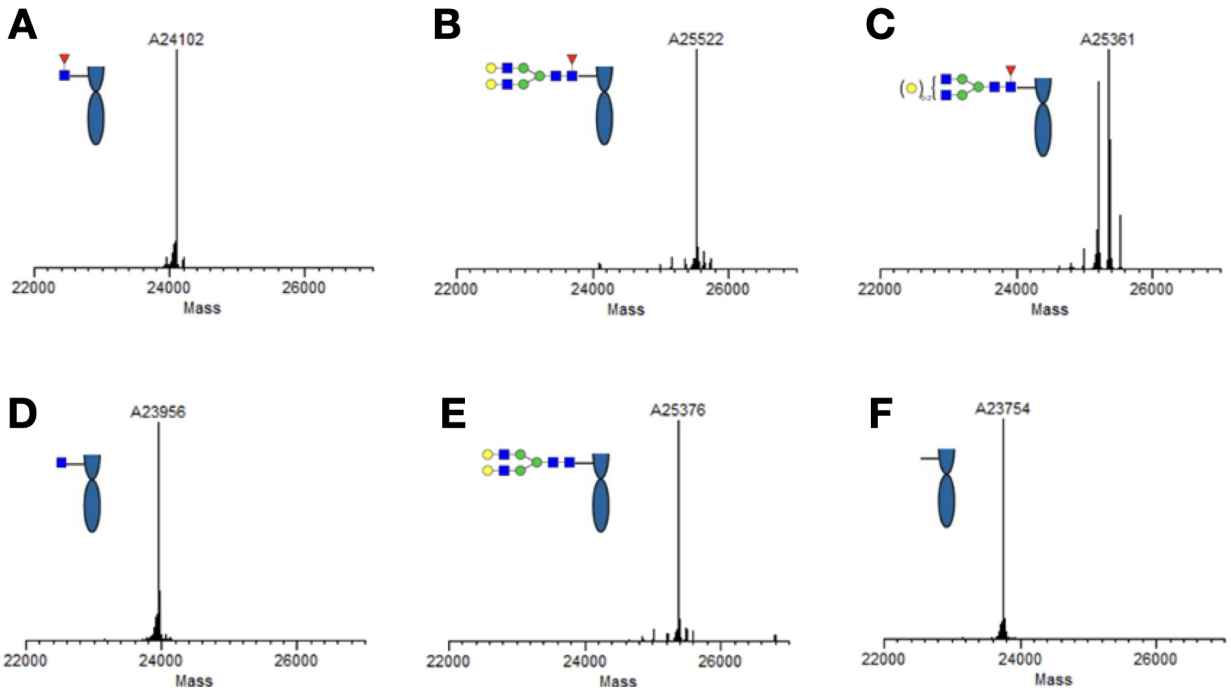

Figure 2.1 | **LC-ESI-MS analysis of the Fc domains released by IdeS treatment of the glycan remodeled and commercial rituximab.** (A) (Fucα-1,6) GlcNAc-rituximab; (B) GlcNAc-rituximab; (C) G2F-rituximab; (D) G2-rituximab; (E) commercial rituximab; (F) The Fc domain of commercial rituximab after PNGase F catalyzed deglycosylation.

Furthermore, to provide quantitative analysis and detection, the Fc N-glycans were released from the antibodies, fluorescently labeled with 2-aminobenzoic acid (2-AA), and analyzed by HPLC. The HPLC separation and quantification indicated that the commercial rituximab carried three different N-glycans, G2F, G1F, and G0F, respectively, in a ratio of 9.3:47.7:43.0. However, the glycoengineered glycoforms carried only the expected single Fc N-glycan without detection of other potential contaminant N-glycans (Fig. 2.2). These results confirm the purity of the glycoengineered rituximab glycoforms.

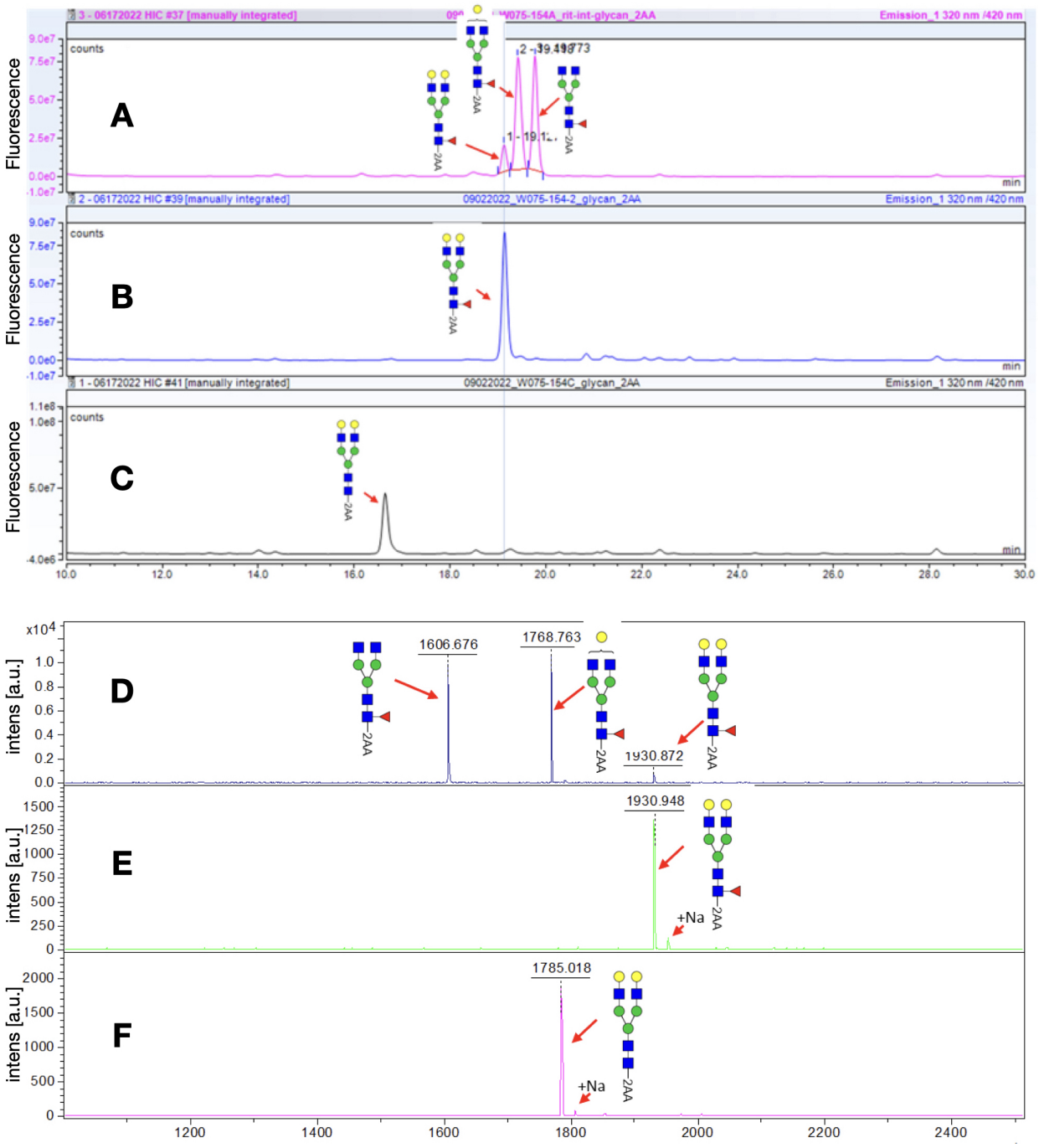
A
B
C
D
E
F
Fluorescence
counts
min
Emission_1 320 nm /420 nm
intens [a.u.]
1606.676
1768.763
1930.872
1930.948
1785.018
+Na
2-AA

Figure 2.2 | .

Figure 2.2 | **Fluorescent HPLC profiles and MALDI-TOF MS analysis of 2-aminobenzoic acid (2-AA) labeled Fc glycans released from rituximab glycoforms.** (A-C) HPLC analysis of the 2-AA labeled Fc glycan from commercial rituximab in **A**, G2F in **B**, and G2 in **C**. (D-F) MALDI-TOF-MS analysis of the 2-AA labeled Fc glycan from commercial rituximab in **D**, G2F in **E**, and G2 in **F**.

G2, G2F, and S2G2F glycoforms were fluorescently labeled with FITC and Alexa647 and yeast displaying nanobodies with specific affinity for the G2 or S2G2F glycoforms were selected through two rounds of magnetic enrichment (MACS) and three rounds of fluorescence-activated cell sorting (FACS)-based enrichment (Fig. 2.3C). High affinity clones were obtained by successively lowering the target glycoform concentration, while specificity was maintained throughout each round by counter-selecting against a high fixed concentration of the undesirable G2F glycoform. After the final round of selection, the resulting library was sequenced and single yeast clones were characterized by flow-cytometry (Fig. 2.3D and F). This screening strategy yielded two nanobodies specific for the G2 glycoform (C11, D3) and two nanobodies specific for the S2G2F glycoform (C5, H9) (Fig. 2E and G). Although D3 bound the G2 glycoform with higher affinity than C11 (K_D = 323 nM vs 22.8 μM), affinity for the G2F glycoform was demonstrably higher (K_D = 1.9 μM vs n.b.). Because glycan binding reagents have typically suffered from poor affinity, we proceeded to mature C11. Sialylated IgG-specific clones C5 and H9 were sufficiently high affinity (K_D = 1.74 nM and 18.8 nM) and did not require further improvement.

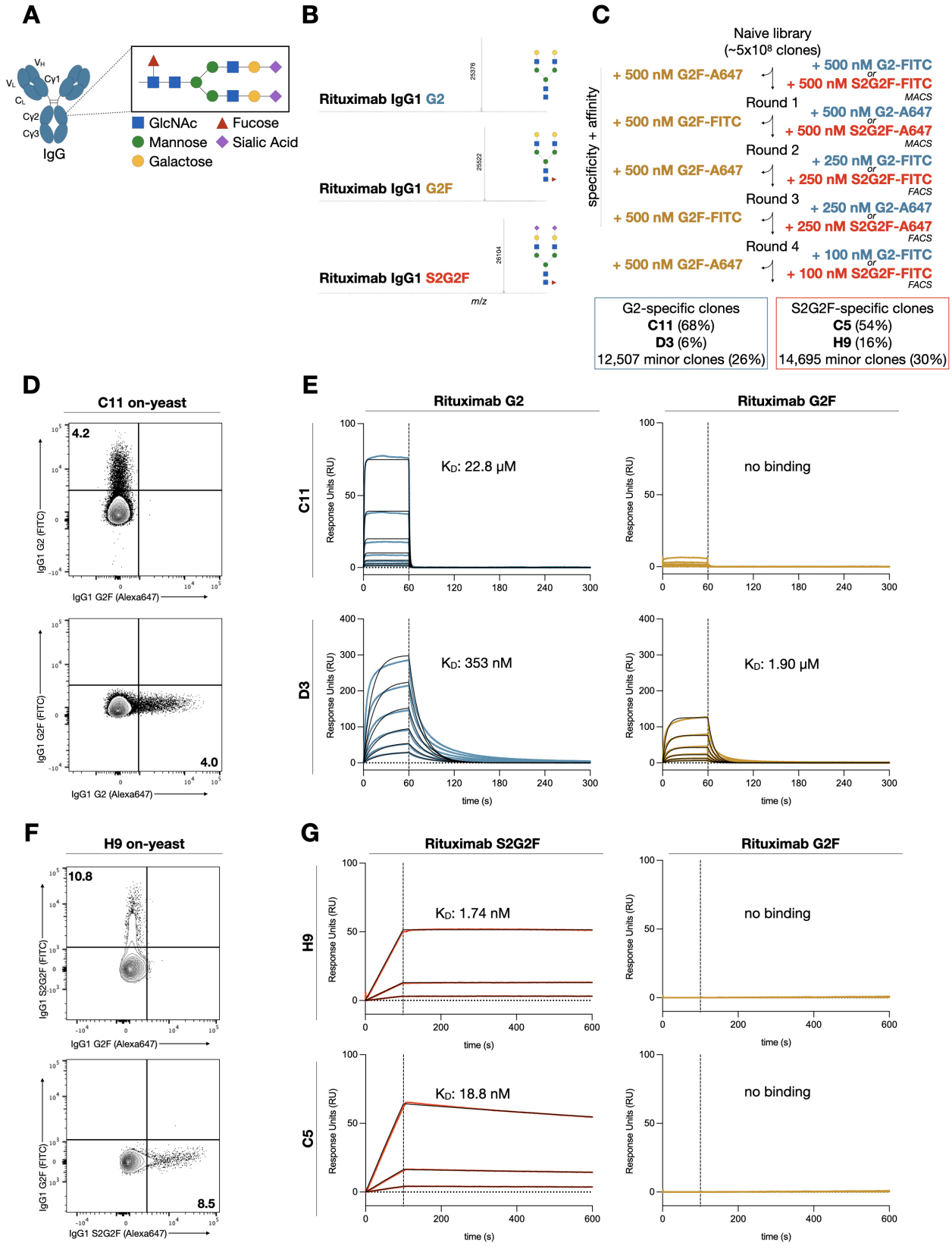
A
IgG
GlcNAc
Fucose
Mannose
Sialic Acid
Galactose
B
Rituximab IgG1 G2
Rituximab IgG1 G2F
Rituximab IgG1 S2G2F
m/z
C
Naive library
(~5x10⁸ clones)
+ 500 nM G2F-A647
+ 500 nM G2-FITC or + 500 nM S2G2F-FITC
MACS
Round 1
+ 500 nM G2F-FITC
+ 500 nM G2-A647 or + 500 nM S2G2F-A647
MACS
Round 2
+ 500 nM G2F-A647
+ 250 nM G2-FITC or + 250 nM S2G2F-FITC
FACS
Round 3
+ 500 nM G2F-FITC
+ 250 nM G2-A647 or + 250 nM S2G2F-A647
FACS
Round 4
+ 500 nM G2F-A647
+ 100 nM G2-FITC or + 100 nM S2G2F-FITC
FACS
specificity + affinity
G2-specific clones
C11 (68%)
D3 (6%)
12,507 minor clones (26%)
S2G2F-specific clones
C5 (54%)
H9 (16%)
14,695 minor clones (30%)
D
C11 on-yeast
4.2
4.0
IgG1 G2 (FITC)
IgG1 G2F (Alexa647)
IgG1 G2F (FITC)
IgG1 G2 (Alexa647)
E
Rituximab G2
Rituximab G2F
C11
D3
Response Units (RU)
KD: 22.8 μM
no binding
KD: 353 nM
KD: 1.90 μM
time (s)
F
H9 on-yeast
10.8
8.5
IgG1 S2G2F (FITC)
IgG1 G2F (Alexa647)
IgG1 G2F (FITC)
IgG1 S2G2F (Alexa647)
G
Rituximab S2G2F
Rituximab G2F
H9
C5
KD: 1.74 nM
no binding
KD: 18.8 nM
time (s)

Figure 2.3 | .

Figure 2.3 | **Generation of IgG glycoform specific nanobodies.** (A) Schematic of the N-linked glycan on Asn-297 of the IgG Fc. (B) Liquid chromatography electrospray ionization mass-spectrometry (LC-ESI-MS) of the G2 and G2F glycoforms of rituximab. G2-Fc, M = 25377 Da; found (m/z) 25376 (deconvolution data), G2F-Fc, M = 25523 Da; found (*m/z*) 25522 (deconvolution data), S2G2F-Fc, M = 26105 Da; found (m/z) 26104. (C) Selection strategy for identification of G2 or S2G2F glycoform-specific nanobodies via magnetic selection (MACS) or fluorescence-activated cell sorting (FACS). Library diversity following five rounds of selection was assessed by next generation sequencing. (D) Flow cytometry of yeast displaying C11 with fluorescently labeled IgG1 G2 and G2F glycoforms. (E) Binding kinetics of the two dominant clones specific for the G2 glycoform of IgG1 Fc, C11 and D3 evaluated by surface plasmon resonance. Blue or yellow traces are raw data, while 1:1 Langmuir global kinetic fits are shown in black. Sample concentrations begin at 1024 nM with 2-fold serial titration until 32 nM. (F) Flow cytometry of yeast displaying H9 with fluorescently labeled IgG1 G2F and S2G2F glycoforms. (G) Binding kinetics of the two dominant clones specific for IgG1 Fc S2G2F, C5 and H9. Blue or yellow traces are raw data, while global kinetic fits are shown in black. Sample concentrations begin at 256 nM with 4-fold serial titration until 16 nM.

2.2.2 Affinity maturation and multimerization of nanobody clones.

To further affinity mature clones specific for afucosylated IgG, we designed a site-saturation mutagenesis library of the CDRs of C11 (Fig. 2.4A). Two rounds of selection of the resulting library, in which G2F was maintained in 50-fold molar excess of G2 bait, yielded numerous clones with penetrant mutations at specific 'hotspots' within each CDR. These clones demonstrated 10 to 1000-fold affinity for G2 while retaining similar levels of specificity as C11 (Fig. 2.4B). Combinatorial assembly of the mutations present in the top clones resulted in a dominant clone, mC11, which exhibited a 1000-fold improvement in affinity for G2 when compared to the C11 parental clone at the cost of marginal specificity (Fig. 2.4C-E). Based on its exquisite specificity, we chose to focus on clone B7 and further engineer it for increased affinity.

Nanobody multimers have been shown to possess drastically higher binding affinities,

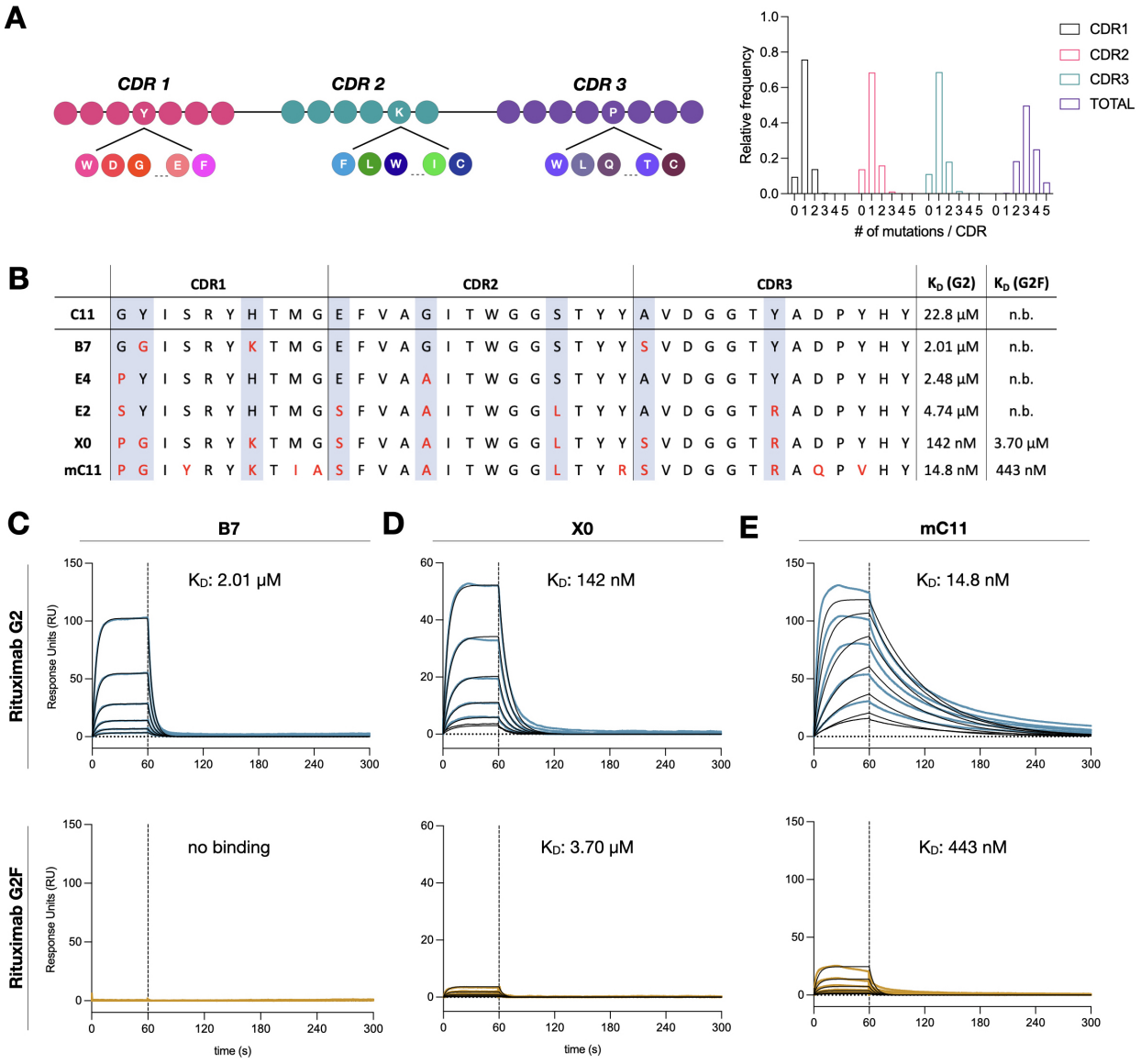

	CDR1									CDR2										CDR3										K_D (G2)	K_D (G2F)
C11	G	Y	I	S	R	Y	H	T	M	G	E	F	V	A	G	I	T	W	G	G	S	T	Y	Y	A	V	D	G	G	T	Y	A	D	P	Y	H	Y	22.8 µM	n.b.
B7	G	G	I	S	R	Y	K	T	M	G	E	F	V	A	G	I	T	W	G	G	S	T	Y	Y	S	V	D	G	G	T	Y	A	D	P	Y	H	Y	2.01 µM	n.b.
E4	P	Y	I	S	R	Y	H	T	M	G	E	F	V	A	A	I	T	W	G	G	S	T	Y	Y	A	V	D	G	G	T	Y	A	D	P	Y	H	Y	2.48 µM	n.b.
E2	S	Y	I	S	R	Y	H	T	M	G	S	F	V	A	A	I	T	W	G	G	L	T	Y	Y	A	V	D	G	G	T	R	A	D	P	Y	H	Y	4.74 µM	n.b.
X0	P	G	I	S	R	Y	K	T	M	G	S	F	V	A	A	I	T	W	G	G	L	T	Y	Y	S	V	D	G	G	T	R	A	D	P	Y	H	Y	142 nM	3.70 µM
mC11	P	G	I	Y	R	Y	K	T	I	A	S	F	V	A	A	I	T	W	G	G	L	T	Y	R	S	V	D	G	G	T	R	A	Q	P	V	H	Y	14.8 nM	443 nM

Figure 2.4 | **Affinity maturation of clone C11 yields nanobodies with nanomolar affinity.** (A) Schematic representation of NNK site-saturation mutagenesis of C11's three CDRs. High-throughput sequencing of resulting affinity maturation library demonstrates 1 mutation per CDR for a total of 3 per clone. (B) CDR sequences and dissociation constants (K_D) for the G2 and G2F glycoforms for five afucosylation-specific high affinity clones. (C-E) Binding kinetics of B7, X0, and mC11 with G2 or G2F glycoforms of rituximab evaluated by SPR. Blue or yellow traces are raw data, kinetic fits are shown in black. Sample concentrations began at 256 nM with 2-fold serial titration until 8 nM (H) Luminex assay comparing the specificity and sensitivity of tetrameric B7 with tetrameric FcγRIIIA for detecting the G2 or G2F glycoforms of rituximab. Vertical dashed lines indicate the range where G2 and G2F can be adequately distinguished. Data was fitted by nonlinear regression analysis.

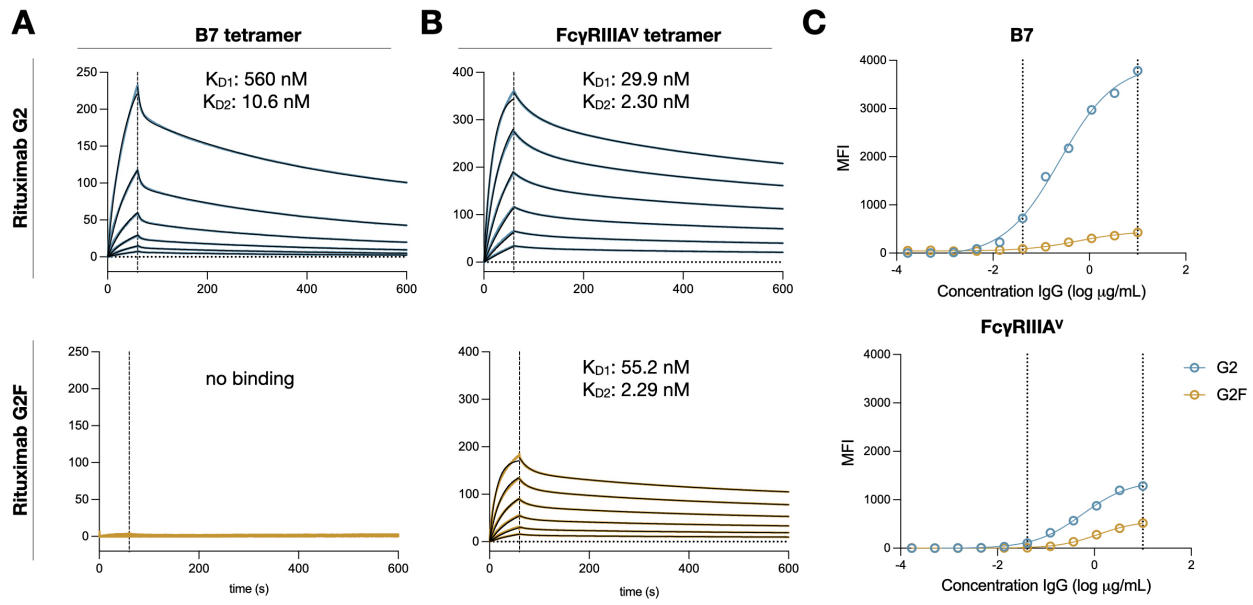

Figure 2.5 | **Comparison of sensitivity and specificity of clone B7 and FcγRIIIA.** (A-B) Binding kinetics of tetrameric B7 and tetrameric FcγRIIIA with G2 or G2F glycoforms of rituximab evaluated by SPR. Blue or yellow traces are raw data, kinetic fits are shown in black. Sample concentrations began at 256 nM with 2-fold serial titration until 8 nM (C) Luminex assay comparing the specificity and sensitivity of tetrameric B7 with tetrameric FcγRIIIA for detecting the G2 or G2F glycoforms of rituximab. Vertical dashed lines indicate the range where G2 and G2F can be adequately distinguished. Data was fitted by nonlinear regression analysis.

largely through avidity[130,131]. To take advantage of this property, we generated biotin-streptavidin tetramers of the most specific nanobody clone, B7. As expected, tetramerization greatly enhanced binding affinity for G2 (K_D1 = 560 nM, K_D2 = 10.6 nM), while preserving specificity (Fig. 2.5A). Though some have proposed the use of soluble Fcγ receptor IIIA (FcγRIIIA) as a detection reagent for afucosylated IgG due to its higher affinity for these glycoforms[132], B7 tetramers demonstrated much greater specificity by SPR as well as greater sensitivity in immunoassays (Fig. 2.5B-C),

2.2.3 IgG glycoform specific nanobodies depend on both protein backbone and glycan composition for binding

Antibodies and lectins specific for glycan residues are ubiquitous in research. However, to the best of our knowledge, reagents for specific complex protein glycoforms have not been reported. To rule out binding to free glycans, we performed an N-linked glycan array using B7 as a probe. As expected, B7 only recognized the human IgG positive control and did not bind any of the N-glycans, regardless of fucosylation (Fig. 2.C-D). The specificity of our glycan array was confirmed using the fucose-binding lectin Aleuria Aurantia Lectin (AAL). Similarly, we confirmed a lack of cross-reactivity to aglycosylated peptide as B7 did not bind IgG1 N297A (Fig. 2.6A-B).

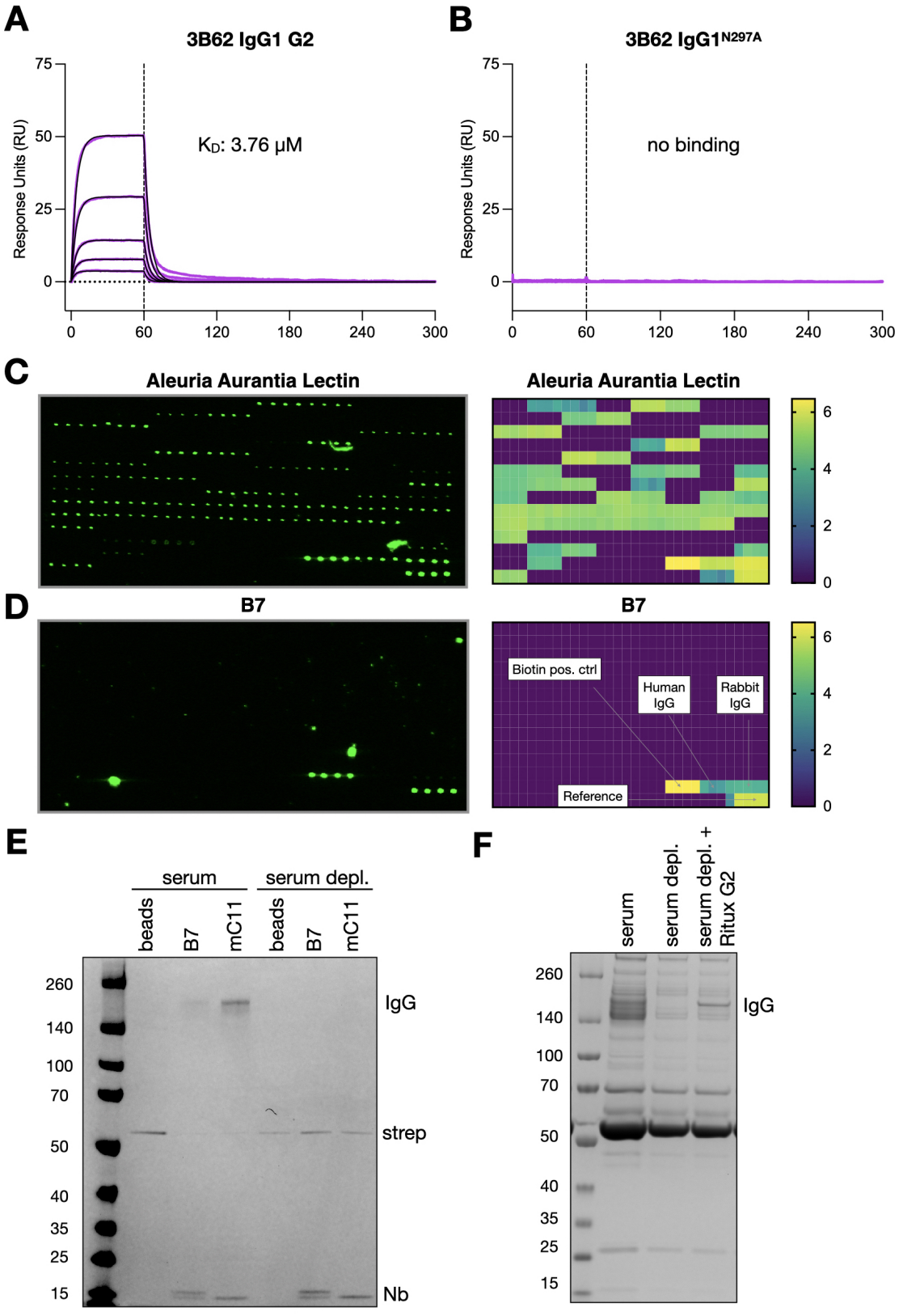
A
3B62 IgG1 G2
Response Units (RU)
75
50
25
0
K_D: 3.76 µM
0
60
120
180
240
300
B
3B62 IgG1N297A
no binding
C
Aleuria Aurantia Lectin
Aleuria Aurantia Lectin
6
4
2
0
D
B7
B7
Biotin pos. ctrl
Human IgG
Rabbit IgG
Reference
E
serum
serum depl.
beads
B7
mC11
beads
B7
mC11
260
140
100
70
50
40
35
25
15
IgG
strep
Nb
F
serum
serum depl.
serum depl. + Ritux G2
260
140
100
70
50
40
35
25
15
IgG

Figure 2.6 | .

Figure 2.6 | **Clone B7 does not bind aglycosylated IgG or free glycans without IgG protein backbone.** (A and B) Binding kinetics of B7 with anti-NP clone 3B62 IgG1 G2 and its aglycosylated 3B62 N297A mutant. Purple traces are raw data, while 1:1 Langmuir global kinetic fits are shown in black. Sample concentrations began at 256 nM with 2-fold serial titration until 16 nM. (C and D) Fluorescent signal (Cy3) of fucose-binding Aleuria Aurantia Lectin (AAL) or clone B7 representing binding to an array of immobilized N-linked glycans. Each condition is provided as a technical quadruplicate oriented horizontally. Conversion of median fluorescent intensity (MFI) to representative heatmap. MFI scale is given as log2. Immobilized biotin is a positive control for streptavidin-Cy3 binding. (E) Coomassie-stained gel comparing B7 and mC11 immunoprecipitation of IgG from intact (left three lanes) or IgG-depleted human serum (right three lanes). (F) Coomassie-stained gel of intact, IgG-depleted, and IgG-depleted serum reconstituted with rituximab G2, confirming appropriate depletion and reconstitution of IgG.

Human IgG is comprised of four subclasses—IgG1, IgG2, IgG3, and IgG4—which share over 90% homology within their Fc domain. To test the subclass cross-reactivity of afucosylation-specific clone B7, we used G2 and G2F glycoforms formatted with human IgG1-4 Fc domains[133]. B7 exhibited subclass specificity (IgG1 > IgG2 > IgG3 >> IgG4) (Fig. 2.7A) but surprisingly maintained specificity for afucosylated glycoforms, with the largest fold-change in specificity for IgG1 and IgG2. In contrast to IgG1, specific glycoforms of other subclasses have a limited biological role in disease, either due to their low abundance in serum or weak FcγR binding. Furthermore, only afucosylated IgG1 has been correlated with the clinical course of inflammatory diseases, while analysis of afucosylated glycoforms of IgG2-4 has demonstrated insignificant predictive power[73].

Finally, we verified that B7 retains binding to all afucosylated forms of IgG1 (G0, G2, S2G2) regardless of galactosylation or sialylation, demonstrating its specificity for all glycoforms lacking the core fucose residue (Fig. 2.7B). Taken together, these studies demonstrate the strict requirements for both peptide sequence and glycan structure necessary for glycoform-specific nanobody binding.

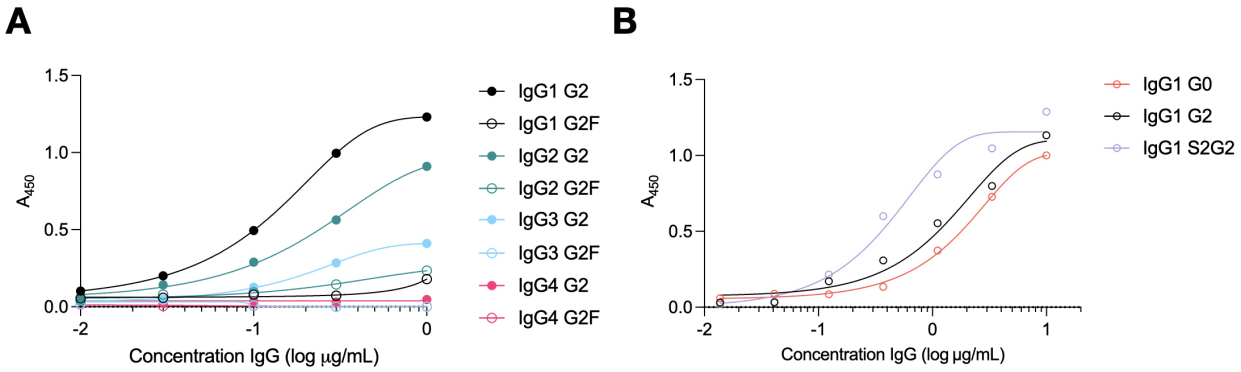

Figure 2.7 | **IgG subclass and glycoform specificity of clone B7.** (A) Sandwich ELISA evaluating subclass and glycoform specificity of clone B7. (B) B7 retains binding to all major afucosylated glycoforms present in human serum. Data in (A-C) were fitted by nonlinear regression analysis.

2.2.4 Crystal structure of apo-X0 and the X0-afucosylated IgG1 Fc complex

Several structures of nanobodies derived from the synthetic camelid nanobody library used in this study have been reported in the literature[126,130]. However, our glycoform-specific nanobodies deviate in CDR sequence from these published models, likely resulting in significantly different loop architecture and requiring that we solve the structure of our clones in isolation. We isolated a pure fraction of the intermediate affinity afucosylated IgG-specific clone, X0, in high concentration and crystallized it in the appropriate solvent conditions (see Methods). We determined the structure at 1.8 Å resolution by molecular replacement and multiple rounds of refinement, using AlphaFold 2's predicted structure for X0 as a search model[134] (Fig. 2.8, Table 6.1). To our surprise, AlphaFold 2's prediction of X0's CDR loops were in complete disagreement with experimentally-derived electron density, though positions of intervening framework regions appeared correct. The CDR loops were manually rebuilt. Consistent with the previously mentioned characteristics of camelid nanobodies, the CDR3 loop protruded considerably from the

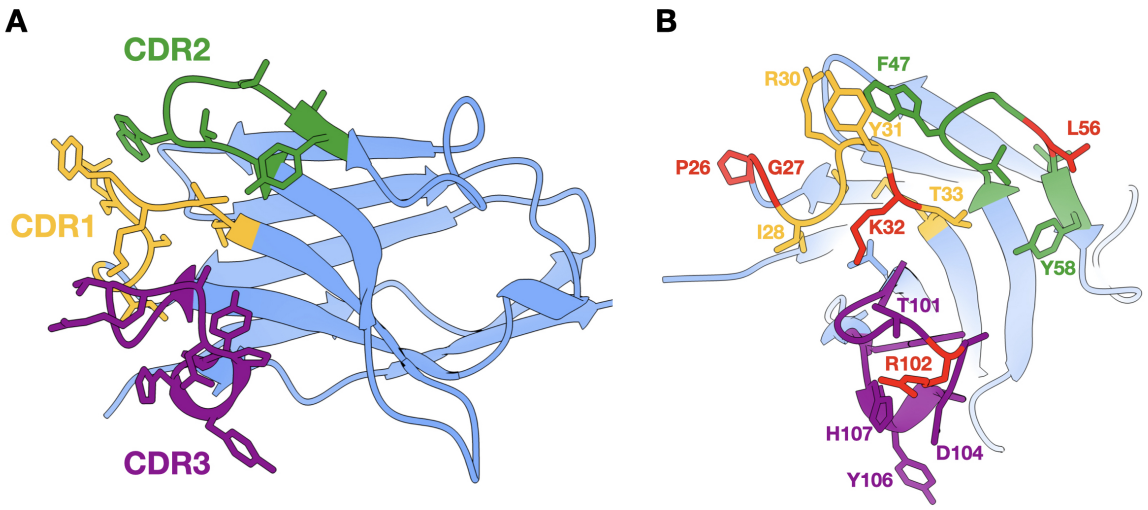

Figure 2.8 | **Crystal structure of the unbound nanobody X0.** (A) Cartoon representation of the overall structure of unbound X0. Stick model of amino acid sidechains are shown for each CDR loop (CDR1 in gold; CDR2 in forest green; CDR3 in dark purple). Framework regions are shown in cornflower blue. (B) Straight-on view of CDR loops. Residues in red were variable during affinity maturation of C11, while those consistent with CDR coloring in A were conserved across all affinity-matured clones.

main body of the molecule, indicating its inherent flexibility and potential to reach recessed epitopes, such as the N-glycans buried in the cleft of IgG molecules[135]. This structure is available as PDB XXXX.

Next, to understand the molecular interactions between afucosylated IgG Fc-specific nanobodies and IgG1, we determined two crystal structures of X0 in complex with afucosylated IgG1^{E382R} Fc (Fig. 2.9A). Co-crystallization of IgG1 Fc is typically difficult due to the propensity of the Fc fragment to crystallize independently of its binding partners. To overcome this potential hurdle, we generated E382X mutants (E382A, E382R, and E382S) that have recently been reported to reduce native crystal contacts in the P212121 space group (such as PDB: 3AVE), more easily allowing for non-canonical crystal packing arrangements[136]. These mutants readily co-migrated with X0 by size exclusion chromatography, indicating that this single polymorphism in the Cγ3 domain of the IgG1 Fc fragment was permissive to nanobody binding. We obtained crystals of the X0-aFuc IgG1

Fc complex that were found to grow in the $P6_1$ and $C2$ space groups in a hexagonal bipyramidal morphology. SDS-PAGE analysis of these crystals revealed that both components were present. The structure was determined by molecular replacement and multiple rounds of refinement using 3AVE and XXXX as search models for the afucosylated IgG1 Fc and X0, respectively. Electron density resolved all amino acids of X0, aa237-444 of IgG1 Fc, and the core N-linked heptasaccharide at Asn 297 on both Fc chains. The final structures were refined to 2.8 Å and 2.7 Å, respectively (Table 6.2). We decided to pursue the $P6_1$ complex based on the completeness of the crystallographic data, and all further discussion will refer to this dataset.

Each asymmetric unit was found to contain two copies of IgG1 Fc and four copies of X0, and thus the complex consists of X0:IgG Fc in a 2:1 ratio, reflecting X0's ability to recognize both open surfaces of the symmetrical homodimer. Importantly, this mode of recognition contrasts with that of FcγR's, which asymmetrically bind with 1:1 stoichiometry. Additionally, since only the Fc fragment was used for these structural studies, it is possible that the presence of a Fab in a full-length afucosylated antibody would prevent secondary X0 binding. We confirmed the stoichiometry of this interaction by analytical ultracentrifugation of X0 mixed with full-length afucosylated IgG1 (data not shown).

2.2.5 Mechanism of nanobody recognition of afucosylated IgG

Overlay of the unbound and bound X0 structures revealed a dramatic shift in the CDR3 loop conformation (Fig. 2.9B). Consistent with an induced-fit model of binding, X0-CDR3 curls down towards the main body of the molecule and wraps around the C'E loop to gain better access to the glycan. This is demonstrated by CDR3 residues that in some cases move >20 Å upon binding (Fig. 2.9C).

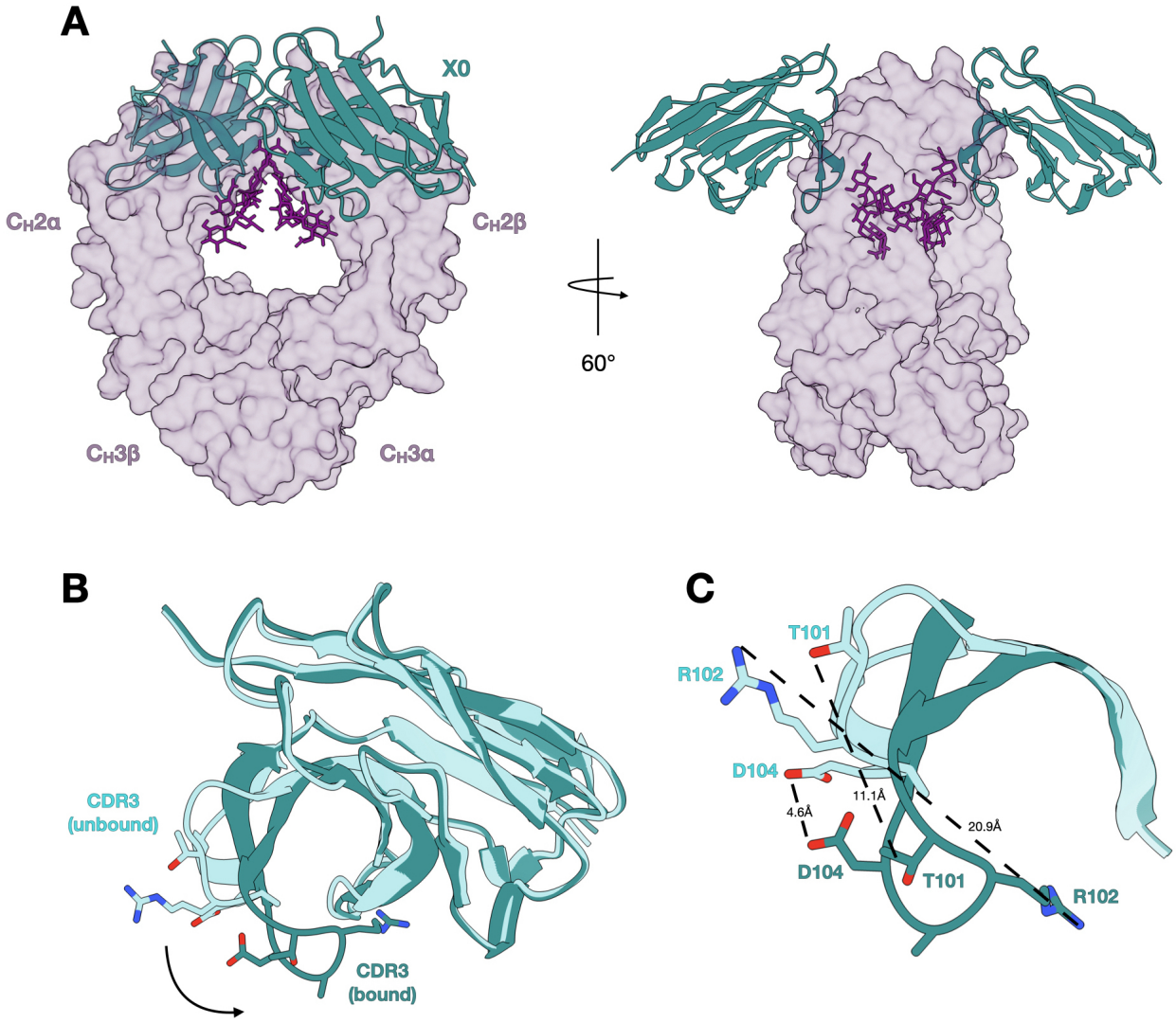

Figure 2.9 | **Overall crystal structure of the X0-afucosylated IgG1 complex.** (A) Side-view (left) and top-view (right) of the complex with transparent surfaces of IgG1 Fc (purple) and superimposed cartoons of X0 (teal) shown. N-linked glycans are shown as sticks in purple. (B) Overlay of unbound X0 (aquamarine) and X0 in complex (teal) superimposed, with sticks of apical CDR3 residue sidechains shown. (C) Overlay of CDR3 loops only with coloring the same as in **B**. Distances between homologous sidechains shown, demonstrating induced fit.

The structure of the complex revealed that all three X0 CDRs contact the Fc protein backbone. Key residues on each molecule were identified by searching for potential contacts under a specified distance threshold and experimentally validated by alanine scanning mutagenesis. We paid special attention to residues that were conserved across all clones during affinity maturation of C11, since we suspected these were essential for high affinity X0-Fc binding. In X0, we mutated residues in CDR1 (Y31), CDR2 (F47, T52, W53, Y58), and CDR3 (Y106). Similarly, we generated afucosylated mutants in the BC loop (H268, E269) and C'E loop (E294, Y296) of the alpha chain, and FG loop (L328, P329, I332) of the beta chain. The relative positions of these putative interactions are highlighted below (Fig. 2.10A-D), and the impact of mutants shown as log2 fold change in K_D relative to wildtype X0-Fc binding (Fig. 2.10E). All X0 CDR mutants reduced binding to wildtype afucosylated IgG by a factor of 4-30x and were generally unable to bind fully fucosylated Fc. α-C'E loop mutants completely abrogated binding, demonstrating that both contacts are individually critical for X0's recognition of the Fc. The importance of these interactions may, in part, explain X0's unfavorable binding to afucosylated IgG3 and IgG4, which both contain Phe at position 296. This substitution likely disrupts H-bonding with Y58 in X0 CDR2. To the contrary, both α-BC loop and β-FG loop contacts were in isolation, dispensable for binding.

Next, we considered the mechanism of X0's glycoform specificity, focusing on two putative glycan-interacting residues in CDR3 of X0, T101 and D104. T101 was absolutely conserved across all clones regardless of affinity, while D104 was also highly conserved, except in the combinatorial mutant, mC11, which contains a D104Q substitution. T101 and D104 are positioned at the apex of the CDR3 loop in close proximity to the α-glycan and β-glycan, respectively. According to our model, T101 H-bonds with the most proximal GlcNAc of the α-glycan, the same residue that is variably bonded to core fucose (Fig. 2.11A-B). Overlaying the X0-Fc complex with previously determined fucosylated IgG1

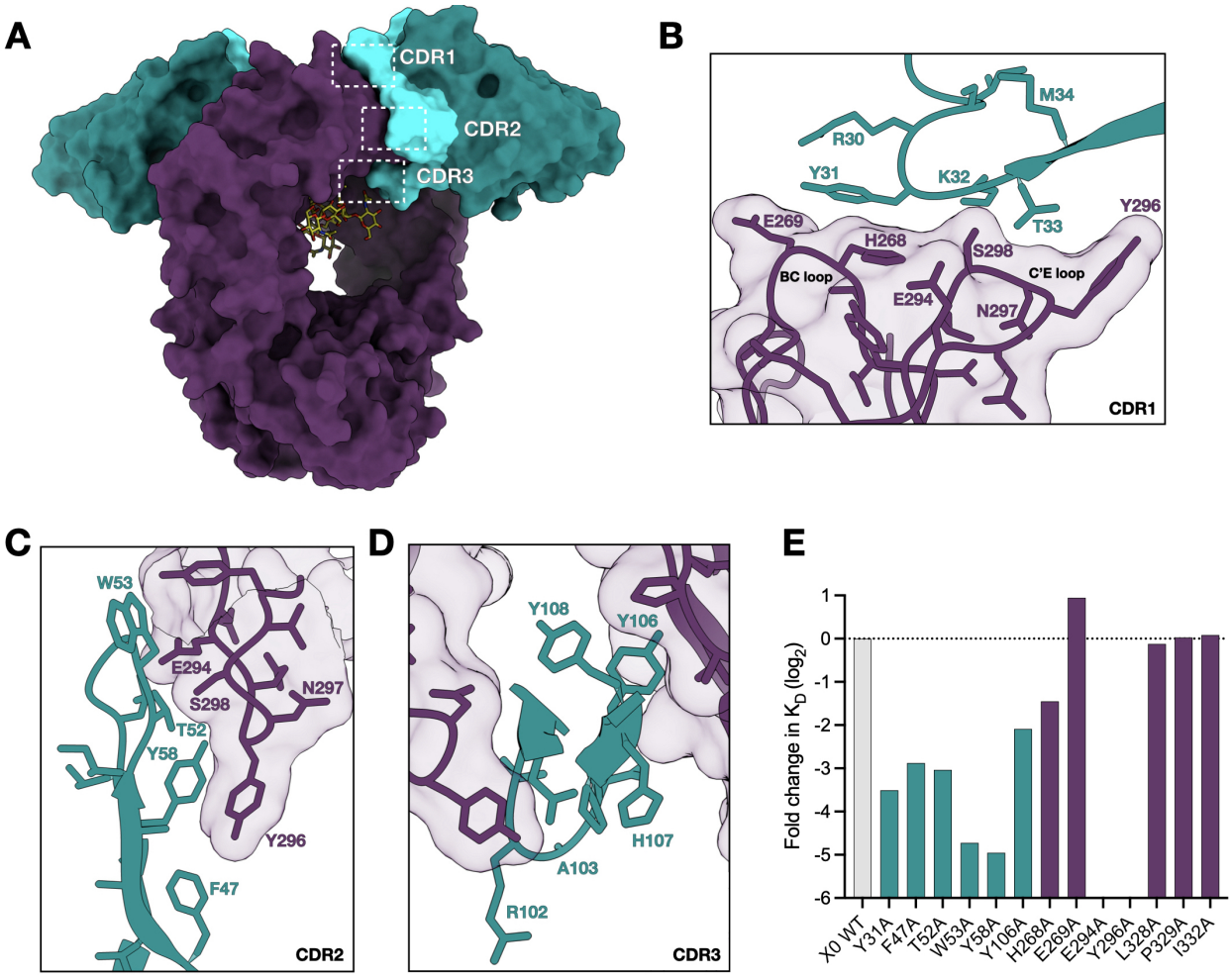

Figure 2.10 | **Protein-protein contacts at the nanobody-IgG binding interface.** (A) Overall structure of the complex showing surfaces of X0 framework regions (teal), X0 CDRs (aquamarine), IgG1 Fc (dark purple), and stick representation of the N-linked glycans in yellow. CDRs are highlighted by dashed white boxes. (B-D) Potential contact residues of CDR1, CDR2, and CDR3 with the IgG1 Fc. (E) Log_2 fold change in K_D of X0 and Fc alanine mutants of putative contact sites. Horizontal dashed line represents the K_D of the wildtype X0-Fc interaction.

Fc structures (i.e. PDB 3AVE) reveals that the core fucose and T101 may clash, possibly revealing a mechanism of glycoform specificity (Fig. 2.11C). Likewise, D104 purportedly contacts the most distal GlcNAc of the β-glycan. Consistent with affinity maturation of C11, saturation mutagenesis at position 101 showed reduced binding across all mutants (Fig. 2.11D). Mutants with residues of similar size (Ile, Ser) or ability to H-bond (Gln, Glu) were generally more favorable than others, but nevertheless revealed a clear preference for Thr. Mutation of D104 had limited impact on overall affinity. Finally, X0 mutants almost uniformly did not bind the G2F glycoform, precluding any claims of altered specificity.

2.2.6 Afucosylated IgG-specific nanobodies block IgG-FcγR interactions *in vitro* and *in vivo*.

Based on structural studies of the X0-Fc complex, we reasoned that X0 and Type I FcγRs would occupy similar epitopes on IgG. Superimposition of the X0-Fc complex and afucosylated IgG1 Fc-FcγRIIIa complex (PDB: 3SGK) confirmed this suspicion (Fig. 2.12A). Strikingly, overlay of these two complexes revealed a similar mode of recognition of the afucosylated glycan. FcγRIIIa's increased affinity for afucosylated IgG1 Fc is a result of glycan-glycan interactions between the two proximal GlcNAc residues on FcγRIIIa-Asn162 and the most proximal glycan on Fc-Asn 297. Those interactions are weakened and/or non-existent when binding fucosylated species. Upon X0 binding, X0-CDR3 moves to a nearly identical space as the FcγRIIIa-Asn162 N-glycan, recapitulating the GlcNAc(2)-GlcNAc(+1) interaction (Fig. 2.12B). Comparison of relevant interacting residues are shown below (Fig. 2.12C).

To better understand the impact of nanobody binding on IgG-FcγR interactions,

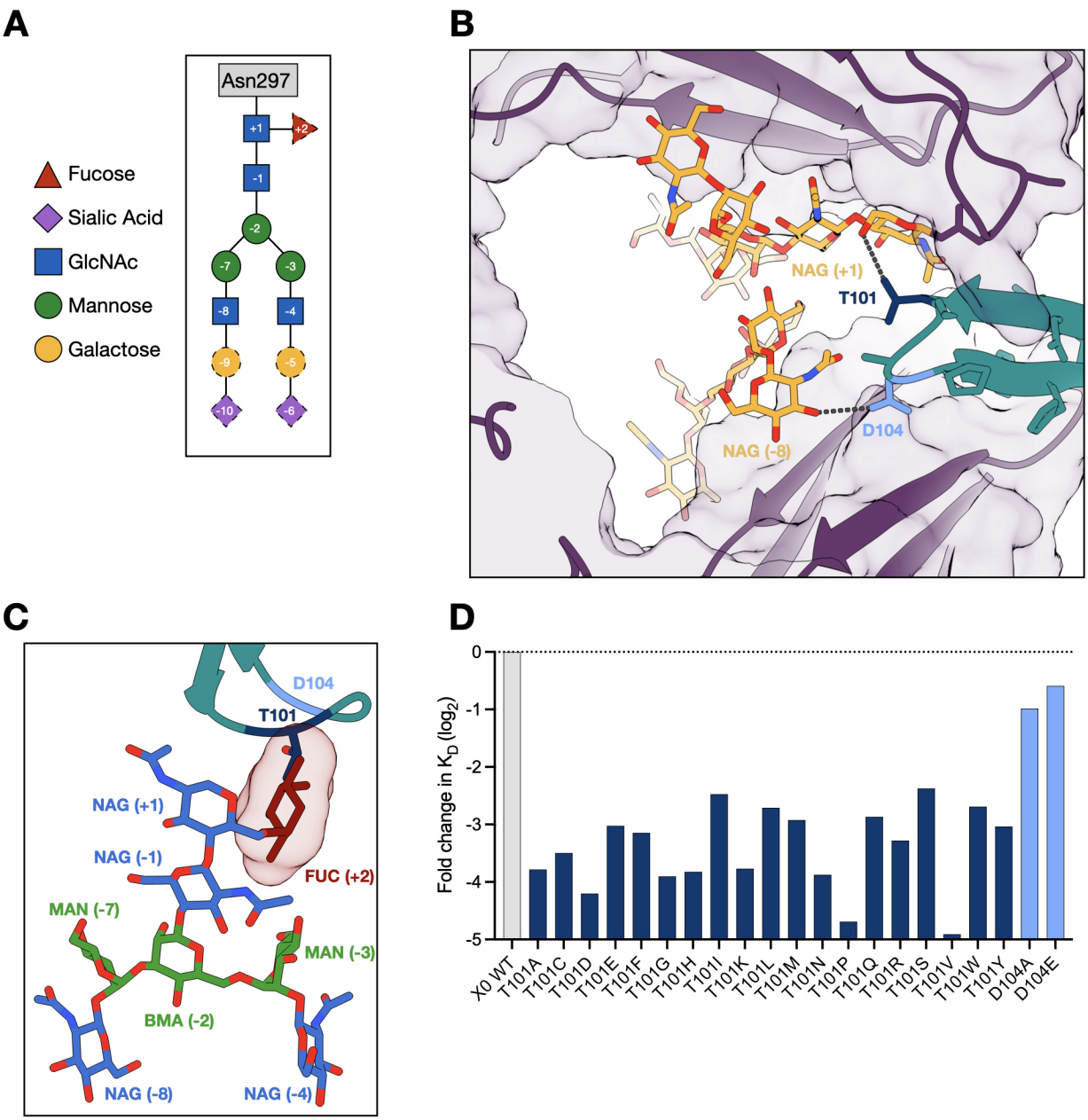

Figure 2.11 | **Protein-glycan contacts at the nanobody-IgG binding interface.** (A) Schematic of the highly conserved N-glycan at IgG-Fc Asn 297. Residues colored and numbered according to SNFG standards. Residues with solid outline are part of the core $Man_3GlcNAc_4$ motif, while those with dashed outlines are variable. (B) X0-CDR3 loop contacts with the Fc glycan. Hydrogen bonds shown by dashed black lines. IgG1 as transparent surface (purple), X0 as cartoon (teal), and glycan as sticks with heteroatoms shown (yellow). Relevant X0 residues highlighted in shades of blue. (C) The X0-CDR3-Fc glycan interface with the core fucose (red sticks with transparent surface) modeled in to reveal potential clashes. (D) Log_2 fold change in K_D of X0 T101 and D104 mutants. Horizontal dashed line represents the K_D of the wildtype X0-Fc interaction.

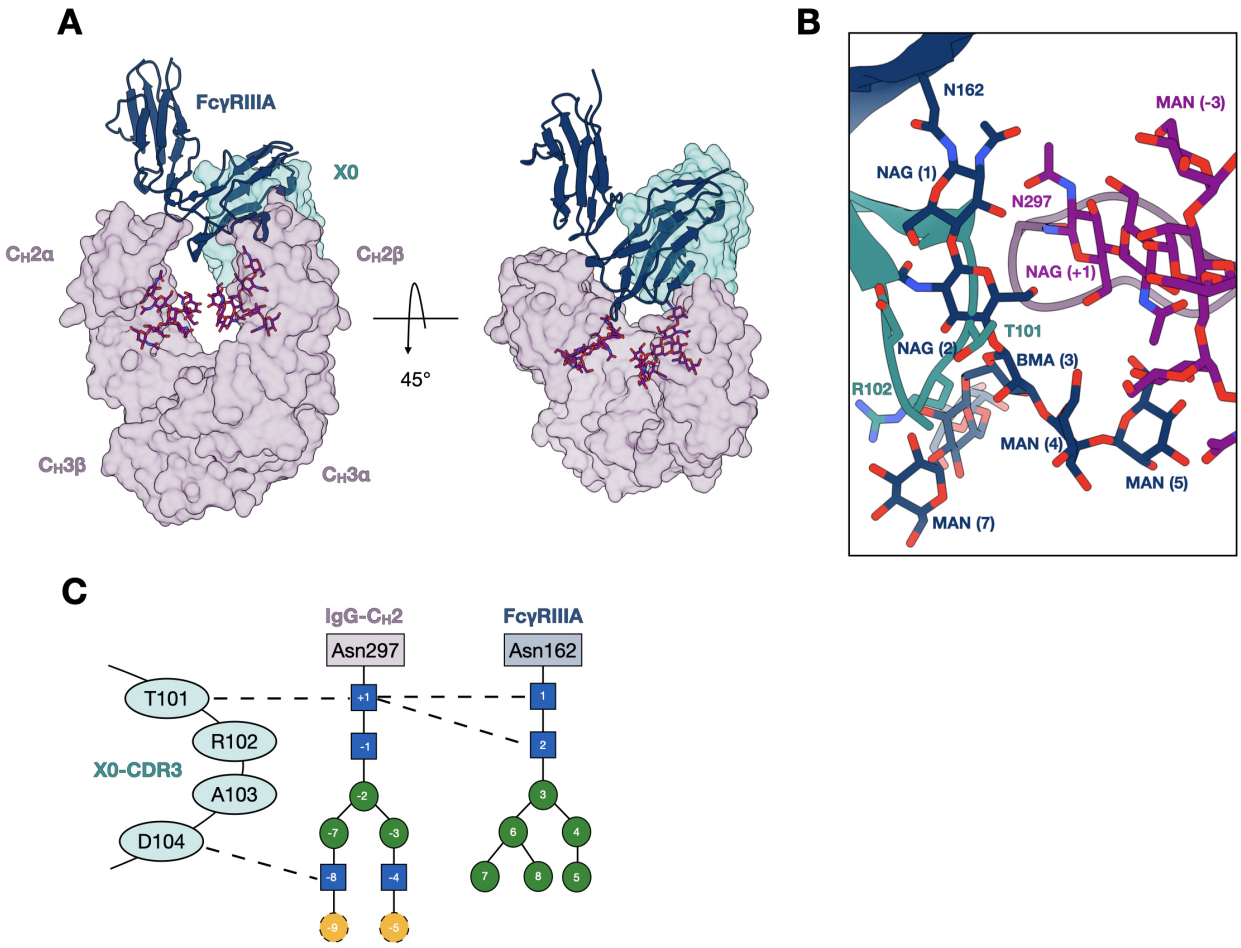

Figure 2.12 | **Overlapping epitopes and similar mode of recognition between X0 and FcγRIIIa.** (A) Side-view (left) and top-view (right) of the superimposed complexes with transparent surfaces of IgG1 Fc (purple) and X0 (teal) shown as well as a cartoon of FcγRIIIa (navy). N-linked glycans are shown as sticks in purple with heteroatoms colored. (B) Close view of X0-CDR3 (teal), FcγRIIIa Asn162 N-glycan (navy), and afucosylated IgG1 Fc Asn 297 N-glycan (purple). X0-CDR3 tracks with the two proximal NAGs of FcγRIIIa. (C) Contact map describing X0-CDR3 and FcγRIIIa-glycan interactions with the Fc glycan. Dashed lines indicated proposed H-bonds.

we performed epitope mapping studies by SPR. Binding the first ligand (either B7 or FcγRIIIa) prevented the second ligand from binding, regardless of orientation. These studies revealed mutually exclusive binding of B7 and FcγRIIIa to afucosylated IgG1. (Fig. 2.13A). Similarly, B7 and its higher affinity variants, X0 and mC11, competitively inhibited monomeric IgG or pre-formed immune complexes from binding multiple FcγR family members (Fig. 2.13B-C).

Afucosylated IgG has been suggested to be a key pathological driver in severe cases of dengue virus and SARS-CoV-2 infection. The mechanisms of this disease enhancement rely on specific IgG-FcγR interactions. Given our preliminary data demonstrating the capacity for nanobody-mediated blockade, we explored whether clone X0, with intermediate affinity and high specificity, could be used *in vivo* as a therapeutic to prevent rituximab-mediated B cell depletion. We chose this model because our group and others have previously shown that only afucosylated rituximab is capable of depleting B cells in humanized FcγR mouse models[129]. To ensure adequate serum half-life of our nanobody therapeutics, we generated nanobody-Fc fusions. Mice were either administered X0-Fc prophylactically or as a treatment following afucosylated rituximab. In both cases, X0-Fc completely blocked B cell depletion compared to isotype controls (Fig. 2.13D-E).

We extended these findings to treat antibody-dependent enhancement (ADE) of dengue infection. In cases of ADE, rather than contributing to antiviral immunity, pre-existing antibodies facilitate viral entry and subsequent infection of host cells, leading to both increased infectivity and virulence. At sub-neutralizing titers, anti-DENV antibodies complex with the DENV virion and attach to the surface of FcγR-expressing leukocytes, utilizing the phagocytic FcγR pathway for entry[137,138,139]. Mechanistic studies have determined that activating FcγRs — specifically FcγRIIa and FcγRIIIa — promote ADE during DENV infection, whereas FcγRIIb acts as a negative regulator for this process[140,141]. In

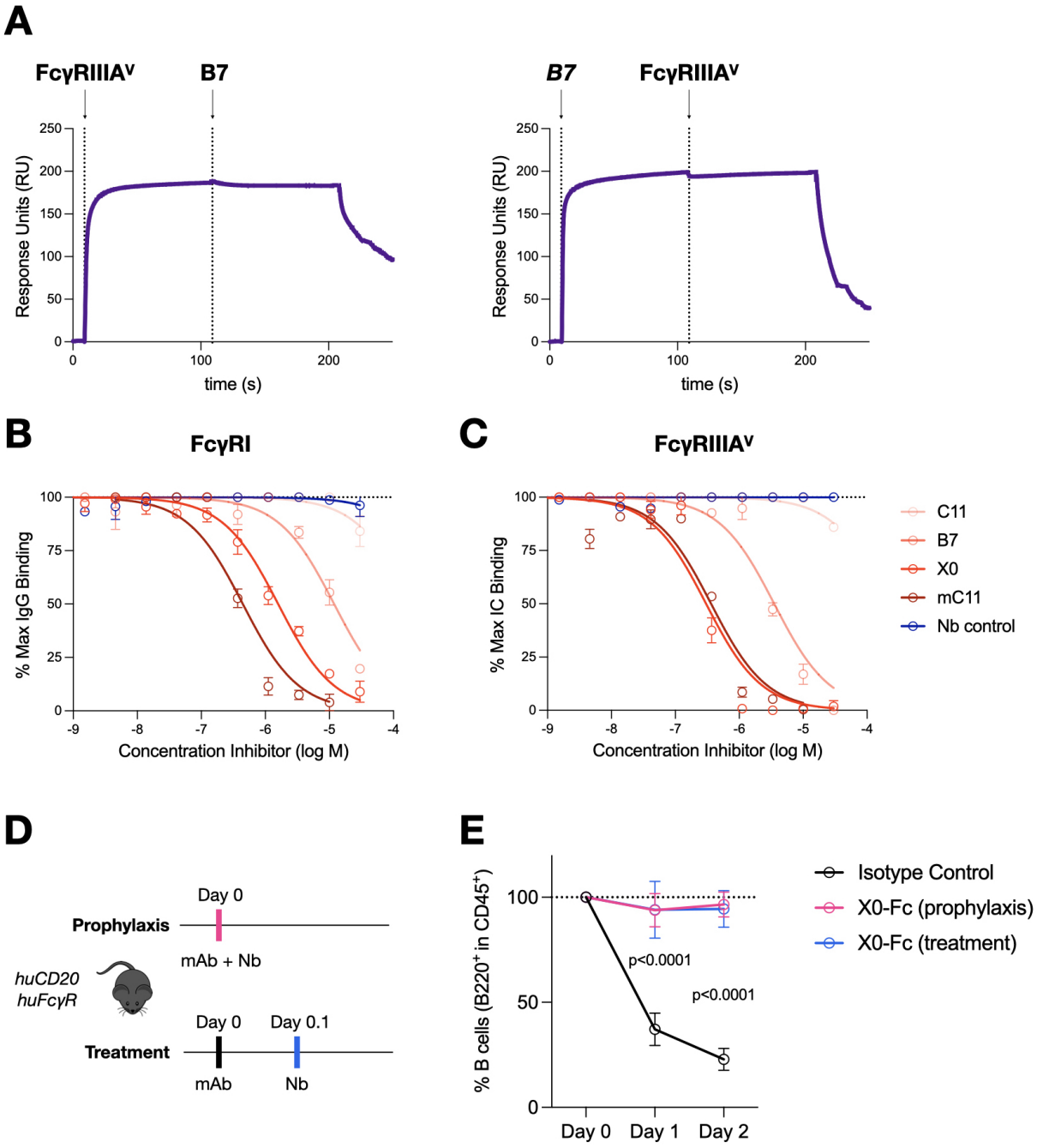

Figure 2.13 | **Afucosylated IgG-specific nanobodies block Fc-FcγR interactions *in vitro* and *in vivo*.** (A) Epitope mapping by SPR shows mutually exclusive binding of B7 and FcγRIIIA to afucosylated IgG1. Vertical dashed lines indicate primary and secondary injection times. (B and C) Enzyme-linked immunosorbent assay (ELISA) evaluating nanobody inhibition of FcγRI or FcγRIIIA binding to afucosylated IgG or immune complexes, respectively. Data displayed as mean ± SEM. Data was fitted by nonlinear regression analysis. (D and E) Mice were administered X0-Fc (2.5 mg/kg) and rituximab G2 (0.5 mg/kg) either prophylactically or as treatment. Data displayed as mean ± SEM (n = 3-4 mice per group).

agreement with these *in vitro* observations, a pathogenic role for antibodies in dengue has been demonstrated *in vivo* in mouse and non-human primate disease models using polyclonal IgG isolated from symptomatic dengue patients or monoclonal anti-dengue IgG[142,143,144,145,146,147]. One recent study from our laboratory generated a novel mouse model of ADE by both knocking out Ifnar1 to allow for murine infection and expressing human FcγRs to recapitulate Fc-FcγR interactions *in vivo*. In this study, the authors identified afucosylated IgG1-FcγRIIIa interactions as the chief determinant of ADE severity. Pre-treatment of mice with Fc null variants protects against dengue infection, while afucosylated variants enhance disease, evident from severe weight loss, thrombocytopenia, and eventual death. As it did in B cell depletion, treatment with X0-Fc fusion disrupted Fc-FcγRIIIa binding and rescued most mice from these disease manifestations (Fig. 2.14).

These studies collectively demonstrate that our glycoform specific nanobodies are potential therapeutics that can selectively target and manipulate specific protein glycoforms.

2.2.7 Afucosylated IgG-specific nanobodies can be adapted to prognostic and diagnostic assays for severe viral infection.

Certain protein glycoforms can serve as powerful markers of specific disease states. Prior reports have demonstrated that the level of afucosylated IgG1 is a robust prognostic marker for severe dengue virus infection. A high level in newly admitted patients predicts disease progression to life-threatening dengue hemorrhagic fever (DHF) or dengue shock syndrome (DSS)[73]. These studies have largely relied on low-throughput mass spectrometry methods to characterize levels of afucosylated IgG in patients. To provide a rapid and inexpensive alternative that can easily be performed in a standard laboratory or delivered at point-of-care, we adapted our nanobodies to biochemical assays, such

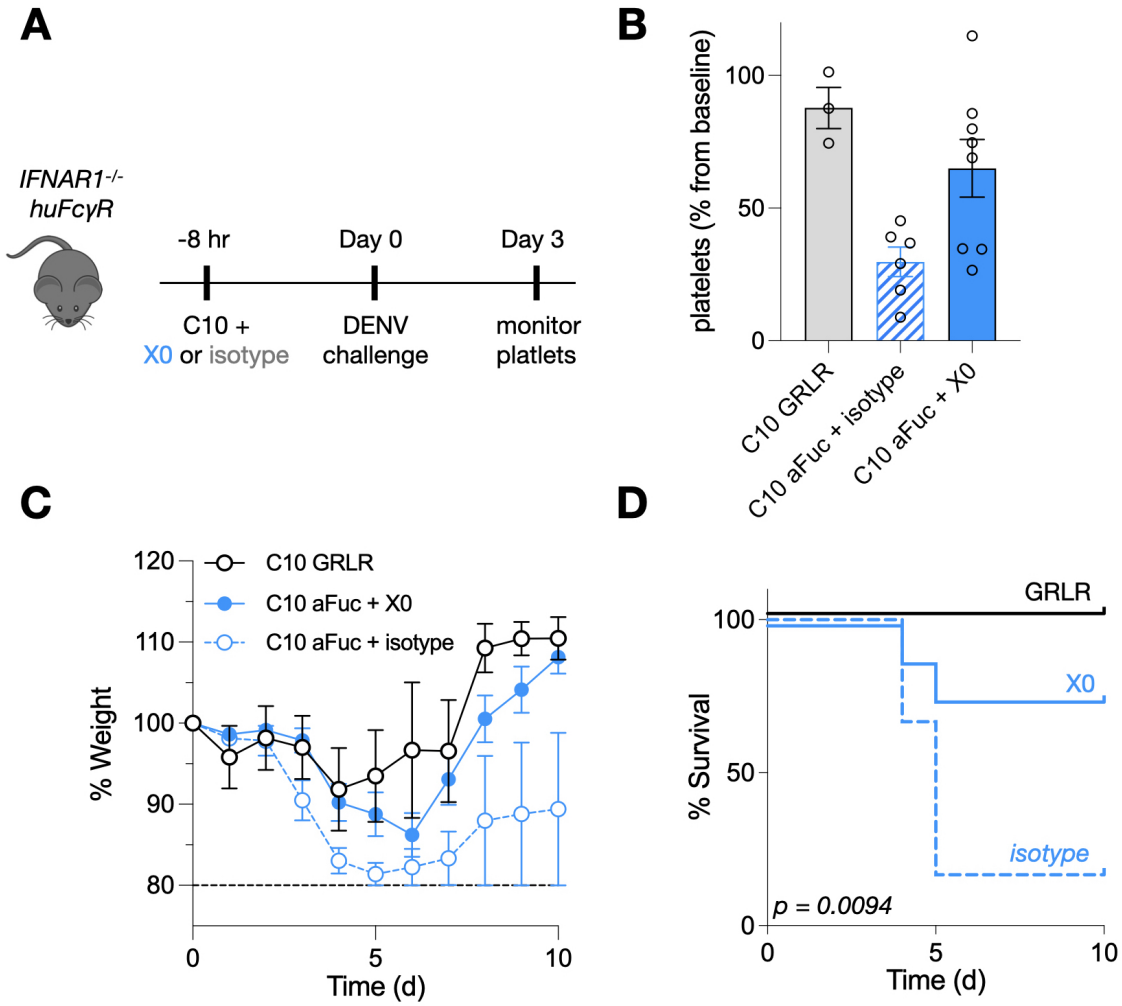

Figure 2.14 | **X0-Fc fusions block afucosylated Fc-FcγRIIa interactions to reverse antibody-dependent enhancement of dengue infection.** (A) 4–6-week-old mice were intravenously administered 20 μg anti-DENV C10 along with 80 μg X0-Fc or isotype, followed 8 hours later by dengue infection. Platelets were counted on Day 3 and monitored for weight loss and survival until Day 10. (B) Platelet levels as a percentage of baseline. (C) Weight as a percentage of baseline. Mice were sacrificed and excluded from further analysis if they lost >20% body mass. Data displayed as mean ± SEM (n = 3-8 mice per group) in B and C. (D) Survival curves of mice treated in A. P value computed by log-rank (Mantel-Cox) test.

as sandwich ELISA or Luminex, to quantify afucosylated IgG1 in patient samples. This contrasts with traditional methods of IgG glycan analysis such as NanoLC-MS, which require purified input material, expensive and highly specialized equipment, and an order of magnitude more time to process samples. We confirmed the specificity of our leading nanobody candidates by immunoprecipitation of IgG from human serum or IgG-depleted serum, demonstrating no binding to other serum glycoproteins (Fig. 2.6E-F). Using serum or purified IgG samples from outpatients from a previously published cohort of convalescent COVID-19 patients[148] whose IgG glycan profiles have been characterized by mass spectrometry, we performed immunoassays capturing human IgG1, and using tetrameric B7 as the detection reagent (Fig. 2.15A). Consistent with our studies of homogeneous IgG glycoforms, nanobody-based quantification of afucosylated IgG in both purified patient IgG and serum demonstrated robust correlation with mass spectrometry values (Fig. 2.15B-C) and using purified IgG or diluted serum had minimal impact on assay output (Fig. 2.15D).

An increase in afucosylated IgG1 has also been observed in SARS-CoV2 infected patients with severe disease[74,76]. To validate these findings and demonstrate the utility of our nanobodies as clinical diagnostics, we used our nanobody-based assay to quantify the levels of afucosylated IgG1 in hospitalized SARS-CoV2 infected patients with moderate or severe COVID-19 as determined by WHO criteria[149]. Expectedly, patients with moderate to severe disease requiring supplemental oxygen therapy had higher levels of afucosylated IgG1 when compared to patients with moderate disease who did not require supplemental oxygen (Fig. 2.16A).

To demonstrate the use of tetrameric B7 as a rapid clinical prognostic, we performed our nanobody-based assay to quantify afucosylated IgG1 in samples collected from dengue-infected pediatric patients at the time of hospital admission (2-6 days after symp-

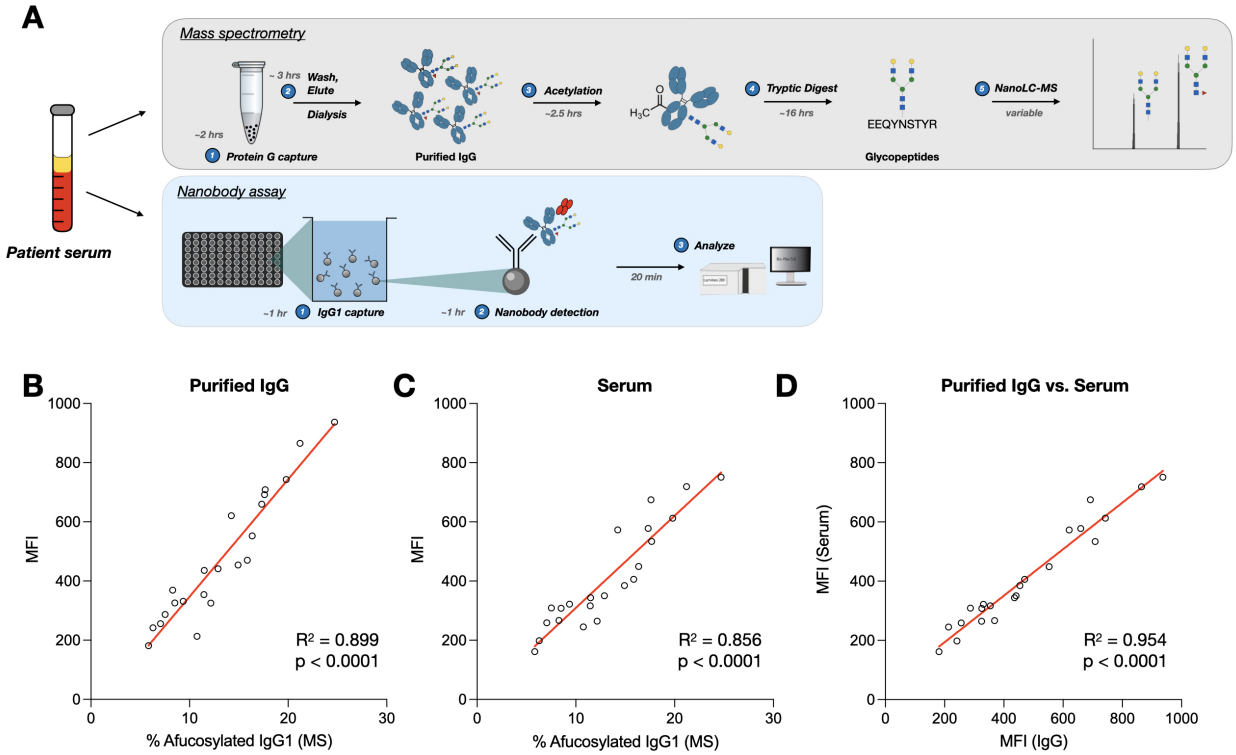

Figure 2.15 | **Nanobody tetramers allow for quantification of IgG glycan composition in patient samples..** (A) Comparison of assay procedures between mass spectrometry and nanobody-based methods of IgG Fc glycan analysis. The nanobody-based assay is simply completed in under 3 hourswithout the need for IgG purification or complex instrumentation. (B and C) Luminex assay quantifying afucosylated IgG1 levels in purified IgG or patient serum. (D) Correlation of afucosylated IgG1 levels detected in purified IgG versus patient serum.

tom onset)[73]. Using the levels of afucosylated IgG1 derived from the assay, we were able to distinguish patients who would days later develop the mildest form of disease, dengue fever (DF), from those who progressed to dengue hemorrhagic fever (DHF) or dengue shock syndrome (DSS) (Fig. 2.16B). Receiver operating characteristic (ROC) analysis of the assay output of both ELISA and Luminex confirmed the prognostic value of IgG glycoform-specific nanobodies in predicting severe dengue disease progression (Fig. 2.16C), comparable to values determined by mass spectroscopy of purified patient IgG.

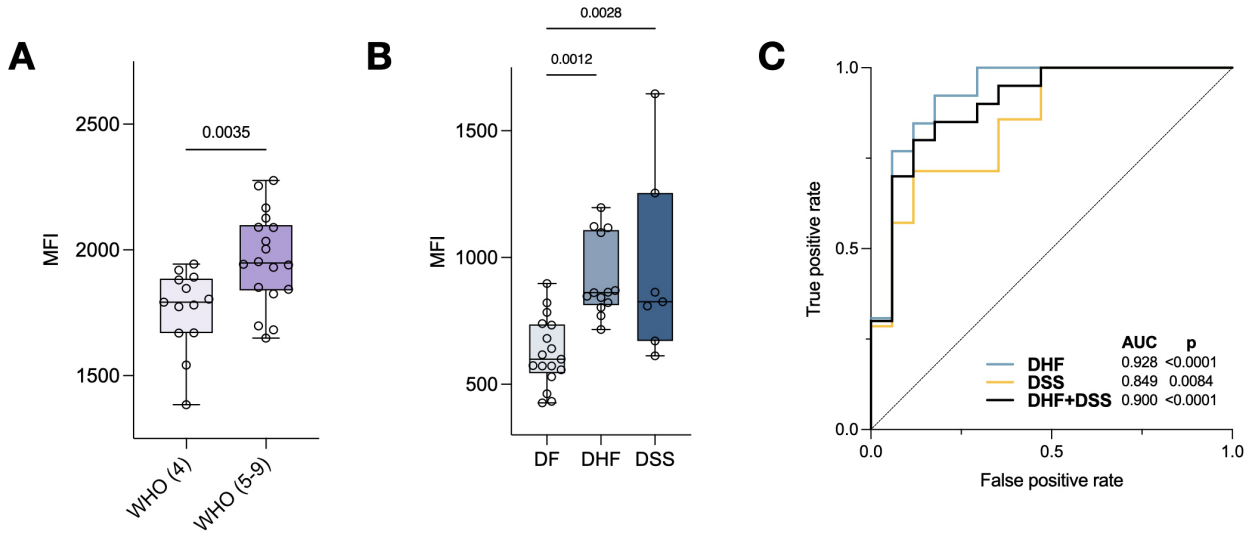

Figure 2.16 | **Nanobody tetramers as diagnostics and prognostics for severe viral disease.** (A) Levels of afucosylated IgG1 in SARS-CoV2-infected hospitalized patients admitted with signs and symptoms of COVID-19, comparing patients with moderate disease not requiring supplemental oxygen (WHO score 4; n = 13) to those with moderate to severe disease requiring supplemental oxygen (WHO scores 5 – 9; n = 18). (B) Levels of afucosylated IgG1 in dengue patients with variable disease severity (dengue fever (DF), dengue hemorrhagic fever (DHF), or dengue shock syndrome (DSS). Data displayed as box plot with all points plotted. Whiskers represent min and max. (C) ROC analysis for the predictive value of afucosylated IgG1 levels at hospital admission for progression to severe dengue infection. AUC, area under curve. Pearson correlation analysis for (B-D); One-way ANOVA/Bonferroni post-hoc for (E and F). Boxes and whiskers represent the median, quartiles, and range (minimum to maximum); numbers above the boxes indicate p values.

2.2.8 Nanobodies can detect IgG glycoforms on live human cells.

Previous approaches characterizing IgG glycosylation have largely focused on secreted antibodies. However, on the surface of B cells there exists an equivalent membrane-bound form, the B cell receptor (BCR), that also harbors the N-linked glycan at Asn 297 (Fig. 2.17A). Little is known about the role of this glycan on the BCR, with previous studies suggesting that specific residues, like the core fucose, may be essential for antigen recognition and receptor-signaling[150,151]. To determine if our nanobodies could be used to interrogate BCR glycan structure, we evaluated binding of tetrameric B7 to the

IgG1-expressing DB lymphoblastic cell line. On analysis, the BCR of wild-type DB cells was almost uniformly fucosylated. However, CRISPR-mediated knockout of the fucosyltransferase FUT8 resulted in robust staining, confirming the specificity of our tool for detecting afucosylated IgG BCR (Fig. 2.17B). Notably, the frequency of cells with afucosylated BCR detected by flow-cytometry correlated with the extent of FUT8 knockout. Next, we extended these methods to primary human class-switched memory B cells derived from peripheral blood. We once again confirmed the specificity of our probes by FUT8 knockout (Fig. 2.17C). Taken together, these findings demonstrate the capability of these nanobody probes to recognize distinct BCR glycoforms and provide a tool to study glycosylation on living cells.

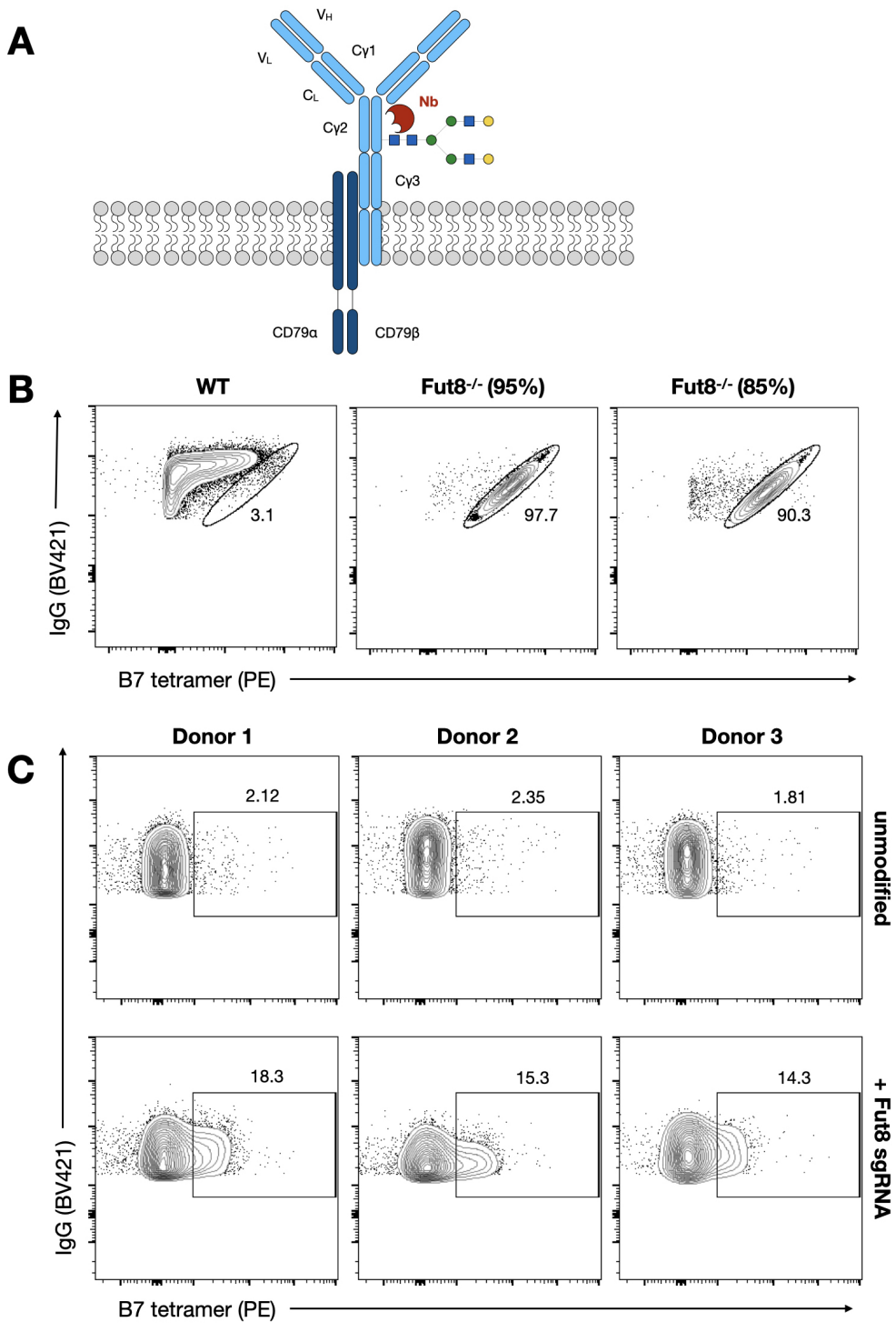
A
VH
VL
Cγ1
CL
Nb
Cγ2
Cγ3
CD79α
CD79β
B
WT
Fut8-/- (95%)
Fut8-/- (85%)
3.1
97.7
90.3
IgG (BV421)
B7 tetramer (PE)
C
Donor 1
Donor 2
Donor 3
2.12
2.35
1.81
unmodified
18.3
15.3
14.3
+ Fut8 sgRNA
IgG (BV421)
B7 tetramer (PE)

Figure 2.17 | .

Figure 2.17 | **Detection of B cell receptor (BCR) glycoforms on live human cells.** (A) Schematic representation of the membrane-bound IgG BCR and its associated glycan. (B) Flow cytometry analysis of BCR afucosylation by B7 tetramer staining of IgG1-expressing B-lymphoblastic cell line DB with and without CRISPR/Cas9-mediated FUT8 knockout. (C) Flow cytometry analysis of BCR afucosylation by B7 tetramer staining of primary human IgG+ peripheral memory B cells with and without CRISPR/Cas9-mediated FUT8 knockout. CRISPR/Cas9 knockout efficiency was determined by TiDE for all experiments.

Chapter 3

THE ROLE OF THE IGG FC GLYCAN IN DEVELOPING ANTIBODY RESPONSES

3.1 Introduction

The IgG Fc glycan is highly conserved across IgG subclasses and species. At minimum, its core heptasaccharide motif is critical for the structural integrity of the Fc fragment and its interactions with FcγRs, as demonstrated by the lack of FcγR binding and effector function of aglycosylated antibodies. Importantly, all secreted IgG found in serum as well as in the membrane-bound BCR is thought to harbor this N-linked glycan. The Fc glycan's ubiquity and persistence throughout evolution may indicate its role in the development of antibody responses as well. Some studies have suggested that the Fc glycan is important for a functional BCR, and that both antigen binding and downstream signaling are compromised by perturbations to the IgG BCR Fc glycan. One such study demonstrated that knockdown of the α-1,6-fucosyltransferase, FUT8, in the immortalized IgG2a-expressing

3-83 B cell line reduced recognition of its cognate antigen, p31[150,151]. 3-83$^{FUT8-/-}$ were less effective at binding p31, ostensibly due to a failure to oligomerize upon antigen stimulation. Similarly, 3-83$^{FUT8-/-}$ were less capable of initiating signaling events downstream of antigen binding, such as phosphorylation of CD79α and Syk. Reconstitution of FUT8 in these cells rescued the phenotype.

However, the conclusions from this study overlook the drawbacks of a FUT8 knockdown model. This enzyme is responsible for α-1,6-fucosylation of multiple target proteins, some of which may be involved in BCR signaling and/or activation. Mouse models of a total FUT8 knockout demonstrate differences between these genotypes, such as significant differences in peripheral leukocyte counts including that of non-IgG expressing B cells. This implies broad and potentially off-target effects of enzymatic ablation and warrants a more precise approach that specifically targets the IgG BCR glycan.

In this chapter, I discuss the generation of genetic mouse models and biochemical tools to study how BCR Fc glycosylation affects the development of antibody responses. I present preliminary data showing the effects that aglycosylated antibodies have on antibody selection as well as future experiments to further interrogate these questions. Finally, I review an attempt at studying the Fc glycan's role in endogenous human Fc-FcγR interactions, and describe an alternative use for this mouse in a tolerance model.

3.2 Results

3.2.1 A genetic mouse model of aglycosylated antibodies.

Mutation of Asn 297 in the Cγ2 domain of recombinant IgG removes the attachment residue for the Fc glycan. Recapitulating this same mutation in a genetic mouse model would result in fully aglycosylated endogenous antibodies that are incapable of binding to FcγRs both in *cis*and trans, but that can be adequately recycled through FcRn. Such a model would allow for investigation of the development of aglycosylated antibody responses, both at the level of serum IgG titers and IgG+ class-switched B cells bearing aglycosylated BCRs. Using CRISPR/Cas9 gene targeting and homology-directed repair, I generated an aglycosylated allele of the IgG1 heavy chain locus of C57BL/6 mice (*Ighg1*) by replacing Asn 297 with Ala (N297A) (Fig. 3.1A). I chose this locus because IgG1 is the dominant subclass in mice and is easily elicited by immunization with standard aluminum-based adjuvants. Backcrossing to wildtype C57BL/6 mice and subsequent F1 x F1 breeding yielded viable heterozygotes and homozygotes (Fig. 3.1B).

When introduced into the genome, the N297A mutation did not cause any obvious abnormalities in B cell development (data not shown). Importantly however, IgG1^{N297A}is not expected to have any bearing on naïve B cells or those expressing isotypes other than IgG1. Thus, the effects of this mutation should be limited to IgG1class-switched cells. Even in the absence of stimuli in specific pathogen free laboratory environments, mice produce a small fraction of class-switched memory B cells, plasma cells, and serum IgG antibodies, likely in response to dietary antigens and intestinal microbiota. In naïve mice, B cell numbers and baseline serum IgM and IgG titers were equivalent among littermates from all three genotypes (Fig. 3.2). This finding indicates that B cells with aglycosylated BCRs are viable and can differentiate into antibody-secreting cells capable of producing

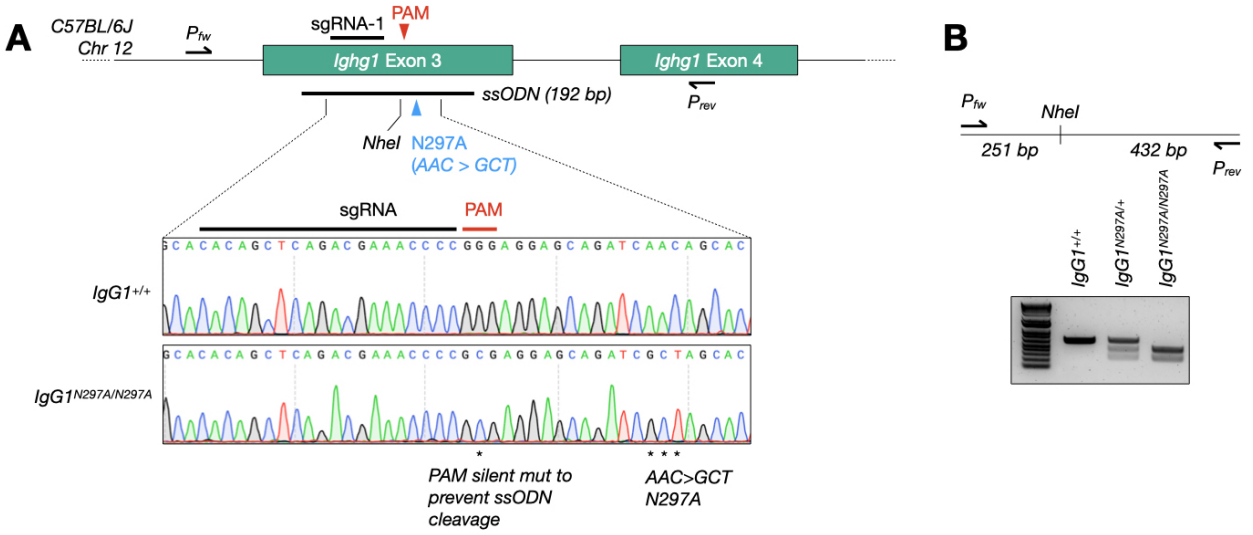

Figure 3.1 | **Design of the IgG1^{N297A}mouse..** (A) Targeting strategy for Exon 3 of IGHG1 to generate the N297A allele using easiCRISPR. Oocytes were microinjected with synthetic sgRNA and single-stranded repair template encoding the N297A mutation and additional silent mutations to destroy the protospacer adjacent motif (PAM) and prevent Cas9 recutting of the template DNA. (B) Genotyping of IgG1$^{+/+}$, IgG1$^{N297A/+}$, IgG1$^{N297A/N297A}$ by restriction fragment length polymorphism (RFLP) analysis of a region spanning Exons 3 and 4 using the NheI restriction enzyme and primers P_{fw} and P_{rev}.

IgG with normal half-life.

3.2.2 The role of the IgG Fc glycan in germinal center responses.

Next, I wanted to understand how the Fc glycan may play a role in B cell and antibody responses to immunization. IgG1$^{+/+}$, IgG1$^{N297A/+}$, and IgG1$^{N297A/N297A}$ mice were immunized subcutaneously in the hind footpad with the canonical haptenated antigen, 4-hydroxy-3-nitro-phenylacetyl (NP) coupled to ovalbumin (NP-OVA). This generates robust germinal center (GC) responses in the draining popliteal lymph node (pLN), where GC B cells are otherwise absent. Quantities of GC B cells is a surrogate for the magnitude of the response. IgG1$^{N297A/+}$and IgG1$^{N297A/N297A}$ mice showed slightly but not always significantly diminished overall GC responses compared to wildtype mice (Fig. 3.3A and D). How-

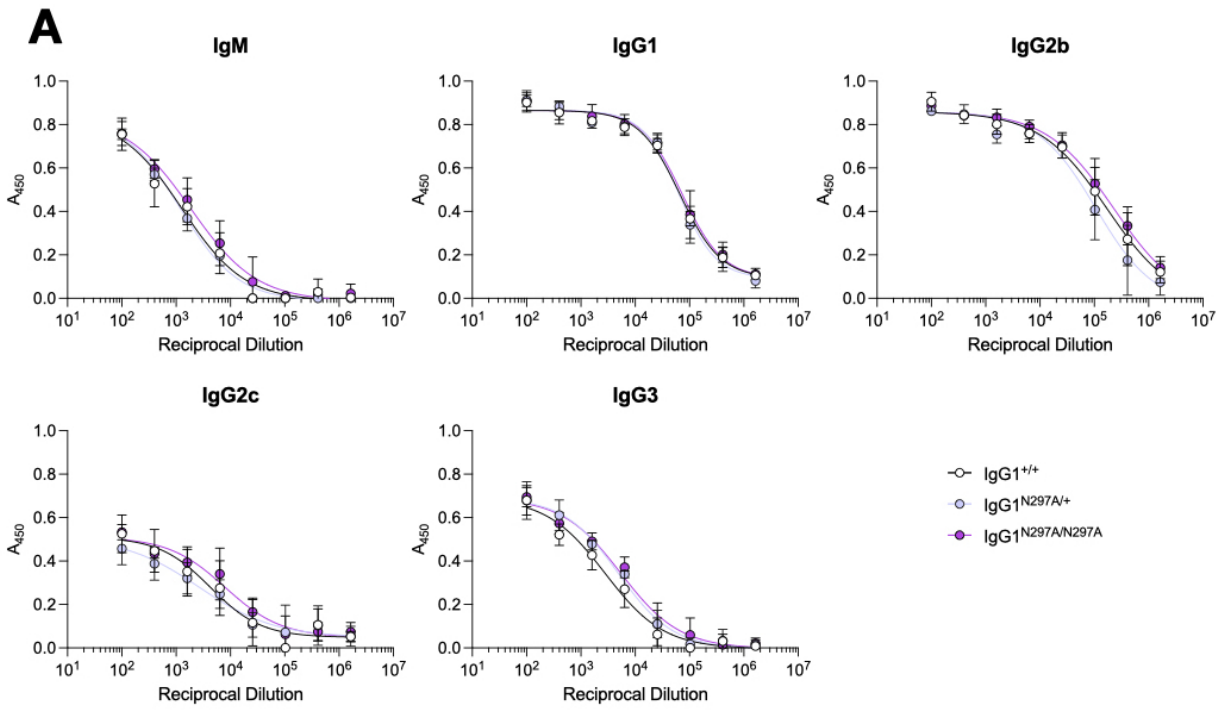

Figure 3.2 | **Baseline Ig titers in IgG1$^{+/+}$, IgG1$^{N297A/+}$, and IgG1$^{N297A/N297A}$ littermates..** (A) Enzyme-linked immunosorbent assay (ELISA) of diluted serum using anti- or light chain F(ab')2 for capture, and subclass-specific anti-IgG-HRP for detection. Data displayed as mean ± SEM. Data was fitted by nonlinear regression analysis.

ever, while IgG1^{+}B cells typically dominate the GC in response to Th2 skewed adjuvants, IgG1$^{N297A/N297A}$ B cells participated to a significantly smaller degree than IgG1$^{+/+}$ B cells (Fig 3.3B and E). GC B cells pass through multiple iterations of selection and hypermutation, and are positively selected in part due their ability to bind antigen, present it to T follicular helper cells, and subsequently proliferate[90,152]. Lower participation in the GC may be due to a defect in any of these processes. This was evident in the antigen-specific compartment of IgG1^{+}GC B cells, where IgG1$^{N297A/N297A}$ cells were less capable of binding fluorescently-labeled NP, reflecting lower rates of affinity maturation toward the target antigen (Fig. 3.3C and F).

These B cell intrinsic defects in germinal center responses may be caused by several

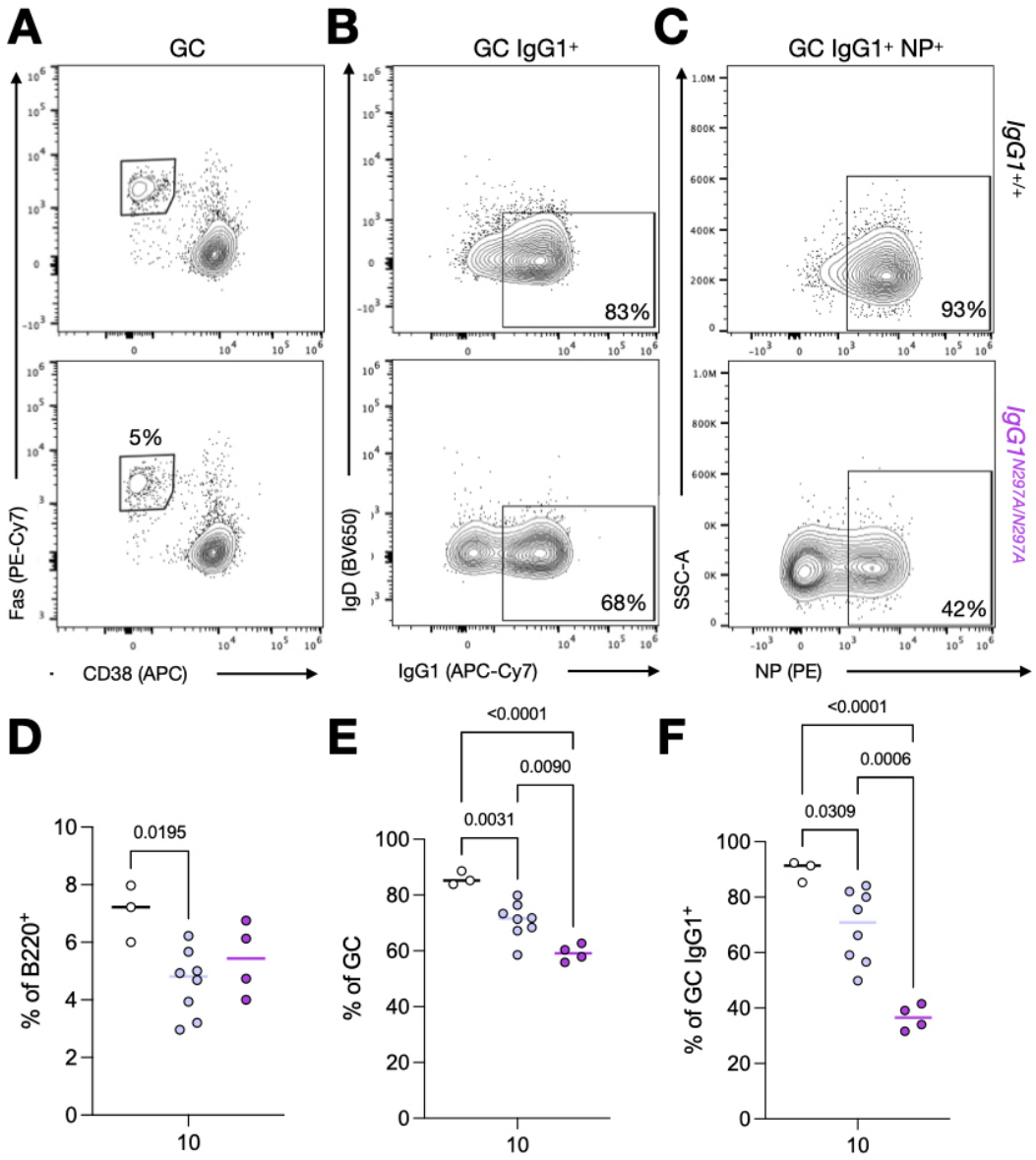

Figure 3.3 | **Diminished germinal center responses to NP-OVA immunization in IgG1^{N297A}germinal center B cells..** (A-C) Flow cytometry staining of live GC B cells ($B220^+CD38^-Fas^+$) (A), GC $IgG1^+$B cells (B), and GC $IgG1^+NP^+$ B cells (C) in the popliteal lymph nodes (pLN) of indicated mice following s.c. immunization of the footpad with 10 μg NP-OVA. (D-F) Quantification of populations defined in A-C across all three genotypes. P values from one-way ANOVA test indicated. Bars indicate median, while each circle represents a mouse (n = 3-8). Mice were 8-10 weeks old and derived from two litters.

factors which determine the affinity and avidity of BCR or proliferation and survival of B cells. This includes low rates of hypermutation or cyclic reentry, inadequate receptor clustering on the B cell surface, and dampened BCR signaling, among many others. To pinpoint the potential cause of diminished IgG1^{N297A}GC B cell responses, I performed ex vivo BCR signaling assays with primary cells derived from mice of glycosylated and aglycosylated genotypes. In both groups, CD43-depleted splenocytes, the vast majority of which are naïve resting B cells, readily class-switched to IgG1 in the presence of lipopolysaccharide (LPS) and interleukin-4 (IL-4) supplied in the growth media (data not shown). Signaling capacity was assessed by crosslinking the IgG1 BCR with anti-IgG1 F(ab')$_2$ at increasing concentrations and by measuring the extent of phosphorylation of downstream molecules by phosphoflow[153]. Such molecules include kinases and signaling adaptors, such as the intracellular BCR signaling component, CD79α, whose phosphorylation serves as a proximal event in BCR signaling. These *ex vivo* studies indicate that upon stimulation, IgG1$^{N297A/N297A}$ B cells are deficient in BCR signaling even at high concentrations of stimulus when wildtype cells achieve saturating levels of detectable phospho-CD79α (Fig. 3.4A-B). Notably, the glycan does not appear to play a role in BCR surface expression, as IgG1 levels measured by flow cytometry across the three genotypes are equivalent, excluding this variable as a reason for signaling differences (Fig. 3.4C). One explanation is that BCR clustering, which occurs following antigen binding and helps to amplify the downstream signaling cascade, is dependent on the Fc glycan. This is congruent with previous data that Fut8$^{-/-}$ IgG2a B cells, whose BCRs exist as monomers at rest, show defects in oligomerization after antigen stimulation[151]. Finally, the BCR is thought to tonically signal, providing a basal survival signal for B cells. This signaling requirement is shown by rapid cell death caused by *in vivo* targeted deletion of surface IgG[154]. At least in the *ex vivo* setting, tonic signaling was equal, shown by equal rates of activation without stimulus.

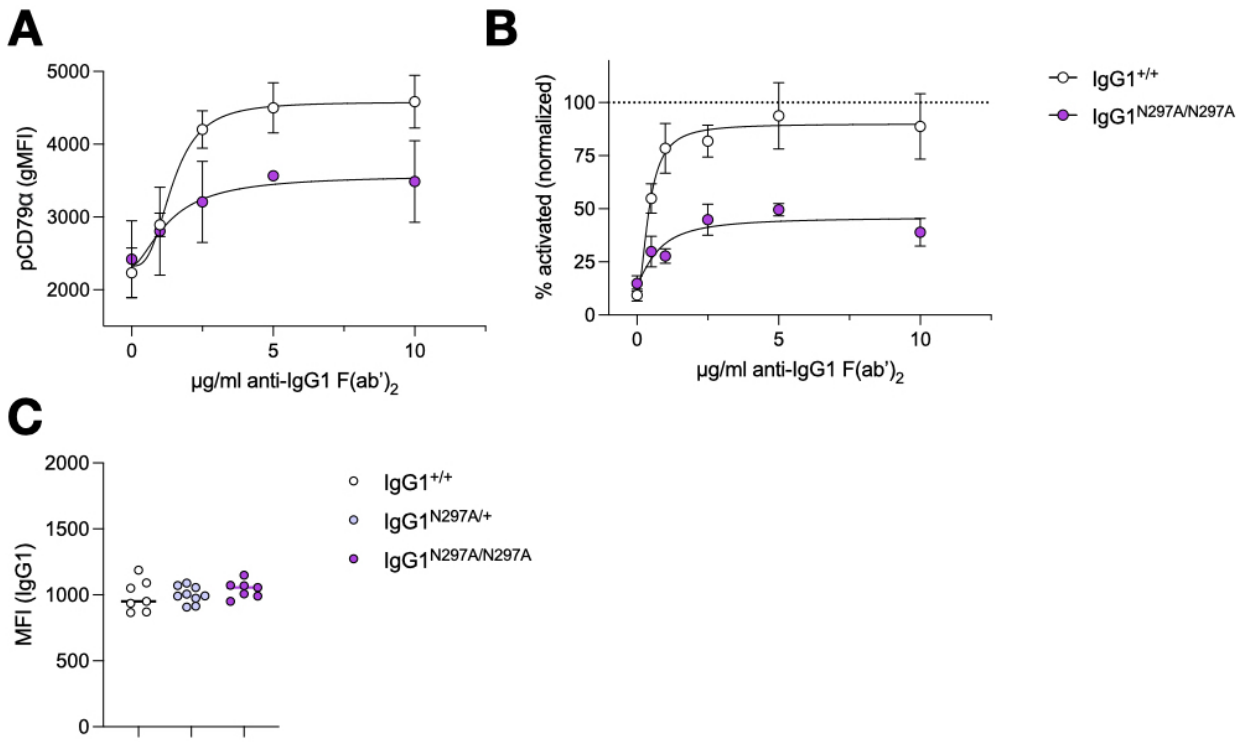

Figure 3.4 | **Stimulation of *in vitro* class-switched B cells by BCR crosslinking..** (A) pCD79α levels measured by intracellular phosphoflow of IgG$^{+/+}$ or IgG1$^{N297A/N297A}$ -derived splenic B cells. Concentration of crosslinking F(ab')$_2$ shown on the x-axis and geometric median fluorescence (gMFI) shown on the y-axis. Higher gMFI correlates with stronger BCR signaling. (B) Data in A shown alternatively as percent activation, using the pCD79α-positive population as a surrogate for the activated state. Values normalized to maximum pCD79α-positive percentage and to account to viability differences between cell populations. (C) gMFI of IgG1 on class switched B cells, eliminating receptor density as a contributing variable to signaling differences.

These preliminary studies show clear intrinsic deficiencies in IgG1^{N297A}B cells in terms of participation in GC responses, antigen binding in the GC, and BCR signaling. As shown, the phenotype is not absolute; B cells bearing aglycosylated IgG1 BCRs are viable, capable of limited signaling, affinity mature toward immunogens, and most importantly, differentiate into antibody-secreting plasmablasts, though at lower frequencies than wildtype cells (Fig. 3.5A). Despite these deficiencies, low and high affinity anti-NP IgG1 serum titers are equivalent following immunization with NP-OVA, regardless of the Ighg1 Asn 297 allele (Fig. 3.5B-C). This discrepancy between a defective IgG1 GC

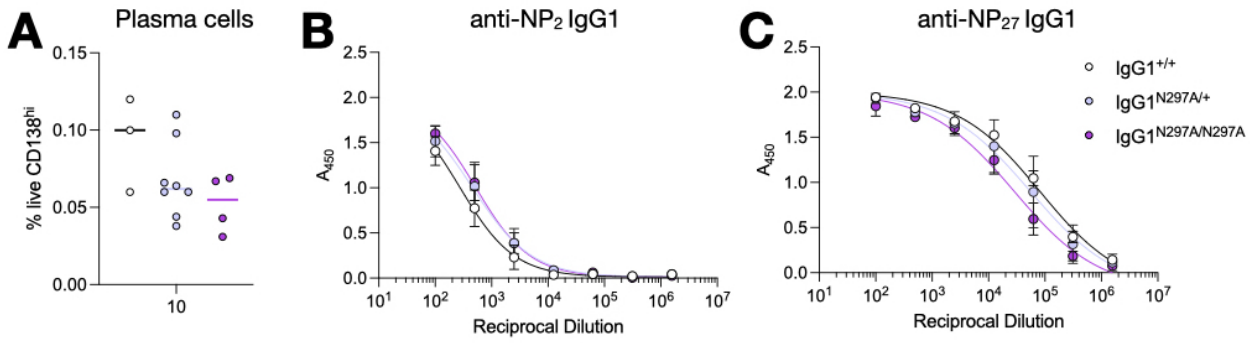

Figure 3.5 | **Comparison of antibody-secreting cells and serum IgG1 titers..** (A) Plasma cell (live CD138^{hi}) percentages in the pLN on Day 10 following s.c. immunization of the hind footpad in IgG1$^{+/+}$, IgG1$^{N297A/+}$, and IgG1$^{N297A/N297A}$ mice. (B-C) ELISA of high affinity (B) and low affinity (C) anti-NP IgG1 serum antibodies using low density (NP_2) and high density (NP_{27}) coupled NP-BSA for capture and anti-IgG1-HRP for detection.

response and serum IgG1 titers is puzzling and requires further study.

3.2.3 Additional genetic and biochemical tools to study aglycosylated responses

Investigation of the Fc glycan's role in the development of antibody responses will require further study using the IgG1^{N297A}mouse model. These studies are ongoing and will be covered in the following chapter. However, it is worth discussing additional tools I have developed to answer related questions.

One such tool is a nanobody specific for aglycosylated mouse IgG1. In heterozygote mice, this reagent is useful for tracking aglycosylated IgG1 B cells among the total IgG1^{+}population. These nanobodies were engineered similarly to those described in Chapter 2, though the bait proteins are different, and clones did not require affinity maturation (Fig. 3.6).

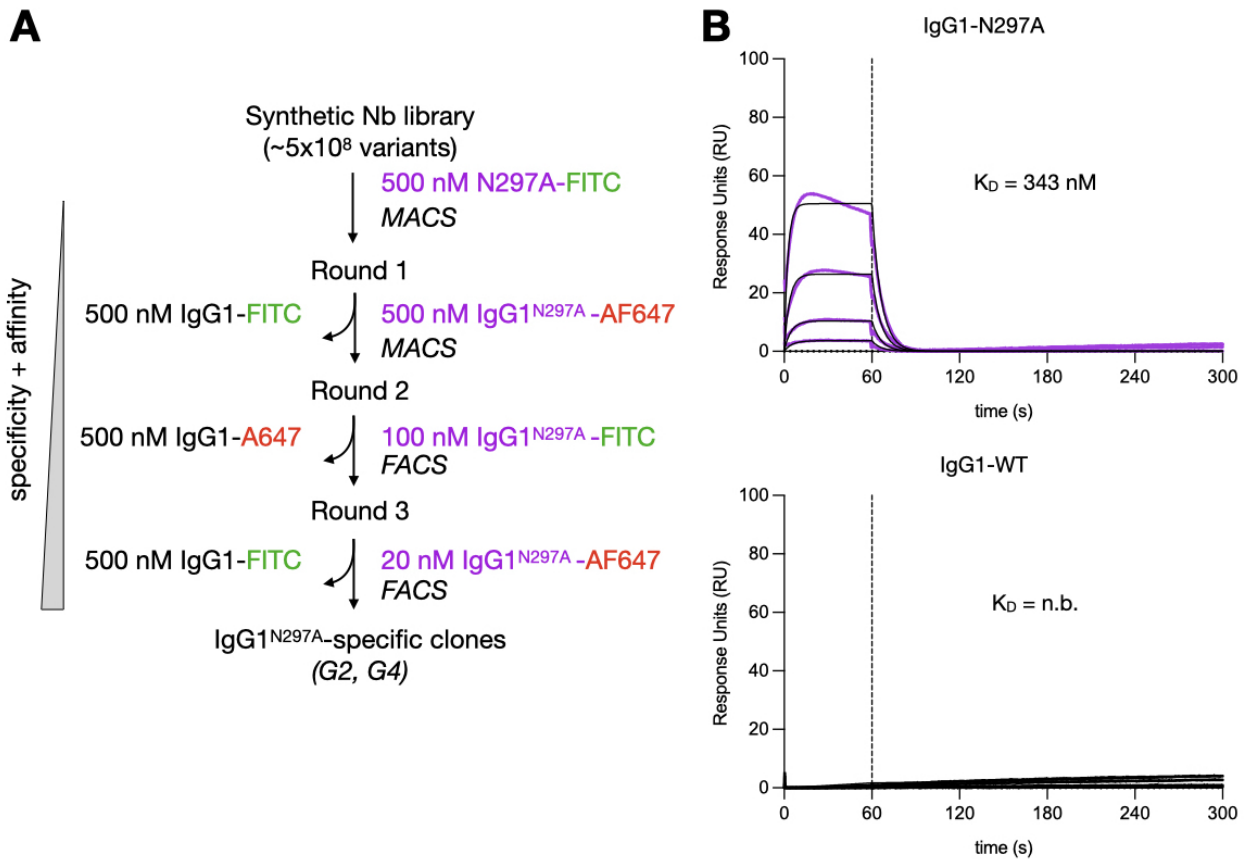

Figure 3.6 | **Discovery of a mIgG1^{N297A}-specific nanobody to track aglycosylated IgG.** (A) Selection and screening strategy to discovery nanobody variants with high specificity for mIgG1^{N297A}via four rounds of magnetic selection (MACS) or fluorescence-activated cell sorting (FACS). Each round of selection increases the requirements for both the affinity and specificity of selected clones by holding mIgG1 concentration constant while incrementally decreasing mIgG1^{N297A}concentration. Fluorophores are swapped each round. (B) Surface plasmon resonance data showing binding kinetics of clone G2 with mIgG1 and its aglycosylated counterpart, mIgG1^{N297A}. Purple traces are raw data, while global kinetic fits are shown in black. Sample concentrations begin at 256 nM with 2-fold serial titration until 64 nM.

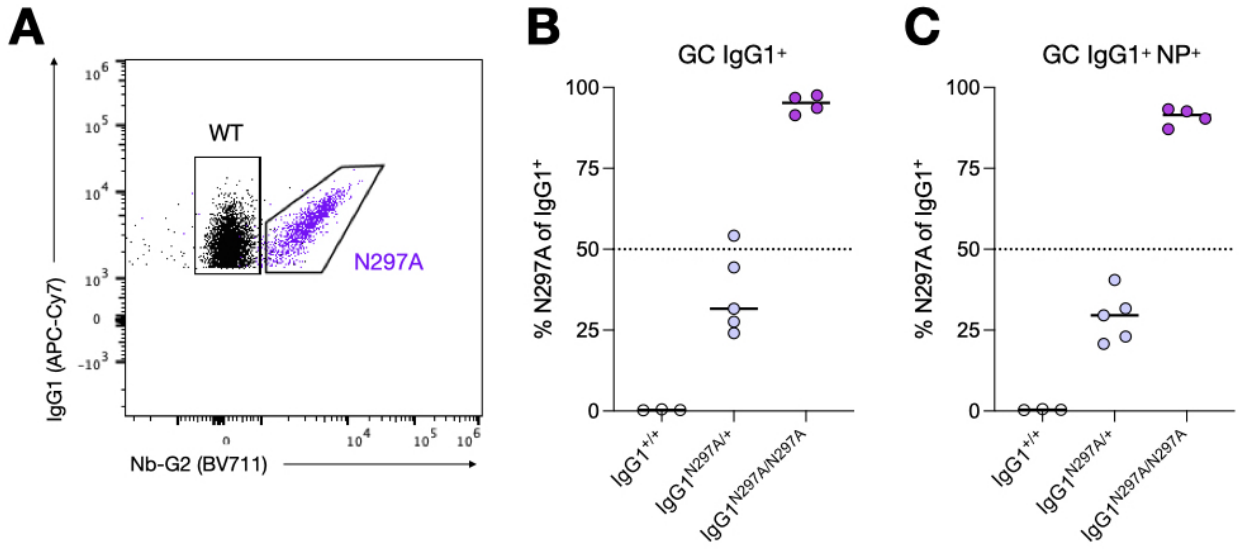

Figure 3.7 | **mIgG1^{N297A} tetramers distinguish glycosylated from aglycosylated surface IgG1 on primary B cells.** (A) Staining with biotin-streptavidin G2 tetramers separates IgG1$^{+/+}$ (black) and IgG1$^{N297A/N297A}$ (purple) B cells. (B-C) Total (B) and NP-specific (C) B cells plotted according to percentage gated as N297A. Bars represent the median, while each dot is a mouse. Horizontal dashed line at 50% for reference.

Fluorescently tagged biotin-streptavidin G2 tetramers can distinguish glycosylated from aglycosylated surface IgG1 on primary B cells by flow cytometry. Co-staining with anti-IgG1 and clone G2 is characteristically linear for aglycosylated IgG1 B cells (Fig. 3.7A). Using this method, analysis of GCs in IgG1$^{N297A/+}$mice immunized with NP-OVA allows for separation of the two alleles. This is made possible in part because B cells typically express only one heavy chain allele typically due to V(D)J recombination of the other allele that leads to a non-functional BCR[155]. Consistent with the phenotype shown in Fig. X, GC B cells from IgG1$^{N297A/+}$mice were skewed toward the wildtype allele, once again reflecting a defect in total and antigen-specific IgG1^{N297A}GC responses (Fig. 3.7B-C). I expect this nanobody reagent will be useful in further studies to track aglycosylated IgG1^{+}B cells in time and space.

Finally, in response to concerns about potential *trans*Fc-FcγR interactions, specifically those between circulating IgG immune complexes and FcγRIIb on B cells that may con-

tribute to B cell signaling, I generated a mouse model completely null for endogenous Fc-FcγR binding. This mouse contains the same IgG1^{N297A}mutation detailed above, but is also knocked out for IgG2b and IgG2c expression (Fig. 3.8A-B). Therefore, all endogenous antibodies are either aglycosylated IgG1 or IgG3, both of which cannot bind FcγRs. Because the IgG1, IgG2b, and IgG2c loci are nearby and are therefore linked, all three genomic edits needed to be on the same chromosome, requiring high editing efficiency. Microinjection of oocytes yielded a single founder pup (1/32), that when backcrossed to wild-type C57BL/6 mice, exhibited linked segregation of all three alleles. In homozygotes, total knockout of IgG2b and IgG2c was confirmed by ELISA (Fig. 3.8C). This colony is currently expanding and will be used to understand developing antibody responses in the complete absence of Fc-FcγR interactions.

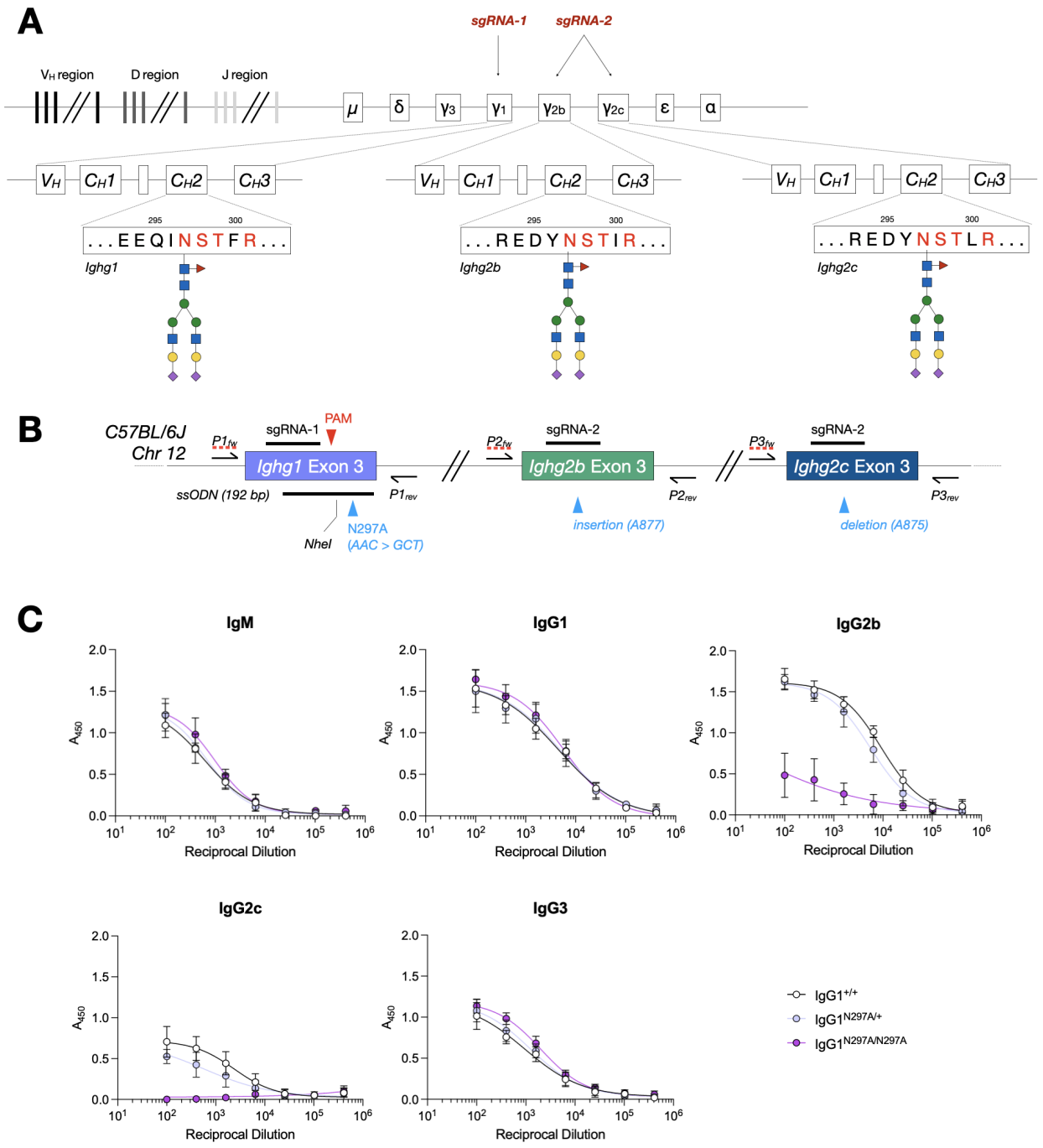

Figure 3.8 | **Design of a mIgG1^{N297A}; IgG2b$^{-/-}$; IgG2c$^{-/-}$ mouse.** (A-B) Schematic of the triple-edited mouse IgH locus, where IgG1, IgG2b, and IgG2c are linked. sgRNA-1 and ssODN targets and repairs IgG1, respectively, while sgRNA-2 targets a conserved site between IgG2b and IgG2c. Sequencing revealed single indels around the expected cleavage site, frameshifting the heavy chain. (B) ELISA of diluted serum using anti-κ or λ light chain F(ab')$_2$ for capture, and subclass-specific anti-IgG-HRP for detection. Data displayed as mean ± SEM. Data was fitted by nonlinear regression analysis.

3.3 An unexpected turn: a novel mouse strain optimized for chronic antibody administration

As another attempt to better understand the role of the IgG Fc glycan in the development of antibody responses, I also generated a mouse model of human IgG and FcγR expression. This mouse was originally meant to study endogenous human aglycosylated antibodies. Unfortunately, frequencies of human IgG1$^+$B cells were too low, and it was not a suitable model. However, the project transformed to take on a new role as a murine system of human antibody tolerance. The results are discussed below.

in vivo assessment of the therapeutic and adverse effects of human antibodies in mouse model systems has long been confounded by intolerance for these agents. Administration of human immunoglobulins to mice inevitably results in mouse anti-human IgG responses, likely due to foreign epitopes present in human IgG proteins. Previous studies have shown that these responses develop within days to weeks of IgG administration and serve to enhance clearance of human IgG[156,157], interfere with antigen binding and effector function, and diminish therapeutic activity[158], while also potentially contributing pathological sequalae of immune complex deposition[159]. For this reason, murine studies of human antibody treatment in our laboratory and others have been limited to the short-term (approximately two weeks) to ensure that anti-human IgG responses are not confounding meaningful results that may apply to patients[160,161,162].

Prior studies have only partially characterized this response and have reported inconsistent results. For instance, some studies argue that the route of immunization (i.e. intravenous vs. intraperitoneal vs. intradermal) may play a role in eliciting an anti-human response[158], though the results are inconsistent. It also has been suggested that IgG1 is the dominant mouse subclass that responds to exogenous human IgG, though there are

substantial mouse IgG2b and IgG2c anti-IgG titers that contribute as well[159]. Further, one study indicated that in order for a mouse anti-human IgG response to develop, the cognate antigen of the administered human antibody must be present in the mouse model[156], implying that immune complexes, not monomeric antibodies, initiate these responses. Finally, the kinetics of this response are unclear; some studies suggest it requires up to nine weeks for a significant anti-human response to develop[163], while others count less than one week. Despite these characterizations, no study to date has provided a robust solution to this intolerance, which continues to limit the extent of in-depth studies of antibody efficacy and safety.

In this study, we present a novel mouse model that is appropriate for the study of long-term, repeated administration of human antibodies. Tolerance to human IgG is conferred by germline knock-in of the human IgG1 heavy chain (IGHG1) in place of mouse Ighg2c. In addition, this knock-in has been combined with a previously described model of human FcγR expression and function[133], so that the relevant effector functions of these exogenous human antibodies can be investigated. In the knock-in mouse, human IgG1 pairs appropriately with mouse light chains, is expressed on the surface of B cells, and is elicited by immunization to both thymic dependent and independent antigens. Knock-in mice are tolerant of repeated administration of human IgG through multiple routes of immunization, and therefore allow for the *in vivo* characterization of antibody-mediated responses in the long term.

3.3.1 Knock-in of hIgG1 into the mouse Ig heavy chain locus.

Human IgG1 (hIgG1) was knocked-in by precise replacement of the native mouse Ighg2c coding sequence with human IGHG1 via CRISPR/Cas9 gene editing of C57BL/6J em-

bryonic stem (ES) cells. In addition to this sequence, a FRT-loxP-neomycin cassette was appended to the 3′ end of the targeting cassette to select properly edited ES cells, as well as 5′ and 3′ homology arms flanking the insert to assist with homology-directed repair (HDR) (Fig. 3.9A). This strategy preserved upstream and downstream switch and regulatory regions, with the intent that hIgG1 would mimic the expression profile of mouse IgG2c, and that other mouse subclasses were undisturbed. Mouse IgG2c was specifically targeted since it most closely approximates the FcγR-binding profile of hIgG1. Mice positive for the knock-in allele were screened using a common forward primer and reverse primers specific for either mIgG2c or hIgG1 (Fig. 3.9B). Serum analysis of heterozygotes (hIgG1/+) and homozygotes (hIgG1/hIgG1) demonstrates pairing of hIgG1 heavy chain with mouse kappa and lambda light chains and successful replacement of the mIgG2c heavy chain (Fig. 3.9C). As expected, the knock-in has normal endogenous mouse IgG levels as compared to C57BL6/J mice. Flow cytometry analysis of B-lineage cells in the spleen shows the knock-in preserves normal B cell development (data not shown). Indeed, analysis of B220+ splenic B cells from knock-in mice shows robust surface expression of hIgG1, indicating pairing of membrane-bound hIgG1 with B-cell receptor (BCR) components is intact. These mice develop normally, are fertile, and have no evidence of spontaneous pathology under the specific pathogen-free conditions maintained in the Rockefeller University animal facility.

3.3.2 hIgG1 knock-in mice mount normal humoral responses.

To determine whether knock-in mice mount hIgG1 responses to specific immunization, wild-type or heterozygote knock-in mice were immunized with the model haptenated antigen, 4-hydroxy-3-nitrophenylacetyl (NP). Thymic-independent (TI) responses were measured by a single immunization with NP-Ficoll adjuvanted with Complete Freund's

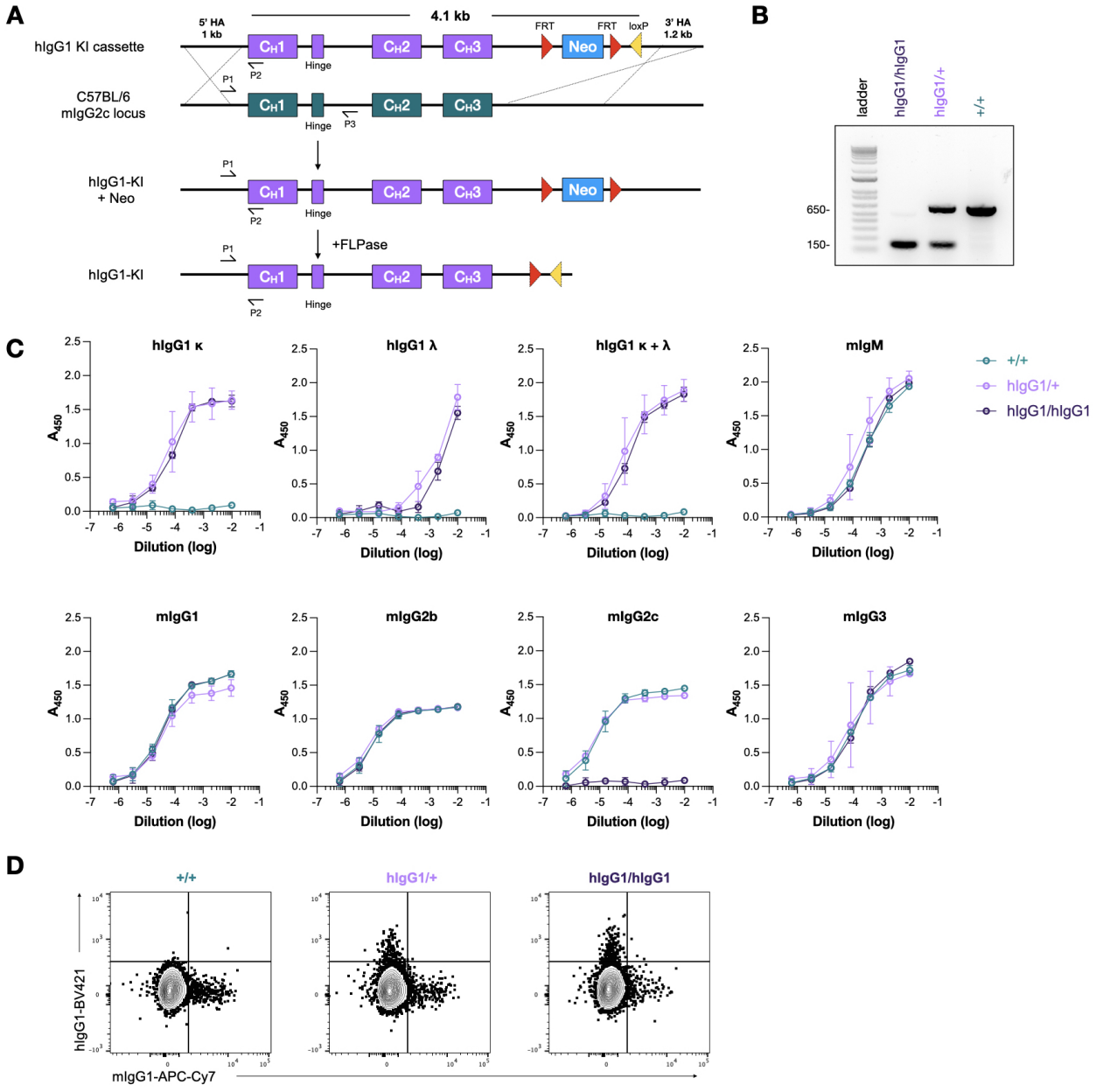

Figure 3.9 | **Generation and characterization of human IgG1 knock-in mouse..** (A) Targeting the mouse IgG2c heavy chain locus for replacement with a construct bearing the human IgG1 heavy chain and FRT-loxP-Neomycin cassette. Red triangles represent FRT sites and the yellow triangle represents a loxP site. (B) Representative (n=5 each strain) genotyping PCR of hIgG1/hIgG1, hIgG1/+, and +/+ mice. (C) Serum IgG titers in +/+, hIgG1/+, and hIgG1/hIgG1 mice on human FcγR background measured by ELISA. Anti-lambda and anti-kappa light chain antibodies were used for capture and HRP-conjugated isotype-specific antibodies for detection. Data displayed as mean ± SEM (n=3). (D) Representative (n=3) flow cytometry analysis of IgG surface expression on splenic B220+ cells.

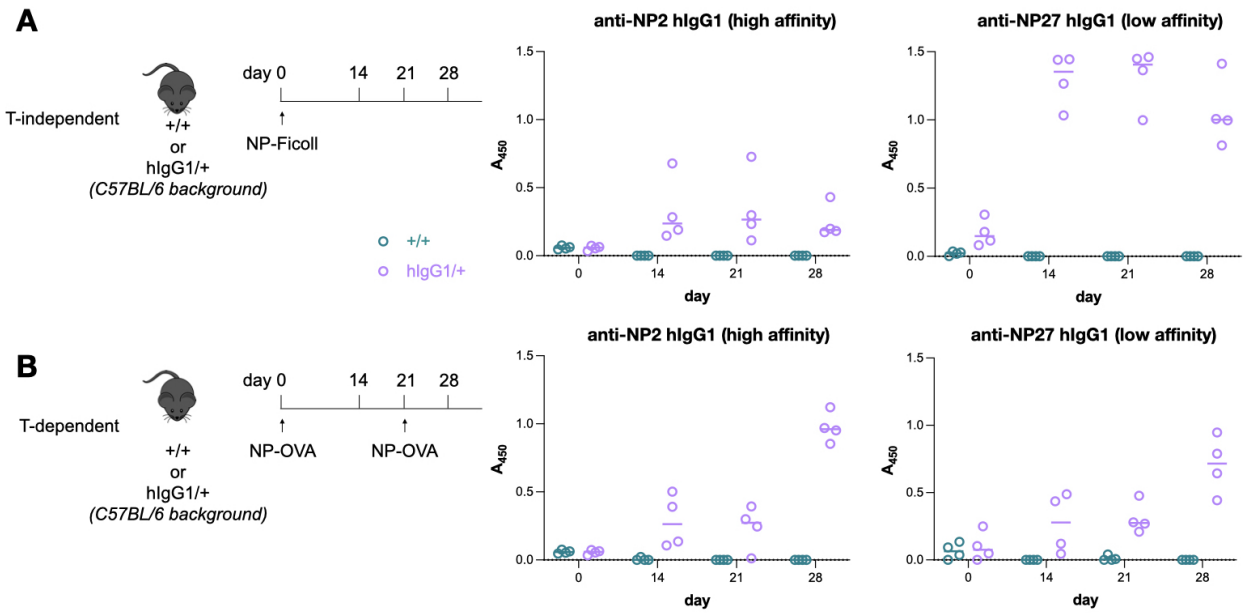

Figure 3.10 | **hIgG1 knock-in mouse has normal shows robust antigen-specific hIgG1 response to immunization.** (A) T-independent intraperitoneal immunization of mice with the indicated genotypes with 50 g NP54-Ficoll in alum. Serum was harvested at the indicated timepoints and analyzed for NP-specific IgG by ELISA. (B) T-dependent intraperitoneal immunization of mice with the indicated genotypes with 50 μg NP17-OVA in alum. Mice were subsequently boosted with 50 g NP17-OVA on Day 21. Serum was harvested at the indicated timepoints and analyzed for NP-specific IgG by ELISA. Data displayed as individual biological replicates with a line representing the mean (n=4 each strain).

Adjuvant (CFA). After two weeks, anti-NP hIgG1 titers were detected, and persisted until the end of the study at four weeks (Fig. 3.10A). Similarly, thymic-dependent (TD) immunization with NP-ovalbumin in a prime-boost dosing schedule two weeks apart induced a strong NP-specific hIgG1 response in the knock-in mice (Fig. 3.10B). The subclass composition of endogenous mouse IgG responses to NP were consistent with previous reports of T-independent and T-dependent immunization[164,165] (data not shown). These studies confirm that hIgG1 can participate in processes of affinity maturation and class switch recombination in response to immunization.

3.3.3 hIgG1 knock-in tolerizes mice to chronic human antibody administration.

Previous studies have demonstrated that repeated dosing of human antibodies induces a strong mouse anti-human response which leads to rapid clearance of human IgG and loss of activity[156,158,159,163]. We hypothesized that native expression of hIgG1 would endow knock-in mice with tolerance to exogenous hIgG1. To investigate the issue of antibody clearance, wild-type C57BL6/J or hIgG1 knock-in mice were dosed weekly with 100 g of the fully human HIV anti-gp120 monoclonal, 3BNC117-hIgG1[166] (Fig. 3.11A). After five cycles of treatment (day 35), knock-in mice were able to maintain high serum levels of 3BNC117, while controls rapidly cleared the antibody to levels at or below the limit of detection of the assay (Fig. 3.11B). We presumed the rapid clearance was due to a strong mouse anti-human IgG1 response that was absent in the knock-in mice, since clearance accelerated considerably after two to three weeks of administration. To test this hypothesis, we immunized knock-in and control mice weekly with 2B8-hIgG1, an anti-CD20 clone with human framework regions, but mouse complementarity-determining regions (CDRs) (Fig. 3.11C). Weekly intravenous administration of 2B8-hIgG1 resulted in mouse anti-human IgG1 titers detectable in control mice by week 3. By week 5, high titers were evident in control mice, while knock-ins had significantly lower levels of mouse anti-hIgG1 antibodies (Fig. 3.11D). Unexpectedly, similar experiments with other human subclasses of IgG routinely used in clinical studies (IgG2 and IgG4) demonstrated that the knock-in mouse is tolerant of 2B8-hIgG4 compared to controls, while 2B8-IgG2 was not strongly immunogenic in either mouse (data not shown). Tolerance to IgG4 may be due to its 90% sequence identity with human IgG1, versus 62% with mouse IgG1 heavy chain. Notably, none of the mice immunized with hIgG1 antibodies mounted a significant response to the constant region of the human kappa light chain, as shown by sandwich

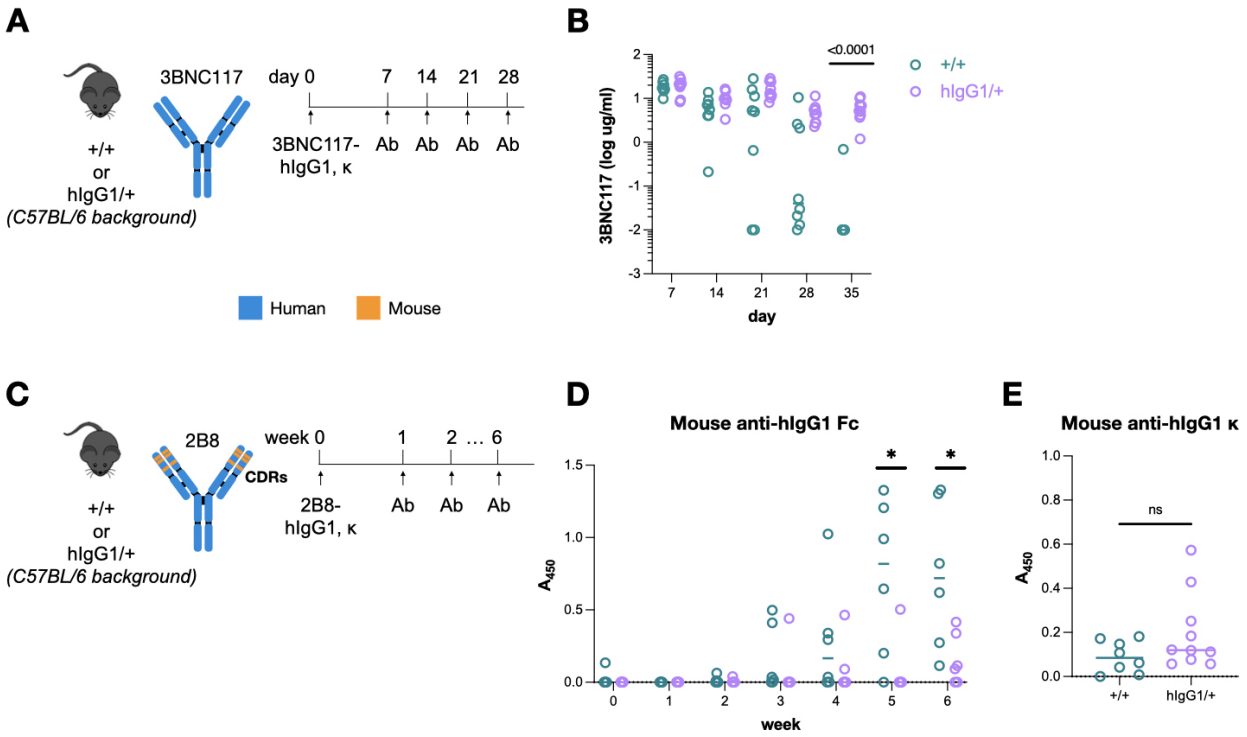

Figure 3.11 | **hIgG1 knock-in tolerizes mice to chronic human antibody administration.** (A and B) Mice of the indicated genotypes were repeatedly administered 100 g 3BNC117-hIgG1 i.p. on the days indicated. Serum levels of 3BNC117-hIgG1 were measured by ELISA using recombinant gp120 for capture and anti-hIgG-HRP for detection. Data shown as individual biological replicates with a horizontal line representing the mean (n=8 each strain). (C and D) Mice of the indicated genotypes were administered 100 g 2B8-hIgG1 i.p. each week for 6 weeks. Mouse anti-hIgG1 Fc titers were measured by ELISA using hIgG1 Fc for capture and anti-mouse IgG-HRP for detection. Data shown as individual biological replicates with a horizontal line representing the mean (n=6 each strain). (E) Mouse anti-human kappa constant region titers were measured by ELISA using an irrelevant mouse IgG1-human kappa chimeric antibody as capture and anti-human Fc-HRP for detection. Data shown as individual biological replicates with a horizontal line representing the mean (n=8-10 each strain).

ELISA using an irrelevant mouse IgG1-human kappa chimeric antibody as capture (Fig. 3.11E).

3.3.4 hIgG1 knock-in mice in a chronic model of immune thrombocytopenia purpura.

Exogenous human antibodies are often used to induce pathology in mouse models of autoimmune diseases, but their efficacy over time is limited by mouse anti-human responses to those antibodies[159]. One common model to induce immune thrombocytopenic purpura (ITP) in mice uses the anti-platelet IIb glycoprotein antibody, 6A6, which when administered intravenously, targets platelets for clearance by macrophages[167,168]. Because the mechanism of platelet clearance in this model relies on Fc-FcγR interactions, it was necessary to cross the hIgG1 knock-in mice to a mouse strain that is fully humanized for FcγRs. To approximate a chronic version of this ITP model[169], mice bearing the knock-in allele and human FcγRs were administered 6A6-hIgG1 for three consecutive days and then let recover for four days, over which time their platelets recovered to normal levels (Fig. 3.12A). Platelet counts were measured on each day. This treatment schedule was repeated twice, for a total of three cycles. In the first two cycles, differences in 6A6-hIgG1 platelet depletion between the two strains were insignificant. In the third cycle, only mice bearing the hIgG1 knock-in allele were able to deplete platelets efficiently (Fig. 3.12C). This difference was accompanied by high mouse anti-hIgG1 Fc titers in control mice, which presumably led to enhanced clearance of 6A6-hIgG1 and therefore interfered with its platelet depleting activity (Fig. 3.12B). This ITP model demonstrates the utility of a mouse that is tolerant of human antibody administration and can therefore recapitulate the pathology of an autoimmune disease in a chronic setting.

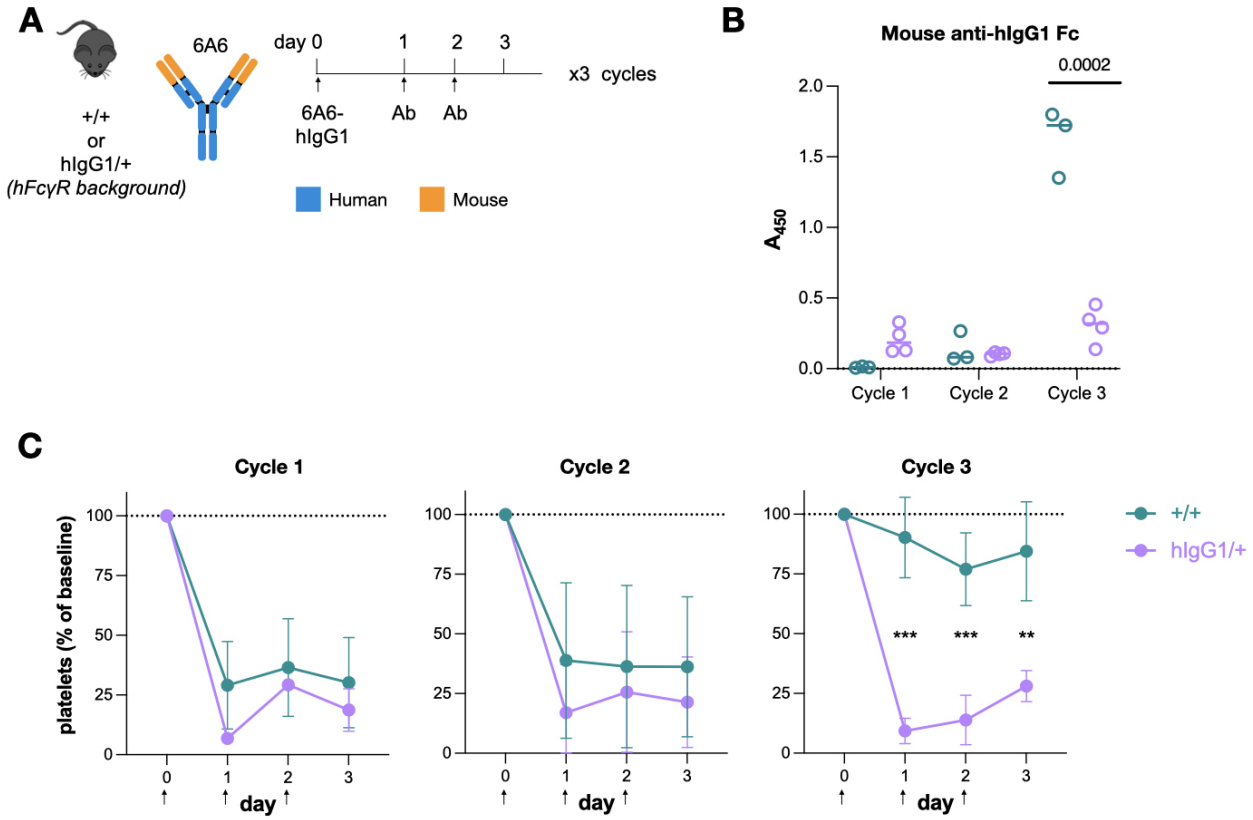

Figure 3.12 | **hIgG1 knock-in mice in a chronic model of immune thrombocytopenic purpura.** (A) Mice of the indicated genotypes were repeatedly administered 10 g 6A6-hIgG1 intravenously 3 times per week for 3 weeks. (B) Mouse anti-hIgG1 Fc titers were measured by ELISA using hIgG1 Fc for capture and anti-mouse IgG-HRP for detection. Data shown as individual biological replicates with a horizontal line representing the mean (n=3-4 each strain). (C) Platelet depletion during 3 cycles of 6A6-hIgG1 treatment. Platelet count is reported as a percentage of platelet count at the start of each cycle. Data displayed as mean ± SEM (n=3-4 each strain).

3.3.5 hIgG1 knock-in mice show improved clinical outcomes in B16-F10 melanoma chronic treatment model.

Human antibody treatment in mouse models of cancer is limited to the short-term by endogenous anti-human IgG responses that limit efficacy of these agents. This is evident from human antibody treatment schedules, which generally take place over a maximum of two weeks. To demonstrate that antibody treatment in the knock-in mouse does not

have such restrictions, we subjected the knock-in and control mice to a chronic treatment model of metastatic B16-F10 melanoma[170]. Mice from each group were pre-treated twice over three weeks with TA99, an antibody clone with mouse variable and human constant regions that targets gp75 on the surface of B16 cells and has been shown to effectively prevent lung metastases in an Fc-dependent manner[6] (Fig. 3.13A). Because TA99 requires strong activating FcγR engagement for efficacy, an Fc optimized variant (GAALIE) of IgG1 was used, which exhibits an improved binding profile to human activating FcγRs[162,171]. As expected, pre-treatment resulted in detectable mouse anti-hIgG1 Fc titers in control, but not in knock-in mice (Fig. 3.13B). Importantly, this study also demonstrates that expression of wild-type hIgG1 tolerizes these mice to an Fc-engineered variant that harbors three mutations in the Cγ2 region, showing the potential use of this model to quantify the immunogenicity of Fc variants. Following pre-treatment, mice were intravenously injected with B16-F10 cells and some groups were treated with four doses of TA99-hIgG1-GAALIE at the timepoints indicated. Two weeks after tumor inoculation, lungs were excised and analyzed for metastases. As expected, mice treated with PBS developed widespread metastases that gave their lungs a blackened appearance. Control mice that were intolerant of human IgG1 after two weeks were only partially treated by TA99-hIgG1-GAALIE, while the lungs of knock-in mice were free of significant metastases (Fig. 3.13C-D). Consistent with these results, TA99 could not be detected in the serum of control mice on Day 14, likely due to enhanced clearance by the formation of mouse anti-hIgG1 immune complexes, while levels persisted at therapeutic levels in most knock-in mice (Fig. 3.13E).

Based on these studies, this knock-in mouse model, which is free of interfering endogenous anti-hIgG1 responses, provides a useful platform to study human antibody efficacy and toxicity in disease models that require long-term treatment.

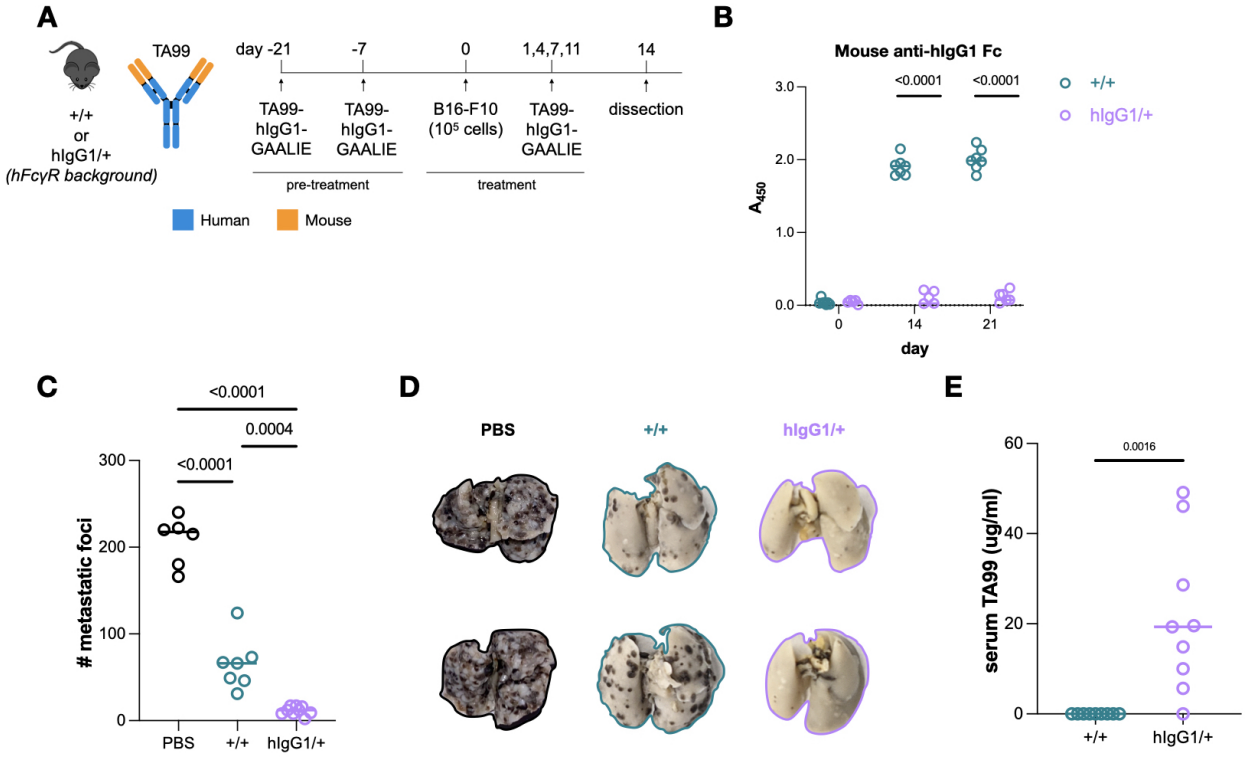

Figure 3.13 | **hIgG1 knock-in mice show improved clinical outcomes in a B16-F10 melanoma chronic treatment model.** (A) Pre-treatment and treatment schedule of mice subjected to the B16-F10 melanoma metastasis model. Mice were pre-treated with TA99-hIgG1 once per week for 3 weeks, inoculated intravenously with B16-F10 cells, and treated 4 times with TA99-hIgG1 at the indicated timepoints. Mice were sacrificed and their lungs excised on Day 14 for analysis. (B) Mouse anti-hIgG1 Fc titers were measured by ELISA using hIgG1 Fc for capture and anti-mouse IgG-HRP for detection. Data shown as individual biological replicates with a horizontal line representing the mean (n=6-9 each strain). (C and D) Lungs were harvested, fixed, and surface lung metastases counted. Data shown as individual biological replicates with a horizontal line representing the mean (n=6-9 each strain). (E) Serum was harvested on Day 14 and TA99-hIgG1 levels were measured by ELISA using recombinant gp75 for capture and anti-hIgG-HRP for detection. Quantification was performed by generating a standard curve with purified TA99-hIgG1. Data shown as individual biological replicates with a horizontal line representing the mean (n=6-9 each strain).

Chapter 4

PERSPECTIVES AND FUTURE DIRECTIONS

Immunoglobulin structural diversity has long captivated researchers around the world. In the mid-1970s, three groups described the crystal structure of the human IgG Fc fragment[172,173]. Despite the technological limitations of this era, these studies provided enormous insight into the overall architecture of the Fc. In one article, Palm and colleagues describe the rigidity of each individual domain, but also the paradoxical inability to resolve both Fab and Fc simultaneously, what we now consider a feature of IgG hinge flexibility. In another, Schwick and colleagues compare their Fc structure to Mickey Mouse, referring to the symmetrical Cγ2 domains as "ellipsoidal ears" protruding from the closely associated Cγ3 domain "head".

In all three primitive descriptions, the authors speculate on the position and composition of the carbohydrate at Asn 297, which is fixed in place and covers the face of the Cγ2 domain. Though Huber and colleagues guesses on Fc glycan composition and positioning were incorrect, they presciently "expect inhomogeneity of the carbohydrate in [their] material which might make the detailed analysis difficult". Such foreshadowing is the basis for the burgeoning field of IgG glycosylation and the stated goals of this thesis.

Here, I have examined novel methods to interrogate and manipulate the diverse IgG Fc glycan and genetic models to study its role in the development of antibody responses.

4.1 Methods to detect and manipulate IgG Fc glycoforms

Historically, antibodies and other glycan-binding reagents have been inadequate for targeting specific glycoproteins. While the field has relied on natural carbohydrate binding proteins like lectins, their recognition of targets is often non-specific. Previous attempts to generate glycan-binding antibodies have been confounded by heterogeneously glycosylated bait proteins for screening. Of course, purely analytical methods are often used to quantify Fc glycan structures, and we indeed employ such methods for validation here, though they are not applicable to standard laboratory techniques or more importantly, *in vivo* targeting of IgG.

In the studies presented here, we exploited the unique structural properties of nanobodies and chemoenzymatic glycoengineering to generate high affinity probes that specifically bind to afucosylated and sialylated IgG glycoforms with minimal cross-reactivity. To our knowledge, these probes are first-in-class molecules that selectively bind complex protein glycoforms of a specific glycoprotein. In characterizing these nanobodies, we demonstrate that their binding is dependent on both protein and glycan structure, and they neither bind aglycosylated protein nor free glycans. To account for a binding mechanism of afucosylated IgG-specific nanobodies, we solved two crystal structures: the apo-nanobody and the nanobody-Fc complex. We provide evidence of the unique recognition interface, whereby the extended and flexible CDR3 loop of the nanobody rotates to accommodate the Fc glycan. In addition to protein-protein contacts, a single residue at the apex of this loop forms hydrogen bonds with the proximal GlcNAc of the

glycan, which is likely obscured in fucosylated species and prevents binding. In experimental validation of the structures, we describe residue dependencies on both molecules by directed mutagenesis, partially confirming our hypotheses of the interactions. Further, we show that we can target specific IgG glycoforms both *in vitro* and *in vivo* to disrupt protein-protein interactions, highlighting the novel utility of these reagents beyond glycoform detection[68,73]. Blocking afucosylated IgG1-FcγRIIIA interactions in a mouse model of anti-dengue antibody-dependent enhancement reversed disease course, promoting survival and alleviating thrombocytopenia.

Due to their high affinity and selectivity, these nanobodies were readily adapted to a variety of standard biochemical assays to quantify IgG glycoforms in unpurified patient serum. They accurately reported levels of afucosylated IgG1 in serum from SARS-CoV-2 patients and in the case of dengue, acted as a prognostic to predict whether certain patients progressed to severe disease. While our assay was sufficient in disease contexts where broad global changes in glycan structure occur, other pathologic conditions with more subtle changes may require reagents with improved affinity or specificity. Additionally, it may be of interest to target other IgG glycan modifications such as galactosylation or bisecting GlcNAc decoration, as the importance of these structures has also been demonstrated in several disease contexts[174]. In particular, the sialylated IgG-specific nanobodies described in this study could be applied in the context of autoimmune or inflammatory conditions that have well-documented changes in IgG sialylation[175,176,177]. Certainly, the mode of sialylated-specific nanobody recognition remains an outstanding question which may shed light on these enigmatic, flexible structures.

Finally, while our studies largely focus on lab-based techniques, it may be reasonable to adapt this technology to low-cost clinical platforms that can be deployed at scale. These could prove useful in resource poor areas, where viral diseases such as dengue infection

are rampant and accurate prognostics could save lives.

4.2 Regulation of IgG Fc glycosylation

Despite burgeoning interest in Fc IgG glycosylation, little is known about its regulation. Various immunizations, infections, autoimmune diseases, and cancers elicit well-defined Fc glycan profiles in patients, but the mechanisms which determine these patterns are unclear. What is known are the main pathways of glycosylation – the cellular machinery responsible for protein and glycan synthesis that result in a diverse array of Fc glycoforms. For example, several studies have used varying expression of glycotransferases such as St6gal1 and Fut8 as evidence of dynamic glycan regulation[176,178]. I would contend that these glycotransferase transcripts are poor surrogates of enzymatic activity and that direct measurement of IgG glycoforms is more accurate. Studies that measure protein levels and dissect the regulatory pathways which control glycosylation machinery in relevant cell types will provide unparalleled insights into pathogenic and protective mechanisms, such as those in dengue virus infection.

Initial experiments should pinpoint the cell types responsible for modulating Fc glycosylation. Some groups have analyzed glycotransferase levels in B cells, but these are precursors of antibody-secreting cells, whose phenotypes may be more relevant for these studies. For example, IgG molecules in B cells are trafficked to the membrane, but it is unknown whether BCR glycoforms are regulated, serve a physiologic role, or match their secreted counterparts following differentiation. No studies to date have specifically interrogated BCR glycan structure. In the work presented here, we demonstrate that our nanobodies recognize afucosylated BCR in synthetic knockouts, opening the door for investigation of the complex genetics and cell types that may govern the nebulous processes

of glycosylation. However, in our hands, staining human peripheral and germinal center from primary patient samples has never revealed native afucosylated glycoforms in the BCR. They may not exist. To follow-up, we plan to analyze IgG glycoforms in plasmablasts and long-lived plasma cells from human peripheral blood and bone marrow using both extra- and intracellular staining. These experiments are novel in their approach and may define specific populations and contexts where the Fc glycan is modulated.

4.3 The IgG Fc's contribution to B cell responses

The idea that Fc structure can determine Fab sequence is a fascinating prospect to those interested in B cell biology. My thesis work focuses primarily on the structure of the Fc glycan, which although buried in the core of the IgG molecule, has major consequences for the integrity of the Fc domain. In Chapter 3, I detailed preliminary data from a mouse model of endogenously expressed aglycosylated IgG1 BCR and serum antibodies. Though baseline serum titers were agnostic to Fc glycosylation, IgG1^{N297A}B cells were less abundant in the germinal center following T-dependent immunization, less avid for the immunogen, and less responsive to BCR stimuli. My initial conclusions from these studies points to a potential defect in BCR clustering, which both impedes effective antigen binding and amplification of downstream BCR signaling. This is partially supported by a single study of *in vitro* signaling and BCR oligomerization in Fut8-/- IgG2a B cells, but warrants further investigation[151]. Regardless, removal the Fc glycan is a major structural disruption, which is already known to abrogate binding with known IgG receptors. Perhaps it also directly impacts signal transduction through IgG or pairing with signaling adaptors.

FcγRIIb, the sole inhibitory FcγR on B cells is a known regulator of B cell responses.

However, it is unclear in FcγRIIb-/- mice whether their high IgG titers are a result of absent tonic signaling or authentic immune complex engagement. One could imagine that because IgG exists in membrane and secreted forms, IgG-FcγRIIb interactions could occur in *cis*or trans. Thus, the N297A mutation should relieve IgG1^{+}B cells of inhibitory *cis*signaling and all B cells of *trans*signaling through aglycosylated immune complexes. To make the distinction between these two possibilities, I generated a mouse that can only express Fc null IgG. This should eliminate *trans*signaling through immune complexes, and when compared to IgG1^{N297A}mice, will show its contribution.

In this study, I also generated a IgG1N297A-specific nanobody to track aglycosylated IgG. Nanobody tetramers accurately distinguish IgG1^{N297A}B cells and were applied to immunization experiments. As before, they demonstrated impaired GC responses in B cells that class-switched to the N297A allele. As an interesting aside, some heterozygote mice did not perfectly exclude one allele or the other, indicating they have productive heavy change rearrangements on both alleles. This is demonstrated by the appearance of two intermediate phenotypes, one skewed towards the wildtype allele and the other skewed toward the N297A allele (Fig. 4.1). Because the V(D)J region of rearranged B cells is clonal, this finding implies that a given V(D)J can pair both intra- and intrachromosomally. This has been reported previously in mice at rates of 10-20%[179]. This reveals that although the Fab participates in allelic exclusion, the Fc does not, and may confound studies of heterozygote mice if these populations overlap, since B cell signaling will be driven by a heterogeneously glycosylated pool of BCRs.

Future experiments with these genetic mouse models and tools include: quantification of somatic hypermutation and affinity maturation by V(D)J sequencing, assessing differentiation into memory B cells and plasma cells, proliferative capacity by nucleoside analog pulsing, immunoprecipitation of membrane IgG to discover differential interact-

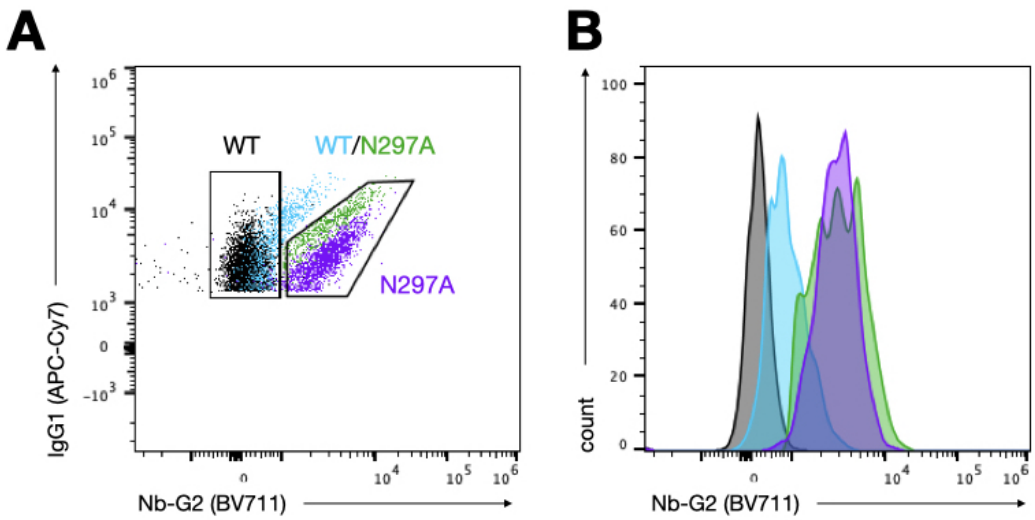

Figure 4.1 | **IgG1$^{N297A/+}$B cells participate in interallelic class-switch recombination.** (A) Staining with biotin-streptavidin G2 tetramers confidently separates IgG1$^{+/+}$ (black) and IgG1$^{N297A/N297A}$ (purple) B cells, but IgG1+/N297A B cells belong to two intermediate populations that are WT dominant (blue) or N297A dominant (green). Gates are drawn as in Fig. X. (B) Histogram of groups shown in A demonstrating overlap of these intermediate populations.

ing partners, super-resolution microscopy to visualize BCR clustering, and more.

4.4 Evaluating long term antibody treatment in preclinical models

We addressed the issue of chronic administration of human antibodies by developing a novel mouse model with tolerance for these agents. By combining this knock-in with our previously published human FcγR model, we have created a system to extensively assess the specific activity and effector function of human antibodies regardless of treatment length or disease chronicity. Importantly, the hIgG1 heavy chain correctly pairs with endogenous mouse kappa and lambda light chains, is adequately expressed in its mem-

brane form on the surface of B cells, and endows these mice with tolerance for exogenous human IgG. This newfound tolerance has major implications for the serum half-life of exogenous antibodies, their ability to opsonize target cells, proteins, or virions, and to perform essential effector functions via Fc-FcγR interactions. Fortunately, knock-in mice avoid the strong mouse anti-human IgG1 Fc response shown in this study to develop as early as two weeks after first treatment. Based on the kinetics of this response and the coinciding decline in hIgG1 activity in models of chronic ITP and metastatic melanoma, it is likely that mouse anti-hIgG1 antibodies directly interfere with antibody effector function. This may be especially true in the models tested, which rely extensively on Fc-FcγR interactions. To our surprise, the 106aa human kappa light chain constant region was not immunogenic to wild-type C57BL6/J mice, despite sharing only 60% sequence identity with its mouse homolog. Therefore, expression of hIgG1 Cγ1-3 appears sufficient to confer tolerance to human IgG1.

Although there are previous reports of hIgG1 knock-ins, tolerance of exogenous hIgG1 has never been characterized[180,181]. Further, though some of these models combine expression of ligand (human IgG) with the full recapitulation of structure and function of their cognate receptors (human FcγRs), they do so on mixed genetic backgrounds, thereby making the present model a unique platform to precisely study human antibodies in mice without confounding factors. This new model will best approximate disease contexts where long-term treatment with human IgG treatment is necessary, such as relapsing and remitting tumors, chronic autoimmune diseases, and chronic infections.

Although the current model presents considerable advantages over previous iterations in terms of human IgG tolerance, it is not well-suited to answer questions about the role of Fc-FcγR interactions in the development of human antibody responses. This is due to species differences in isotype expression, B-cell receptor components, regula-

tion of class-switch recombination, and a host of other genetic factors that govern these responses. In addition, although the knock-in mice express endogenous hIgG1, it is at levels lower than in humans, in which it is the dominant subclass. Here, hIgG1 is regulated similarly to mouse IgG2c, a less abundant subclass in mice. Further, in mice and humans, endogenous serum IgG competes for receptor occupancy of the neonatal Fc receptor (FcRn), thereby setting the bounds for the half-life of antibodies, so expression of the human FcRn would be required to accurately recapitulate half-life in humans. Other improvements to the model include human versions of the Type II FcRs CD23 and DC-SIGN.

In summary, we conclude that this novel mouse model is tolerant of human antibodies and will be a useful tool for researchers who wish to study human antibody treatment and pathology in the long term.

4.5 Final words

Nearly five decades after the Fc glycan first puzzled structural biologists, we now have a high-resolution view into its heterogeneous composition, functional characteristics, and overall impact on IgG function. Despite that, many questions remain unanswered. What determines its structure and how is it regulated? What host or pathogenic factors instruct B-lineage cells to produce certain Fc glycoforms? Are antibody-secreting cells imprinted and/or do they have a memory of the glycoforms they produce? Can this memory be recalled? Why do some antigens elicit certain Fc glycoform responses? Answers to these questions will take time and likely require high fidelity reagents and models that will help us understand how these processes occur in humans. In the future, they may help us design more effective vaccines and therapies that elicit desired antibody effector func-

tions.

Work on glycoform-specific nanobodies was particularly inspiring, because it proves our capability to engineer molecules with exquisite specificity that target highly variable motifs. I would hope that we can extend these findings to other important glycoproteins that will aid the development of more targeted diagnostics, therapeutics, and research tools.

Chapter 5

METHODS

5.1 Methods for 'Synthetic nanobodies as tools to distinguish IgG Fc glycoforms'

5.1.1 Expression and purification of IgG

Recombinant antibodies were generated using the Expi293 or Expi293 FUT8$^{-/-}$ system (ThermoFisher) using previously described protocols[171]. Briefly, an equal ratio of heavy and light chain plasmids was complexed with Expifectamine in OptiMEM and added to Expi293 cells in culture at 3 x 10^6 cells/ml. Enhancer 1 and Enhancer 2 were added 20 hours after transfection. After 6 days, recombinant IgG antibodies were purified from cell-free supernatants by affinity purification using protein G sepharose beads (GE Healthcare), dialyzed in PBS, filter-sterilized (0.22 μm), concentrated with 100 kDa MWCO spin concentrator (Millipore), purified with Superdex 200 Increase 10/300 GL

(GE Healthcare), and finally assessed by SDS–PAGE followed by SafeBlue staining (ThermoFisher). All antibody preparations were more than 95% pure and endotoxin levels were less than 0.05 EU mg^{-1}, as measured by the limulus amebocyte lysate assay. Purified IgG was fluorescently labeled with Alexa647-NHS or FITC-NHS (ThermoFisher) at a 15-fold molar excess for 1 hour at room temperature, and double-dialyzed into PBS.

5.1.2 Chemoenzymatic glycoengineering of IgG

LC-ESI-MS analysis of the Fc domains released by IdeS treatment of rituximab derivatives

LC-ESI-MS analysis was performed with Exactive Plus Orbitrap Mass Spectrometer (Thermo Scientific) equipped with an Agilent Poroshell 300SB C8 column (5 μm, 1.0×75 mm) with a gradient elution of 2535% aq MeCN containing 0.1% FA for 6 min, 0.4 mL/min. Mass spectra were deconvoluted using MagTran (ver 1.03 b2).

Preparation of (Fucα1,6)GlcNAc-rituximab with immobilized Endo-S2 WT.

Commercial rituximab (22.0 mg, 100 mg/mL, RefDrug Inc.) was incubated with immobilized (on agarose resin) wild-type Endo-S2 (200:1, wt/wt) at 37 °C with gentle shaking for 6 h, when LC-ESI-MS analyses indicated complete cleavage of the N-glycans on the Fc. The resin was centrifuged, and the deglycosylated antibody was purified by protein A chromatography, exchanged to Tris buffer (100 mM, pH 7.2) to yield (Fucα1,6)GlcNAc-rituximab (20.3 mg, 94%). ESI-MS: calcd for IdeS treated Fc of (Fucα1,6)GlcNAc-rituximab, M = 24,104 Da; found (m/z), 24,102 Da (deconvolution data).

Preparation of GlcNAc-rituximab with immobilized Endo-S2 WT and AlfC a-fucosidase in a one-pot manner.

To generate GlcNAc-rituximab, commercial rituximab (RefDrug Inc., 18.0 mg, 100 mg/mL) was incubated with immobilized wild-type Endo-S2 following the procedure above. After the Fc glycan was completely removed, α-fucosidase AlfC from Lactobacillus casei (50:1, wt/wt) was added to the mixture and incubated at 37 °C for 16 h, when LC-MS analyses indicated complete cleavage of the core fucose on the Fc. The resin was centrifuged down, and the antibody was isolated by purified by protein A chromatography, exchanged to Tris buffer (100 mM, pH 7.2) to yield GlcNAc-rituximab (15.2 mg, 86%). ESI-MS: calcd for IdeS treated Fc of GlcNAc-rituximab, M = 23,958 Da; found (m/z), 23,956 Da (deconvolution data).

Enzymatic Transglycosylation of (Fucα1,6)GlcNAc-rituximab or GlcNAc-rituximab to Generate rituximab Glycoforms.

A solution of (Fucα1,6)GlcNAc-rituximab (9.0 mg) or GlcNAc-rituximab (9.0 mg) in a Tris buffer (100 mM, pH 7.2, final antibody concentration 15 mg/mL) and G2-glycan oxazoline (30 eq) was incubated with Endo-S2 D184M mutant (0.05 mg/mL) at 30 °C for 15 min. LC-MS analyses indicated the complete transglycosylation. The mixture was purified by protein A chromatography, exchanged to PBS buffer (100 mM, pH 7.4) to yield G2F-rituximab (8.1 mg, 88%) or G2-rituximab (8.3 mg, 90%). ESI-MS: calcd for IdeS treated Fc of G2F-rituximab, M = 25,523 Da; found (m/z), 25,522 Da (deconvolution data); calcd for IdeS treated Fc of G2-rituximab, M = 25,377 Da; found (m/z), 25,376 Da (deconvolution data). The homogeneity of glycoengineered rituximab was further confirmed by fluorescence labeling of released N-glycans with 2-AA, compared to the heterogeneity of glycans for native rituximab. The identity of the 2-AA labeled released glycans were confirmed by MALDI-TOF-MS analysis.

2-AA glycan labeling and release.

For 2-AA glycan labeling, the Fc N-glycans were released from rituximab by PNGase F treatment and were subsequently labeled by reductive amination with a-aminobenzoic acid, following the manufacturer's protocol (Sigma-Aldrich GlycoProfileTM 2-AA Labeling Kit). Analytical RP-HPLC was performed on a Thermo ScientificTM VanquishTM UHPLC system equipped with a fluorescence detector F (excitation, 320 nm; emission, 420 nm). Separations were performed using a C18 column (Thermo Scientific AccucoreTM, 3 × 150 mm, 2.6 m) at a flow rate of 0.6 mL/min using a linear gradient of 0-15% MeCN containing 0.1% TFA over 30 min at 30°C. Fluorescent HPLC analysis and quantification indicated that the Fc N-glycans from commercial rituximab consisted of three forms, G2F, G1F, and G0F, which were present in the ratios of 9.3 : 47.7 : 43.0. The glycoengineered rituximab glycoforms G2F and G2 showed a single homogeneous N-glycan (G2F and G2 respectively), without detection of other N-glycans.

5.1.3 Identification of IgG Fc glycoform specific nanobodies

We used a previously published yeast surface display library (¿5x10^8 variants) that recapitulates the native llama VHH repertoire[126]. The library displays an HA-tagged nanobody at the terminus of a synthetic stalk sequence, whose expression is controlled by an inducible Gal promoter. In the presence of galactose, 12-18% of the naïve library typically expresses the nanobody protein.

For round 1, 5x10^9 yeast (10x expected diversity) were induced for 48 hours in YEP-galactose tryptophan dropout (-Trp) medium, and washed in staining buffer (20 mM HEPES, pH 7.5, 150 mM sodium chloride, 0.1% (w/v) bovine serum albumin). For negative selection, yeast were resuspended in 5 mL of staining buffer containing 500 nM rituximab-G2F-Alexa647. Yeast were incubated for 1 hour at 4°C, washed in cold staining

buffer, and resuspended in 4.5 mL of staining buffer with 500μLanti-Alexa647 microbeads (Miltenyi). Yeast were incubated with microbeads for 20 minutes at 4°C, washed in cold staining buffer, and depleted of G2F-binders on a MACS LS column (Miltenyi). For positive selection, yeast were resuspended in 5 mL staining buffer with 500 nM rituximab-G2-FITC or rituximab-S2G2F-FITC. Yeast were incubated for 1 hour at 4°C, washed in cold staining buffer, and resuspended in 4.5 mL of staining buffer with 500μLanti-FITC microbeads. Yeast were incubated with microbeads for 20 minutes at 4°C, washed in cold staining buffer, and G2- or S2G2F-binders were captured on a MACS LS column and recovered in YEP-glucose (-Trp) medium.

For round 2 of selection, 1.5x10^8 induced yeast, the procedure outlined in round 1 was performed with the fluorophores swapped (i.e. rituximab-G2F-FITC and rituximab-G2-Alexa647 or rituximab-S2G2F-Alexa647). For rounds 3-5, fluorescence-activated cell sorting (FACS) was used in place of MACS. For round 3, 1.5x10^7 induced yeast was stained with 500 nM rituximab-G2F-Alexa647 and 250 nM rituximab-G2-FITC or rituximab-S2G2F-FITC. FITC+Alexa647- clones were sorted into YEP-glucose (-Trp) and expanded. For round 4, 1.5x10^7 induced yeast was stained with 500 nM rituximab-G2F-FITC and 250 nM rituximab-G2-Alexa647 or 250 nM rituximab-S2G2F-Alexa647. FITC-Alexa647$^+$ clones were sorted into YEP-glucose (-Trp) and expanded. For round 5, 1.5x10^7 induced yeast was stained with 500 nM rituximab-G2F-Alexa647 and 100 nM rituximab-G2-FITC or 100 nM rituximab-S2G2F-FITC. FITC+Alexa647- clones were sorted into YEP-glucose (-Trp) and expanded.

8x10^6 yeast were spun down and resuspended in 30μL0.2% sodium dodecyl sulfate (v/v) and heated at 94°C for 4 minutes to lyse yeast. Yeast were spun down at 10000 x g and 1μL of supernatant was used as template for a PCR reaction using [primer3, primer4]. Next-generation sequencing of post-round 5 nanobody sequences was performed by a

MiSeq Nano (Illumina) with 10% PhiX to yield dominant clones (G2: C11 and D3) and (S2G2F: H9 and C5).

5.1.4 Expression and purification of nanobodies

Nanobodies were expressed and purified similarly to previously reported methods[126,130,182]. Nanobody sequences were amplified with [primer 5, primer 6] and cloned into pET26-b(+) expression vector with His tag and AviTag using Gibson Assembly (NEB), and transformed into BL21(DE3) *E. coli* (NEB). Nanobody multimers were generated using multi-part Gibson Assembly with unique linker regions to preserve correct orientation. Bacteria were grown in terrific broth at 37°C overnight, and the next day a 1:100 culture was grown until an OD of 0.7-0.9, when 1 mM IPTG was added. After 20-24 hours of shaking at 25°C, *E. coli* were pelleted and resuspended in SET buffer (200 mM Tris, pH 8.0, 500 mM sucrose, 0.5 mM EDTA, 1X cOmplete protease inhibitor (Sigma)) and rocked for 30 minutes at room temperature, followed by the addition of 2x volume of deionized water and 45 minutes more rocking. NaCl was added to 150 mM, MgCl2 to 2 mM, and imidazole to 20 mM before pelleting cell debris at 17,000 x g for 20 minutes. The periplasmic fraction was filtered with a 0.22 um filter and incubated with 4 mL 50% Ni-NTA resin equilibrated in wash buffer (20 mM HEPES, pH 7.5, 150 mM NaCl, 40 mM imidazole) (Qiagen) per liter of initial bacterial culture. Supernatant and resin was rocked for 1 hour at room temperature, and then pelleted at 50 x g for 1 minute. Resin was washed on column with 10 volumes of wash buffer before elution with elution buffer (20 mM HEPES, pH 7.5, 150 mM NaCl, 250 mM imidazole). Eluted protein was concentrated with 3 kDa MWCO filters (Amicon) before size-exclusion chromatography (GE Healthcare). Proteins were stable at 4°C.

For tetramerization, nanobody monomers were biotinylated *in vitro* with BirA (Avidity) for 1 hour at room temperature according to manufacturer's directions, double desalted using Zeba Spin Desalting columns 7K MWCO (ThermoFisher), and purified by size-exclusion chromatography. For *in vivo* biotinylation, CVB-T7 POL *E. coli* (Avidity) were used to express nanobodies, and at the time of induction, 50 μM of D-biotin was added to the culture. Streptavidin conjugates were complexed in a 1:4 ratio with biotinylated monomers by adding 1/4th volume of conjugate every 10 minutes for a total of 40 minutes.

For nanobody-Fc fusions, nanobody sequences were directly fused to human IgG1 Fc residues 216-447. Importantly, Asn 297 was mutated to alanine to prevent nanobody binding. These constructs were expressed and purified in the same manner as antibodies (see 'Expression and purification of IgG').

5.1.5 Surface Plasmon Resonance (SPR)

SPR was performed on a Biacore T200 machine (Cytiva Life Sciences). In some experiments, purified IgG glycoforms diluted in HBS-EP+ were immobilized on the surface of a Protein A or Protein G CM5 sensor chip at 1000 RU (50 nM). Purified nanobodies were flowed over IgG-bound sensor chips at the indicated concentrations at 30 μL/minute for 60 seconds, followed by 600 seconds of dissociation. Sensor chips were regenerated with 10 mM Glycine-HCl pH 1.5.

In other experiments, purified His-tagged nanobodies were immobilized on the Ni^{2+}-activated surface of NTA sensor chips at 500 RU (50 nM). Purified IgG was flowed over nanobody-bound sensor chips at the indicated concentrations at 30 μL/minute for 60 seconds, followed by 600 seconds of dissociation. Sensor chips were regenerated with 350

mM EDTA.

All kinetic constants were calculated using GraphPad Prism v9. For nanobody monomer binding, sensorgrams were fit using a 1:1 Langmuir binding model and kinetic constants reported. For tetramer binding, the association phase was fit separately using an association kinetics model simultaneously fitting the association rate constant for each concentration. The dissociation phase was fit to a biexponential decay model with two dissociation rate constants (one fast, one slow) shared between each concentration.

For epitope mapping experiments, rituximab G2 diluted in HBS-EP+ was immobilized on the surface of a Protein A or Protein G CM5 sensor chip at 1000 RU (50 nM). Purified B7 or FcγRIIIA was injected at 10s at 30 μL/minute for 100 seconds to achieve saturation. Immediately after, a mixture of purified B7 and FcγRIIIA at the same concentration as in the primary injection was injected at 30 μL/minute for 100 seconds, followed by dissociation.

5.1.6 Affinity maturation of C11

Using degenerate NNK oligos, assembly PCR was used to generate a site saturation mutagenesis library of C11, where one codon in each CDR was mutated at a time, for a total of 0-3 amino acid CDR mutations per nanobody clone. The pooled assembly PCR reaction was amplified so that its ends overlapped with the surface display vector used in the initial rounds of selection. Vector and insert DNA was electroporated into Saccharomyces cerevisiae strain BJ5465 (ATCC 208289) to generate a library of $1.4x10^7$ transformants, which were plated on YEP-glucose (-Trp) agar. Plates were scraped and $1.4x10^8$ induced in YEP-galactose (-Trp) for 48 hours. For round 1, yeast were washed in staining buffer and co-stained with 125 nM rituximab-G2F-FITC and 2.5 nM rituximab-G2-

Alexa647 (50-fold excess G2F). FITC-Alexa647$^+$ clones were sorted into YEP-glucose (-Trp), expanded, and induced for round 2. Clones were induced, and co-stained with 37.5 nM rituximab-G2F-Alexa647 and 750 pM rituximab-G2-FITC (50-fold excess G2F). FITC$^+$Alexa647$^+$ clones were sorted and plated onto YEP-glucose (-Trp) agar. 288 individual clones were induced in duplicate 96-well plates and stained with 200 pM rituximab-G2-A647 or 10 nM rituximab-G2F-A647. Highly selective clones were selected and sequenced for further experiments.

5.1.7 Nanobody ELISA

For some experiments, half-well 96-well plates were coated with 30μLof 10 μl/mL mouse anti-IgG1 (ThermoFisher) overnight. Plates were washed with PBST (0.05% Tween-20) 3 times, blocked with 2% BSA in PBS for 1 hour at room temperature, washed, incubated with recombinant IgG, purified patient IgG, or patient serum, washed, incubated with nanobody-streptavidin-HRP conjugates (1:1000, Biolegend), washed, developed with TMB substrate, quenched with 1M phosphoric acid, and read at 450 nm on a spectrophotometer.

For other experiments, half-well 96-well plates were coated with 30μLof 10 μl/mL nanobody overnight. Plates were washed with PBST (0.05% Tween-20) 3 times, blocked with 2% BSA in PBS for 1 hour at room temperature, washed, incubated with recombinant IgG, purified patient IgG, or patient serum, washed, incubated with anti-human IgG-HRP conjugates (1:5000, JacksonImmunoResearch), washed, developed with TMB substrate, quenched with 1M phosphoric acid, and read at 450 nm on a spectrophotometer.

5.1.8 Nanobody Luminex

Magplex microspheres (region 45) were conjugated to mouse anti-human IgG1 (ThermoFisher) using xMAP Ab Coupling kit, per manufacturer's instructions, and blocked with 1% BSA in PBS overnight. 50μLmicrospheres and 50μLof diluted recombinant IgG, purified patient IgG, or patient serum were shaken at 500 rpm in a 96-well plate for 1 hour. Microspheres were washed 3 times with 1% BSA in PBS and shaken with nanobody-streptavidin-PE conjugates for 30 minutes. Microspheres were washed and median fluorescent intensities calculated using Luminex 200 Instrument System (ThermoFisher).

For other experiments, Magplex microspheres (region 45) were conjugated to S2G2F-specific clone H9 (10 μg/106 beads), per manufacturer's instructions, and blocked with 1% BSA overnight. 50μLmicrospheres and 50μLof diluted recombinant IgG was shaken at 500 rpm in a 96-well plate for 1 hour. Microspheres were washed 3 times with 1% BSA in PBS and shaken with R-PE-conjugated Fab¬2 goat anti-human IgG Fc (Jackson Immunoresearch) for 30 minutes. Microspheres were washed and median fluorescent intensities calculated using Luminex 200 Instrument System (ThermoFisher).

5.1.9 ELISA-based FcγR binding assay

Recombinant FcγR ectodomains were expressed in Expi-293F and purified with Ni-NTA resin as in previously described protocols[171]. High-binding 96-well microtiter plates (Nunc) were incubated with 10μl/mL of recombinant FcγRI or FcγRIIIA(V) overnight at 4°C. Plates were then blocked with PBS plus 2% (w/v) BSA. IgG immune complexes were prepared by incubation of an anti-NP (4-hydroxy-3-nitrophenylacetyl) antibody 3B62 with NP-BSA (27 conjugation) at a 10:1 molar ratio for 1h at 4°C. Nanobodies were serially diluted 1:3 in PBS, with a starting concentration of 19.2nM. IgG immune com-

plexes or monomeric 3B62 were brought to concentration of 20 ug ml-1 or 2 ug ml-1 respectively and pre-complexed at a 1:1 (v/v) ratio for 1h at room temperature and then captured on FcγR-coated plates. Following 1h incubation, bound IgG was detected using a 1:5000 dilution of horseradish peroxidase (HRP)-conjugated goat F(ab')2 anti-human IgG (H+L) (Jackson Immunoresearch). Plates were developed with TMB (3,3',5,5'-tetramethylbenzidine) two-component peroxidase substrate kit. Reactions were quenched with 1M phosphoric acid. Absorbance at 450 nm was recorded using a SpectraMax Plus spectrophotometer (Molecular Devices). Background absorbance was subtracted for samples and % maximum binding was determined against an IgG or immune complex only control.

5.1.10 IgG Fc glycan and IgG subclass analysis

The subclass distribution and Fc glycan composition of IgGs was determined by mass spectrometry at the Institute of Biotechnology of the Cornell University, as described previously[68,73]. Briefly, IgGs were purified from plasma or serum samples by protein G purification and dialyzed against PBS. Assay reproducibility was determined by assessing the Fc glycan profile from three subjects in two independent experiments. Research personnel involved in Fc glycan analysis had no access to clinical information and characteristics of the patient samples.

5.1.11 Glycan Array

N-glycan arrays (Z-Biotech) were used according to manufacturer instructions. Briefly, slides were blocked with Glycan Array Blocking Buffer for an hour on shaker at 85 rpm.

After an hour, blocking buffer was removed and 200μLof B7 (0.5 mg/mL or 0.05 mg/mL) or biotinylated-AAL (10 μl/mL) was added. Slides were incubated for 2 hours shaking at 200 rpm and then washed three times with Wash Buffer (50mM Tris-HCl, 137 mM NaCl, 0.05% Tween 20, pH 7.6). 200 μl of 1 μg/mL of Streptavidin-Cy3 (Vector labs) was added for 1 hour shaking at 85 rpm. Slides were washed three times with Wash Buffer, dried, and then scanned with a Typhoon FLA-9500 (GE Healthcare).

5.1.12 Immunoprecipitation

Streptavidin-coated Dynabeads (ThermoFisher) were incubated with 5:1 molar excess biotinylated nanobody for 1 hour at room temperature, then washed 3 times with PBS. Dynabeads were incubated with serum, or IgG-depleted serum for 1 hour, after which they were washed 3 times with PBS. Beads were boiled for 5 minutes at 95°C in SDS loading buffer, and loaded onto a 4-12% Bis-Tris protein gel for analysis.

5.1.13 Generation of FUT8 Knockout Expi-293F and DB cell lines

CRISPR–Cas9 guide RNAs targeting human FUT8 were assembled with Cas9-3NLS nuclease (Synthego) via incubation at 37°C for 15 min. Cas9/RNP complexes were nucleofected into 2 x 10^6 cells using the SF Cell Line 4D-Nucleofector kit according to manufacturer's instructions (Lonza). After a week of culture, indel frequencies were quantified using TIDE software as described previously[183]. Sequence for the single-guide RNA (sgRNA) molecule used is as follows: ACAGCCAAGGGTAAATATGG.

5.1.14 B cell depletion model

All *in vivo* experiments were performed in compliance with federal laws and institutional guidelines and have been approved by the Rockefeller University Institutional Animal Care and Use Committee. Mice were bred and maintained at the Comparative Bioscience Center at the Rockefeller University. For all experiments, huCD20 transgenic mice on a FcγR-humanized background[129] (males and females; 8-12 weeks old) were administered 0.5 mg/kg rituximab G2 (anti-huCD20) to deplete B cells. For nanobody prophylaxis, nanobody-Fc fusion proteins were administered (2.5 mg/kg) together with rituximab. For nanobody treatment nanobody-Fc fusion proteins were administered (2.5 mg/kg) 2 hours after rituximab. Mice were bled on Day 0, 1, and 2 for analysis. Whole blood was lysed (RBC lysis buffer; Biolegend) for 5 minutes at room temperature, and resuspended in FACS buffer (PBS containing 1% w/v BSA and 2 mM EDTA). Cells were labeled with fluorescently-conjugated antibodies anti-CD45 (PE-Cy7) and anti-huCD20 (APC), as well as 7-AAD viability dye (ThermoFisher). Samples were collected on an Attune NxT (ThermoFisher) and B cell frequencies (B220 in $CD45^+$) were calculated using FlowJo (v10.6).

5.1.15 Surface BCR analysis

The B lymphoblast cell line, DB (ATCC), was utilized for evaluating nanobody binding to surface BCR. Cells were stained in FACS buffer and labeled with fluorescently-conjugated anti-hIgG Fc (BV421) at 1:200 (Biolegend), B7-tetramer (PE) at 1 μg/ml, as well as 7-AAD viability dye (ThermoFisher) at 1:1000. For analysis of primary human B cells, buffy coats were obtained from the New York Blood Center. Samples were diluted in RPMI-1640, and peripheral blood mononuclear cells separated by Ficoll gradient centrifugation. Class-switched B cells were enriched by MACS using a class-switched memory B cell enrich-

ment kit (Miltenyi). B cells with cultured for 24 hours in B cell media (RPMI-1640 supplemented with 10% fetal bovine serum, 55 μM β-mercaptoethanol, 2 mM L-glutamine, 1 mM sodium pyruvate, penicillin/streptomycin (1x), 10 mM HEPES, and 2 μg/ml anti-RP105 (clone MHR73-11, Biolegend). CRISPR–Cas9 guide RNAs targeting human FUT8 were assembled with Cas9-3NLS nuclease (Synthego) via incubation at 37°C for 15 min. Cas9/RNP complexes were nucleofected into 1 x 10^6 cells using the P3 Primary Cell 4D-Nucleofector kit and program EH-140 (Lonza). After 48 hours, indel frequencies were quantified using TIDE software as described previously. Sequence for the single-guide RNA (sgRNA) molecule used is as follows: ACAGCCAAGGGTAAATA**TGG** (PAM sequence in bold). Cells were stained as described for the DB cell line. Samples were collected on an Attune NxT and data was analyzed with FlowJo.

5.1.16 Patient samples

For serum or purified IgG in Fig. X, samples were obtained from a previously described patient cohort of convalescent COVID-19 patients[148]. For dengue virus infected patients in Fig. X, purified IgG from a previously published dengue virus infected cohort was used[73]. All samples were de-identified and obtained under approval from the Rockefeller University Institutional Review Board.

Sera from adult patients (≥21 years old) with COVID-19, presenting to the Emergency Room of Weiler Hospital, the Einstein Campus of Montefiore Medical Center (MMC) in the Bronx, New York, were collected between September 2020 and May 2021. Inclusion criteria were signs and symptoms associated with COVID-19, documented new SARS-CoV-2 infection, diagnosed by real-time reverse transcription PCR (RT-PCR) of nasopharyngeal secretions (obtained via deep nasopharyngeal swabs), and admission to the

hospital. Exclusion criteria were age < 21, history of prior SARS-CoV-2 infection, or no COVID-19 associated symptoms. Patients were categorized by WHO score[149].

Hospitalized patients were grouped into those with moderate disease but not requiring supplemental oxygen therapy (WHO score 4; n = 13) and those with moderate - severe disease (WHO scores 5 – 9; n = 18) requiring supplemental oxygen by nasal canular (WHO 5), high flow, Bilevel Positive Airway Pressure (BiPAP), and/or mechanical ventilation (WHO 6 – 9). There were no significant differences in demographics between the groups. Patients with WHO score 4 had a mean age of 64 ± 15 years and 8/13 (61.5%) were male; patients with WHO score 5 – 9 had a mean age of 66 ± 12 years and 9/18 (50%) were male. Left over sera (from clinical lab evaluations), stored at 4°C in the clinical hematology lab for 24-48 hours, were collected, coded without identifiers, aliquoted, and stored at -80°C on the day obtained until tested. The study was approved by the Albert Einstein College of Medicine and MMC Institutional Review Board.

5.1.17 Statistics

An unpaired two-tailed t test was used when comparing two groups. One-way ANOVA with Bonferroni's post hoc test was used when comparing more than two groups. GraphPad Prism software (v9.1) was used for all statistical analysis. P values of ≤0.05 were considered statistically significant.

5.2 Methods for 'The role of the IgG Fc glycan in developing antibody responses'

5.2.1 Generation of IgG1^{N297A} mice

IgG1^{N297A} mice were generated in C57BL/6 zygotes by following standard easiCRISPR protocols[184]. Briefly, zygotes were injected with sgRNA targeting Exon 3 of *IGHG1* and single-stranded repair template coding for the N297A mutation, a *NheI* cut-site, and a silent protospacer adjacent motif (PAM) mutation to prevent Cas9 recutting. sgRNA sequence was CACAGCTCAGACGAAACCCC**GGG**, with PAM sequence in bold. Repair template contained 88 bp 5' and 3' homology arms. Mice were backcrossed to C57BL/6 and littermates were used as controls in all experiments. Genotyping was performed using primers P_{fw} and P_{rev} (Table 3) and restriction digest with *NheI*.

To generate the IgG1^{N297A}; IgG2b$^{-/-}$; IgG2c$^{-/-}$ mouse, a similar strategy was used, but sgRNA targeting the *Ighg2b Ighg2c* were included in the micro-injection solution. sgRNA sequence was TCAGACACAAACCCATAGAG**AGG**, with PAM sequence in bold. Mice were screened for the IgG1^{N297A} allele as described above, and Exon 3 of *Ighg2b Ighg2c* amplified by PCR and sequenced for indels. In 1/32 pups, the Igh locus was determined to be IgG1$^{N297A/N297A}$;IgG2b$^{+/-}$; IgG2c$^{+/-}$. Mice were backcrossed to C57BL/6 and homozygotes for the Fc null allele were sequenced and IgG subclass titers measured by ELISA.

5.2.2 Generation of the hIgG1 knock-in mouse

The *Ighg2c* targeting construct was generated by joining a 1 kb 5′ homology arm upstream of the mouse Ighg2c Cγ1 region, human *IGHG1* Cγ1-Cγ3, and a 1.2 kb 3′ homology arm downstream of the mouse Ighg2c Cγ3 region. Homology arms were generated by PCR amplification (Pfu Turbo DNA Polymerase, Agilent Technologies) from C57BL/6 genomic DNA, and human *IGHG1* Cγ1-Cγ3 from PCR amplification of from a DNA library isolated from human blood (BAC clone RCPI-11-417P24, CHORI). These fragments were placed within the pBluescript II SK+ cloning vector (Agilent Technologies). In between the *IGHG1* Cγ3 and mouse 3′ homology arm, a FRT-LoxP-Neo cassette was inserted.

The two gRNAs CAGTCCACAGCAATTTCGGC**AGG** and CAAGAACACCG-CAACAGTCC**TGG** (PAMs in bold) were used to guide the Cas9D10A (nickase), along with the targeting construct, into C57BL/6 embryonic stem (ES) cells. Transfection and subsequent neomycin selection of targeted ES cell clones were performed by the Rockefeller University Gene Targeting Facility.

The first round of screening ES cell clones by PCR for both the 5′ and 3′ regions of hIgG1 sequence identified positive events that were confirmed by southern blot analysis of XbaI-digested genomic DNA. A probe that hybridized outside of the targeting vector identified a 3.9 kb band, indicating the presence of a successfully targeted allele, while a 7.0 kb band identified the wild-type *Ighg2c* allele. Positive clones were selected and microinjected into C57BL/6 mouse blastocysts and implanted into surrogate mice. Pups born were screened for presence of the targeted allele and crossed to mice expressing FLPase for removal of the FRT-flanked Neomycin cassette.

5.2.3 Flow cytometry

Single-cell suspensions of mouse peripheral blood, popliteal lymph nodes (pLNs) or splenocytes were obtained by mechanical homogenization and 70μm filtration, red blood cells lysed for 5 min at room temperature with RBC Lysis Buffer (Biolegend), resuspended in PBS containing 0.5% (w/v) BSA and 2 mM EDTA (FACS buffer), and labeled with the following antibodies (all used at 1:200 dilution unless otherwise stated): anti-B220-(clone RA3-6B2), anti-NK1.1-(clone PK136), anti-Gr-1-(clone RB6-8C5), anti-F4/80, anti-CD3-(clone 17A2), anti-CD11b-(clone M1/70), anti-human FcγRIIa (clone IV.3) (5 μg ml^{-1}), anti-human FcγRIIb (clone 2B6) (5 μg ml^{-1}), anti-human FcγRIIIa/b (clone 3G8) (5 μg ml^{-1}), anti-human FcγRI (clone 10.1) (5 μg ml^{-1}), anti-TCRβ (clone H57-597), anti-IgD (clone 11-26c.2a), anti-mouse IgG1 (clone RMG1-1), anti-mouse Fas (clone Jo2 at 1:800), anti-mouse CD138 (clone 281-2 at 1:400), anti-mouse CD38 (clone 90), NP-PE (5 μg/ml), anti-mouse IgG3 (clone R40-82), anti-mouse IgG2a/b (clone R2-40), anti-human IgG1 (clone M1310G05), and anti-mouse phospho-CD79α (Y182) (clone D1B0). For FcγR staining, isotype staining was performed with mouse IgG1 isotype control (5 μg ml^{-1}), mouse IgG2b kappa isotype control (5 μg ml^{-1}), mouse IgG1 kappa isotype control (5 μg ml^{-1}), mouse IgG1 kappa isotype control (5 μg ml^{-1}). Viability was determined by 7-AAD staining (1 μg ml^{-1}, ThermoFisher) or Fixable Aqua Live/Dead stain (ThermoFisher). Data was collected using an Attune NxT flow cytometer (ThermoFisher) and data were analyzed using FlowJo (v10.8) software.

5.2.4 ELISA

For baseline IgG titers, diluted sera were added to ELISA plates (Nunc) coated with goat anti-mouse κ light chain and/or goat anti-mouse λ light chain antibodies (1 μg ml-

1 each, Bethyl Laboratories), and plates were developed with species/isotype-specific horseradish peroxidase (HRP)-conjugated antibodies: goat anti-mouse IgM, goat anti-mouse IgG1, goat anti-mouse IgG2b, goat anti-mouse IgG2c, goat anti-mouse IgG3, or goat anti-human IgG (all from JacksonImmunoResearch). Detection was performed using a TMB Peroxidase Substrate Kit (SeraCare) and reactions stopped with the addition of 0.16 M phosphoric acid. Absorbance was measured at 450 nm using a SpectraMax Plus spectrophotometer (Molecular Devices). Background absorbance of negative controls was subtracted from experimental samples and duplicate wells were then averaged.

Serum TNP- and NP-specific IgG levels were quantified by ELISA. Sera were diluted and added to ELISA plates coated with TNP-BSA or NP-BSA (10 μg/mL, Biosearch Technologies), and plates were developed with the same secondary antibodies listed above.

5.2.5 Immunizations

IgG1^{N297A} mice were immunized subcutaneously (s.c.) in the hind footpad with 10 μg NP-OVA adjuvanted with alhydrogel (InVivoMab) at a 2:1 ratio in a total volume of 20 μL.

hIgG1 knock-in mice were immunized intraperitoneally (i.p.) with TNP-LPS (50 μg; Biosearch Technologies) in 200 μL of PBS or NP-OVA (50 μg; Biosearch Technologies) in 200 μL of Alum (Thermo Scientific). Some mice were boosted i.p. with 50 μg of NP-OVA in 200 μL of PBS 21 days after primary immunization.

5.2.6 Antibody engineering and production

The Expi293F expression system was used to generate antibodies. Briefly, Expi293F cells were maintained in Expi293 Expression Medium (Thermo Fisher Scientific), and transfected with heavy-chain and light-chain constructs using an ExpiFectamine 293 Transfection Kit (Thermo Fisher Scientific). The Fc engineered GAALIE variant was generated by site-directed mutagenesis using specific primers, as previously described[18]. Five days after transfection, supernatants were collected, centrifuged, and sterile-filtered (0.22 μm). Clarified supernatants were incubated with constant agitation with Protein G Sepharose 4 Fast Flow (GE Healthcare) at 4°C overnight. The next day Protein G beads were washed with PBS, bound antibodies were eluted using IgG elution buffer (Thermo Fisher Scientific), dialyzed (MWCO 100,000 kDa) in PBS, and sterile-filtered again. Purity was assessed by SDS–PAGE followed by SafeStain blue staining (ThermoFisher), as well as by size exclusion chromatography (SEC) using a Superdex 200 Increase 10/300GL column (GE Healthcare) on an Äkta Pure 25 HPLC system (data analysed using Unicorn v.6.3 software).

5.2.7 *Ex vivo* B cell stimulation

Spleens from mice of the indicated genotypes were harvested, homogenized, filtered through a 70 μm strainer, red blood cells lysed for 5 min at room temperature with RBC Lysis Buffer, and resuspended in MACS buffer (PBS + 0.5% (w/v) BSA + 2 mM EDTA). $CD43^+$ cells were depleted using CD43 MACS beads (Miltenyi) and the flow through collected. After washing in MACS buffer, cells were cultured in RPMI-1640 supplemented with 10% fetal bovine serum (FBS), 20 ng/mL recombinant mouse interleukin-4 and 50 μg/mL lipopolysaccharide for 5 days at 37°C to class-switch B cells to the IgG1 isotype.

Cells were analyzed for class-switching by flow cytometry using procedures outlined above.

Cells were washed with ice-cold PBS twice and then incubated for 20 min in 50 μL Fixable Aqua stain (ThermoFisher) diluted in PBS. Cells were washed and seeded in a round-bottom 96-well plate (Nunc) at a density of 10^5 cells/well in 50 μL of RPMI-1640 + 2% FBS. Cells were kept on ice at all times, besides during stimulation. For stimulation, 50 μL of anti-mouse IgG1 F(ab')$_2$ diluted in media at 2x the concentrations indicated in Figure 3.4 and plates were placed in a shallow 37°C water bath for 5 minutes. For fixation, 100 μL of fixation buffer (eBioscience FoxP3/Transcription Factor Fixation and Permeabilization Buffer : diluent in a 1:1 ratio, ThermoFisher) was added to each well and incubated for 10 min in the water bath. Cells were then washed with eBioscience Wash Buffer (ThermoFisher) before fluorescent staining. Cells were stained intracellularly/extracellularly simultaneously with anti-B220, anti-IgD, anti-IgG1, anti-pCD79α (clones indicated in section above) and analyzed on FlowJo (v10.8).

5.2.8 Tolerance studies

To study tolerance to human IgG1 antibodies, 100 μg of 3BNC117 (anti-HIV gp120)-hIgG1, 2B8 (anti-CD20)-hIgG1, 2B8-hIgG2, 2B8-hIgG3, or 2B8-hIgG4 were administered i.p. according to the schedule indicated in Figure 3.11. Serum was collected at the timepoints indicated. To detect serum 3BNC117 levels, diluted sera were added to ELISA plates coated with recombinant gp120 (2 μg ml-1, Sino Biological), and detected with HRP-conjugated goat anti-human IgG (JacksonImmunoResearch). OD_{450} values were converted to μg ml-1 using a standard curve generated with purified 3BNC117. To detect mouse anti-human IgG1 levels, diluted sera were added to plates coated with human IgG1 Fc or an irrelevant

mouse chimeric antibody with a mouse IgG1 heavy chain and human kappa light chain (both 2 μg ml-1, produced in-house), and detected with HRP-conjugated goat anti-mouse IgG1/2b/2c/3.

5.2.9 Chronic immune thrombocytopenic purpura model

Mice were injected intravenously (i.v.) with 10 μg of anti-glycoprotein IIb antibody (clone 6A6)-hIgG1 on Days 0, 1, and 2, of each week for three weeks. Whole blood was harvested on days 0-3 of each week. Platelet counts were measured using an automated hematologic analyzer (Heska HT5). To detect mouse anti-human IgG1 levels, diluted sera were added to plates coated with human IgG1 Fc (2 μg ml-1, produced in-house), and detected with HRP-conjugated goat anti-mouse IgG1/2b/2c/3.

5.2.10 Melanoma chronic treatment model

For the B16-F10 lung metastasis model, mice were pretreated i.v. with 40 μg of anti-gp75 (clone TA99)-hIgG1-GAALIE 21 and 7 days before they were injected i.v. with 1 ×105 B16-F10 tumor cells. They received 40 μg of recombinant TA99-hIgG1-GAALIE i.p. on days 1, 4, 7, and 11. On day 14 after tumor challenge, mice were killed and lungs were analyzed for the presence of surface metastases by counting the number of metastatic foci. To detect mouse anti-human IgG1 levels, diluted sera were added to plates coated with human IgG1 Fc (2 μg ml-1, produced in-house), and detected with HRP-conjugated goat anti-mouse IgG1/2b/2c/3. To detect serum TA99-hIgG1-GAALIE levels, diluted sera were added to ELISA plates coated with 5 μg ml-1 recombinant gp75 (Creative Biomart), and detect with HRP-conjugated goat anti-human IgG.

5.2.11 Statistics

An unpaired two-tailed t test was used when two groups were being compared. One-way ANOVA with Bonferroni's post hoc test was used when more than two groups were compared. GraphPad Prism software (v9.1) was used for all statistical analysis. P values of ≤0.05 were considered statistically significant (indicated as *$P \leq 0.05$, **$P \leq 0.01$, ***$P \leq 0.001$, and ****$P \leq 0.0001$).

Chapter 6

APPENDIX

	unbound X0
Data collection	
Beamline	NSLS-II FMX
Space group	$I2_1I2_1I2_1$
Cell dimensions (a, b, c) (Å)	(59.3, 95.1, 110.4)
Cell dimensions (α, β, γ) (°)	(90, 90, 90)
Resolution (Å)	50-1.8 (1.84-1.80)
Wavelength (Å)	0.97934
R_{pim}	0.045 (0.339)
$CC_1/2$	0.991 (0.708)
<I>/< σI>	29.9 (1.8)
Completeness (%)	99.2 (95.8)
Redundancy	9.5 (6.7)
Unique Reflections	27855
Phasing	
Search model	Alphafold (X0)
Refinement	
R_{work} / R_{free}	0.192/0.222
B-factors (Å^2) (Avg/Wil)	31.2/23.4
RMS deviations	
bond lengths (Å)	0.007
bond angles (°)	0.959
Ramachandran plot	
% favored	98.3
% allowed (°)	1.7
% outliers	0
Model contents	
Protomers / ASU	2
Protein residues	240
Water	175
PDB ID	XXXX

Table 6.1 | **Refinement and collection statistics for unbound X0 crystal structure.** Values in parentheses refer to the highest resolution shell. R_{free} set consists of 5% of data chosen randomly against which structures was not refined.

	Complex I	Complex II
Data collection		
Beamline	NSLS-II AMX	NSLS-II AMX
Space group	$C2$	$P6_1$
Cell dimensions (a, b, c) (Å)	(125.6, 92.2, 76.5)	(170.6, 170.6, 126.2)
Cell dimensions (α, β, γ) (°)	(90, 117.0, 90)	(90, 90, 120)
Resolution (Å)	50-2.6 (2.64-2.60)	50-2.7 (2.75-2.70)
Wavelength (Å)	0.92010	0.92010
R_{pim}	0.050 (0.574)	0.035 (0.522)
$CC_1/2$	0.996 (0.504)	1.000 (0.604)
$<I>/<\sigma I>$	23.6 (1.4)	31.1 (1.5)
Completeness (%)	90.7 (90.4)	98.2 (98.9)
Redundancy	2.5 (2.5)	4.6 (4.8)
Unique Reflections	21352	56382
Phasing		
Search model(s)	3AVE (Fc) + XXXX (X0)	Complex I
Refinement		
R_{work} / R_{free}	0.208/0.279	0.220/0.255
B-factors (Å^2) (Avg/Wil)	78.1/60.2	94.0/71.1
RMS deviations		
bond lengths (Å)	0.015	0.012
bond angles (°)	1.95	2.06
Ramachandran plot		
% favored	96.5	97.5
% allowed (°)	3.5	2.4
% outliers	0	0.1
Model contents		
Protomers / ASU	2	4
Protein residues	653	1308
Water	10	14
PDB ID	YYYY	ZZZZ

Table 6.2 | **Refinement and collection statistics for the X0-IgG1 Fc Complex I and II crystal structures.** Values in parentheses refer to the highest resolution shell. R_{free} set consists of 5% of data chosen randomly against which structures was not refined.

Bibliography

[1] M. F. Jennewein and G. Alter. The immunoregulatory roles of antibody glycosylation. *Trends Immunol*, 38(5):358–372, 2017.

[2] T. Takai, M. Ono, M. Hikida, H. Ohmori, and J. V. Ravetch. Augmented humoral and anaphylactic responses in fc gamma rii-deficient mice. *Nature*, 379(6563):346–9, 1996.

[3] F. Li, P. Smith, and J. V. Ravetch. Inhibitory fc receptor is required for the maintenance of tolerance through distinct mechanisms. *J Immunol*, 192(7):3021–8, 2014.

[4] R. J. Brownlie, K. E. Lawlor, H. A. Niederer, A. J. Cutler, Z. Xiang, M. R. Clatworthy, R. A. Floto, D. R. Greaves, P. A. Lyons, and K. G. Smith. Distinct cell-specific control of autoimmunity and infection by fcgammariib. *J Exp Med*, 205(4):883–95, 2008.

[5] R. Clynes, J. S. Maizes, R. Guinamard, M. Ono, T. Takai, and J. V. Ravetch. Modulation of immune complex-induced inflammation in vivo by the coordinate expression of activation and inhibitory fc receptors. *J Exp Med*, 189(1):179–85, 1999.

[6] R. A. Clynes, T. L. Towers, L. G. Presta, and J. V. Ravetch. Inhibitory fc receptors modulate in vivo cytotoxicity against tumor targets. *Nat Med*, 6(4):443–6, 2000.

[7] V. Goede, K. Fischer, R. Busch, A. Engelke, B. Eichhorst, C. M. Wendtner, T. Chagorova, J. de la Serna, M. S. Dilhuydy, T. Illmer, S. Opat, C. J. Owen, O. Samoylova, K. A. Kreuzer, S. Stilgenbauer, H. Döhner, A. W. Langerak, M. Ritgen, M. Kneba, E. Asikanius, K. Humphrey, M. Wenger, and M. Hallek. Obinutuzumab plus chlorambucil in patients with cll and coexisting conditions. *N Engl J Med*, 370(12):1101–10, 2014.

[8] F. Li and J. V. Ravetch. Antitumor activities of agonistic anti-tnfr antibodies require differential fcriib coengagement in vivo. *Proc Natl Acad Sci U S A*, 110(48):19501–6, 2013.

[9] S. Bournazos, A. Gupta, and J. V. Ravetch. The role of igg fc receptors in antibody-dependent enhancement. *Nat Rev Immunol*, 20(10):633–643, 2020.

[10] J. V. Ravetch and S. Bolland. Igg fc receptors. *Annu Rev Immunol*, 19:275–90., 2001.

[11] M. J. Zhou and E. J. Brown. Cr3 (mac-1, alpha m beta 2, cd11b/cd18) and fc gamma riii cooperate in generation of a neutrophil respiratory burst: requirement for fc gamma riii and tyrosine phosphorylation. *J Cell Biol*, 125(6):1407–16, 1994.

[12] L. Marois, G. Paré, M. Vaillancourt, E. Rollet-Labelle, and P. H. Naccache. Fc gammariiib triggers raft-dependent calcium influx in igg-mediated responses in human neutrophils. *J Biol Chem*, 286(5):3509–19, 2011.

[13] J. M. Green, A. D. Schreiber, and E. J. Brown. Role for a glycan phosphoinositol anchor in fc gamma receptor synergy. *J Cell Biol*, 139(5):1209–17, 1997.

[14] A. Coxon, X. Cullere, S. Knight, S. Sethi, M. W. Wakelin, G. Stavrakis, F. W. Luscinskas, and T. N. Mayadas. Fc gamma riii mediates neutrophil recruitment to immune complexes. a mechanism for neutrophil accumulation in immune-mediated inflammation. *Immunity*, 14(6):693–704, 2001.

[15] S. Bournazos, T. T. Wang, R. Dahan, J. Maamary, and J. V. Ravetch. Signaling by antibodies: Recent progress. *Annu Rev Immunol*, 35:285–311, 2017.

[16] S. Bournazos, J. M. Woof, S. P. Hart, and I. Dransfield. Functional and clinical consequences of fc receptor polymorphic and copy number variants. *Clin Exp Immunol*, 157(2):244–54, 2009.

[17] P. Sondermann, J. Kaiser, and U. Jacob. Molecular basis for immune complex recognition: a comparison of fc-receptor structures. *J Mol Biol.*, 309(3):737–49., 2001.

[18] B. Dhaliwal, D. Yuan, M. O. Pang, A. J. Henry, K. Cain, A. Oxbrow, S. M. Fabiane, A. J. Beavil, J. M. McDonnell, H. J. Gould, and B. J. Sutton. Crystal structure of ige bound to its b-cell receptor cd23 reveals a mechanism of reciprocal allosteric inhibition with high affinity receptor fcri. *Proc Natl Acad Sci U S A*, 109(31):12686–91, 2012.

[19] A. M. Duchemin, L. K. Ernst, and C. L. Anderson. Clustering of the high affinity fc receptor for immunoglobulin g (fc gamma ri) results in phosphorylation of its associated gamma-chain. *J Biol Chem*, 269(16):12111–7, 1994.

[20] M. H. Jouvin, M. Adamczewski, R. Numerof, O. Letourneur, A. Vallé, and J. P. Kinet. Differential control of the tyrosine kinases lyn and syk by the two signaling chains of the high affinity immunoglobulin e receptor. *J Biol Chem*, 269(8):5918–25, 1994.

[21] A. D. Hoppe and J. A. Swanson. Cdc42, rac1, and rac2 display distinct patterns of activation during phagocytosis. *Mol Biol Cell*, 15(8):3509–19, 2004. Hoppe, Adam D Swanson, Joel A 2004/6/1.

[22] J. C. Unkeless, Z. Shen, C. W. Lin, and E. DeBeus. Function of human fc gamma riia and fc gamma riiib. *Semin Immunol*, 7(1):37–44, 1995.

[23] J. A. Swanson and A. D. Hoppe. The coordination of signaling during fc receptor-mediated phagocytosis. *J Leukoc Biol*, 76(6):1093–103, 2004.

[24] D. L. Durden and Y. B. Liu. Protein-tyrosine kinase p72syk in fc gamma ri receptor signaling. *Blood*, 84(7):2102–8, 1994.

[25] D. L. Durden, H. M. Kim, B. Calore, and Y. Liu. The fc gamma ri receptor signals through the activation of hck and map kinase. *J Immunol*, 154(8):4039–47, 1995.

[26] E. Eiseman and J. B. Bolen. Engagement of the high-affinity ige receptor activates src protein-related tyrosine kinases. *Nature*, 355(6355):78–80, 1992.

[27] P. Selvaraj, O. Carpén, M. L. Hibbs, and T. A. Springer. Natural killer cell and granulocyte fc gamma receptor iii (cd16) differ in membrane anchor and signal transduction. *J Immunol*, 143(10):3283–8, 1989.

[28] C. Pignata, K. V. Prasad, M. J. Robertson, H. Levine, C. E. Rudd, and J. Ritz. Fc gamma riiia-mediated signaling involves src-family lck in human natural killer cells. *J Immunol*, 151(12):6794–800, 1993.

[29] R. J. Botelho, M. Teruel, R. Dierckman, R. Anderson, A. Wells, J. D. York, T. Meyer, and S. Grinstein. Localized biphasic changes in phosphatidylinositol-4,5-bisphosphate at sites of phagocytosis. *J Cell Biol*, 151(7):1353–68, 2000. Botelho, R J Teruel, M Dierckman, R Anderson, R Wells, A York, J D Meyer, T Grinstein, S 2001/1/3.

[30] A. D. Hoppe and J. A. Swanson. Cdc42, rac1, and rac2 display distinct patterns of activation during phagocytosis. *Mol Biol Cell*, 15(8):3509–19, 2004.

[31] G. Sánchez-Mejorada and C. Rosales. Fcgamma receptor-mediated mitogen-activated protein kinase activation in monocytes is independent of ras. *J Biol Chem*, 273(42):27610–9, 1998.

[32] M. Bracke, P. J. Coffer, J. W. Lammers, and L. Koenderman. Analysis of signal transduction pathways regulating cytokine-mediated fc receptor activation on human eosinophils. *J Immunol*, 161(12):6768–74, 1998.

[33] J. Aramburu, L. Azzoni, A. Rao, and B. Perussia. Activation and expression of the nuclear factors of activated t cells, nfatp and nfatc, in human natural killer cells: regulation upon cd16 ligand binding. *J Exp Med*, 182(3):801–10, 1995.

[34] R. N. Pearse, T. Kawabe, S. Bolland, R. Guinamard, T. Kurosaki, and J. V. Ravetch. Ship recruitment attenuates fc gamma riib-induced b cell apoptosis. *Immunity*, 10(6):753–60, 1999.

[35] S. Amigorena, C. Bonnerot, J. R. Drake, D. Choquet, W. Hunziker, J. G. Guillet, P. Webster, C. Sautes, I. Mellman, and W. H. Fridman. Cytoplasmic domain heterogeneity and functions of igg fc receptors in b lymphocytes. *Science*, 256(5065):1808–12, 1992.

[36] T. Muta, T. Kurosaki, Z. Misulovin, M. Sanchez, M. C. Nussenzweig, and J. V. Ravetch. A 13-amino-acid motif in the cytoplasmic domain of fc gamma riib modulates b-cell receptor signalling. *Nature*, 368(6466):70–3, 1994.

[37] M. Ono, S. Bolland, P. Tempst, and J. V. Ravetch. Role of the inositol phosphatase ship in negative regulation of the immune system by the receptor fc(gamma)riib. *Nature*, 383(6597):263–6, 1996.

[38] M. Ono, H. Okada, S. Bolland, S. Yanagi, T. Kurosaki, and J. V. Ravetch. Deletion of ship or shp-1 reveals two distinct pathways for inhibitory signaling. *Cell*, 90(2):293–301, 1997.

[39] R. M. Anthony, F. Nimmerjahn, D. J. Ashline, V. N. Reinhold, J. C. Paulson, and J. V. Ravetch. Recapitulation of ivig anti-inflammatory activity with a recombinant igg fc. *Science*, 320(5874):373–6, 2008.

[40] R. M. Anthony, F. Wermeling, M. C. Karlsson, and J. V. Ravetch. Identification of a

receptor required for the anti-inflammatory activity of ivig. *Proc Natl Acad Sci U S A*, 105(50):19571–8, 2008.

[41] Y. Kaneko, F. Nimmerjahn, and J. V. Ravetch. Anti-inflammatory activity of immunoglobulin g resulting from fc sialylation. *Science*, 313(5787):670–3, 2006.

[42] R. M. Anthony, T. Kobayashi, F. Wermeling, and J. V. Ravetch. Intravenous gammaglobulin suppresses inflammation through a novel t(h)2 pathway. *Nature*, 475(7354):110–3, 2011.

[43] V. Ghetie and E. S. Ward. Multiple roles for the major histocompatibility complex class i- related receptor fcrn. *Annu Rev Immunol.*, 18:739–66., 2000.

[44] K. E. Mostov. Transepithelial transport of immunoglobulins. *Annu Rev Immunol.*, 12:63–84., 1994.

[45] I. J. Seppälä, H. Sarvas, and O. Mäkelä. Low concentrations of gm allotypic subsets g3 mg and g1 mf in homozygotes and heterozygotes. *J Immunol*, 151(5):2529–37, 1993. Seppälä, I J Sarvas, H Mäkelä, O 1993/9/1.

[46] A. Morell, F. Skvaril, A. G. Steinberg, E. Van Loghem, and W. D. Terry. Correlations between the concentrations of the four sub-classes of igg and gm allotypes in normal human sera. *J Immunol*, 108(1):195–206, 1972. Morell, A Skvaril, F Steinberg, A G Van Loghem, E Terry, W D 1972/1/1.

[47] Xinyu Ma, Yuwei Zhu, De Dong, Yan Chen, Shubo Wang, Dehui Yang, Zhuo Ma, Anqi Zhang, Fan Zhang, Changyou Guo, et al. Cryo-em structures of two human b cell receptor isotypes. *Science*, 377(6608):880–885, 2022.

[48] Qiang Su, Mengying Chen, Yan Shi, Xiaofeng Zhang, Gaoxingyu Huang, Bangdong Huang, Dongwei Liu, Zhangsuo Liu, and Yigong Shi. Cryo-em structure of the human igm b cell receptor. *Science*, 377(6608):875–880, 2022.

[49] Jianying Yang and Michael Reth. Oligomeric organization of the b-cell antigen receptor on resting cells. *Nature*, 467(7314):465–469, 2010.

[50] Jinmin Lee, Prabuddha Sengupta, Joseph Brzostowski, Jennifer Lippincott-Schwartz, and Susan K Pierce. The nanoscale spatial organization of b-cell receptors on immunoglobulin m–and g–expressing human b-cells. *Molecular biology of the cell*, 28(4):511–523, 2017.

[51] T. T. Wang and J. V. Ravetch. Functional diversification of iggs through fc glycosylation. *J Clin Invest*, 129(9):3492–3498, 2019. Wang, Taia T Ravetch, Jeffrey V 2019/9/4.

[52] R. M. Anthony and F. Nimmerjahn. The role of differential igg glycosylation in the interaction of antibodies with fcgammars in vivo. *Curr Opin Organ Transplant*, 2010.

[53] C. Ferrara, F. Stuart, P. Sondermann, P. Brunker, and P. Umana. The carbohydrate at fcgammariiia asn-162. an element required for high affinity binding to non-fucosylated igg glycoforms. *J Biol Chem*, 281(8):5032–6, 2006.

[54] Kai-Ting C Shade, Michelle E Conroy, Nathaniel Washburn, Maya Kitaoka, Daniel J Huynh, E Laprise, Sarita U Patil, Wayne G Shreffler, and Robert M Anthony. Sialylation of immunoglobulin e is a determinant of allergic pathogenicity. *Nature*, 2020.

[55] K. T. Shade, B. Platzer, N. Washburn, V. Mani, Y. C. Bartsch, M. Conroy, J. D. Pagan, C. Bosques, T. R. Mempel, E. Fiebiger, and R. M. Anthony. A single glycan on ige is indispensable for initiation of anaphylaxis. *J Exp Med*, 212(4):457–67, 2015. Shade, Kai-Ting C Platzer, Barbara Washburn, Nathaniel Mani, Vinidhra Bartsch, Yannic C Conroy, Michelle Pagan, Jose D Bosques, Carlos Mempel, Thorsten R Fiebiger, Edda Anthony, Robert M 2015/4/1.

[56] J. N. Arnold, M. R. Wormald, D. M. Suter, C. M. Radcliffe, D. J. Harvey, R. A. Dwek, P. M. Rudd, and R. B. Sim. Human serum igm glycosylation: identification of glycoforms that can bind to mannan-binding lectin. *J Biol Chem*, 280(32):29080–7, 2005. Arnold, James N Wormald, Mark R Suter, David M Radcliffe, Catherine M Harvey, David J Dwek, Raymond A Rudd, Pauline M Sim, Robert B 2005/6/16.

[57] R. Sitia, A. Rubartelli, and U. Hämmerling. The role of glycosylation in secretion and membrane expression of immunoglobulins m and a. *Mol Immunol*, 21(8):709–19, 1984. Sitia, R Rubartelli, A Hämmerling, U 1984/8/1.

[58] T. Anelli, S. Ceppi, L. Bergamelli, M. Cortini, S. Masciarelli, C. Valetti, and R. Sitia. Sequential steps and checkpoints in the early exocytic compartment during secretory igm biogenesis. *EMBO J*, 26(19):4177–88, 2007. Anelli, Tiziana Ceppi, Stefania Bergamelli, Leda Cortini, Margherita Masciarelli, Silvia Valetti, Caterina Sitia, Roberto 2007/9/7.

[59] Pamela Stanley, Harry Schachter, Naoyuki Taniguchi, A Varki, R Cummings, J Esko, and H Freeze. N-glycans, essentials of glycobiology. *Varki A., Cummings RD, Esko JD, Freeze HH, Stanley P., Bertozzi CR, Hart GW, Etlzler ME, Cold Spring Harbor Laboratory Press, New York*, pages 101–114, 2009.

[60] C. Ferrara, S. Grau, C. Jager, P. Sondermann, P. Brunker, I. Waldhauer, M. Hennig, A. Ruf, A. C. Rufer, M. Stihle, P. Umana, and J. Benz. Unique carbohydrate-carbohydrate interactions are required for high affinity binding between fcgammariii and antibodies lacking core fucose. *Proc Natl Acad Sci U S A*, 108(31):12669–74, 2011.

[61] S Krapp, Y Mimura, R Jefferis, R Huber, and P Sondermann. Structural analysis of human igg-fc glycoforms reveals a correlation between glycosylation and structural integrity. *Journal of Molecular Biology*, 325(5):979–989, 2003.

[62] A. A. Ahmed, J. Giddens, A. Pincetic, J. V. Lomino, J. V. Ravetch, L. X. Wang, and P. J. Bjorkman. Structural characterization of anti-inflammatory immunoglobulin g fc proteins. *J Mol Biol*, 426(18):3166–3179, 2014.

[63] P. Sondermann, A. Pincetic, J. Maamary, K. Lammens, and J. V. Ravetch. General mechanism for modulating immunoglobulin effector function. *Proc Natl Acad Sci U S A*, 110(24):9868–72, 2013.

[64] A. Pincetic, S. Bournazos, D. J. DiLillo, J. Maamary, T. T. Wang, R. Dahan, B. M. Fiebiger, and J. V. Ravetch. Type i and type ii fc receptors regulate innate and adaptive immunity. *Nat Immunol*, 15(8):707–16, 2014.

[65] T. T. Wang, J. Maamary, G. S. Tan, S. Bournazos, C. W. Davis, F. Krammer, S. J. Schlesinger, P. Palese, R. Ahmed, and J. V. Ravetch. Anti-ha glycoforms drive b cell affinity selection and determine influenza vaccine efficacy. *Cell*, 162(1):160–9, 2015.

[66] J. Maamary, T. T. Wang, G. S. Tan, P. Palese, and J. V. Ravetch. Increasing the breadth and potency of response to the seasonal influenza virus vaccine by immune complex immunization. *Proc Natl Acad Sci U S A*, 114(38):10172–10177, 2017.

[67] G. Zauner, M. H. Selman, A. Bondt, Y. Rombouts, D. Blank, A. M. Deelder, and M. Wuhrer. Glycoproteomic analysis of antibodies. *Mol Cell Proteomics*, 12(4):856–65, 2013. Zauner, Gerhild Selman, Maurice H J Bondt, Albert Rombouts, Yoann Blank, Dennis Deelder, André M Wuhrer, Manfred 2013/1/18.

[68] T. T. Wang, J. Sewatanon, M. J. Memoli, J. Wrammert, S. Bournazos, S. K. Bhaumik, B. A. Pinsky, K. Chokephaibulkit, N. Onlamoon, K. Pattanapanyasat, J. K. Taubenberger, R. Ahmed, and J. V. Ravetch. Igg antibodies to dengue enhanced for fcriiia binding determine disease severity. *Science*, 355(6323):395–398, 2017.

[69] H. U. Scherer, D. van der Woude, A. Ioan-Facsinay, H. el Bannoudi, L. A. Trouw, J. Wang, T. Häupl, G. R. Burmester, A. M. Deelder, T. W. Huizinga, M. Wuhrer, and R. E. Toes. Glycan profiling of anti-citrullinated protein antibodies isolated from human serum and synovial fluid. *Arthritis Rheum*, 62(6):1620–9, 2010.

[70] F. E. van de Geijn, M. Wuhrer, M. H. Selman, S. P. Willemsen, Y. A. de Man, A. M. Deelder, J. M. Hazes, and R. J. Dolhain. Immunoglobulin g galactosylation and sialylation are associated with pregnancy-induced improvement of rheumatoid arthritis and the postpartum flare: results from a large prospective cohort study. *Arthritis Res Ther*, 11(6):R193, 2009.

[71] S. Shinzaki, H. Iijima, T. Nakagawa, S. Egawa, S. Nakajima, S. Ishii, T. Irie, Y. Kakiuchi, T. Nishida, M. Yasumaru, T. Kanto, M. Tsujii, S. Tsuji, T. Mizushima, H. Yoshihara, A. Kondo, E. Miyoshi, and N. Hayashi. Igg oligosaccharide alterations are a novel diagnostic marker for disease activity and the clinical course of inflammatory bowel disease. *Am J Gastroenterol*, 103(5):1173–81, 2008.

[72] Y. C. Bartsch, S. Eschweiler, A. Leliavski, H. B. Lunding, S. Wagt, J. Petry, G. M. Lilienthal, J. Rahmöller, N. de Haan, A. Hölscher, R. Erapaneedi, A. D. Giannou, L. Aly, R. Sato, L. A. de Neef, A. Winkler, D. Braumann, J. Hobusch, K. Kuhnigk, V. Krémer, M. Steinhaus, V. Blanchard, T. Gemoll, J. K. Habermann, M. Collin, G. Salinas, R. A. Manz, H. Fukuyama, T. Korn, A. Waisman, N. Yogev, S. Huber, B. Rabe, S. Rose-John, H. Busch, F. Berberich-Siebelt, C. Hölscher, M. Wuhrer, and M. Ehlers. Igg fc sialylation is regulated during the germinal center reaction following immunization with different adjuvants. *J Allergy Clin Immunol*, 146(3):652–666.e11, 2020.

[73] Bournazos S, My Vo HT, Duong V, Auerswald H, Ly S, Sakuntabhai A, Dussart

P, Cantaert T, and Ravetch JV. Antibody fucosylation predicts disease severity in secondary dengue infection. *Science*, in press, 2021.

[74] M. D. Larsen, E. L. de Graaf, M. E. Sonneveld, H. R. Plomp, J. Nouta, W. Hoepel, H. J. Chen, F. Linty, R. Visser, M. Brinkhaus, T. Šuštić, S. W. de Taeye, A. E. H. Bentlage, S. Toivonen, C. A. M. Koeleman, S. Sainio, N. A. Kootstra, P. J. M. Brouwer, C. E. Geyer, N. I. L. Derksen, G. Wolbink, M. de Winther, R. W. Sanders, M. J. van Gils, S. de Bruin, A. P. J. Vlaar, T. Rispens, J. den Dunnen, H. L. Zaaijer, M. Wuhrer, C. Ellen van der Schoot, G. Vidarsson, Amsterdam UMC COVID-19, and biobank study group. Afucosylated igg characterizes enveloped viral responses and correlates with covid-19 severity. *Science*, 371(6532), 2021.

[75] S. Chakraborty, J. C. Gonzalez, B. L. Sievers, V. Mallajosyula, M. Dubey, U. Ashraf, B. Y. Cheng, N. Kathale, K. Q. T. Tran, C. Scallan, A. Sinnott, A. Cassidy, S. T. Chen, T. Gelbart, F. Gao, Y. Golan, X. Ji, S. Kim-Schulze, M. Prahl, S. L. Gaw, S. Gnjatic, T. U. Marron, M. Merad, P. S. Arunachalam, S. D. Boyd, M. M. Davis, M. Holubar, C. Khosla, H. T. Maecker, Y. Maldonado, E. D. Mellins, K. C. Nadeau, B. Pulendran, U. Singh, A. Subramanian, P. J. Utz, R. Sherwood, S. Zhang, P. Jagannathan, G. S. Tan, and T. T. Wang. Early non-neutralizing, afucosylated antibody responses are associated with covid-19 severity. *Sci Transl Med*, page eabm7853, 2022. Chakraborty, Saborni Gonzalez, Joseph C Sievers, Benjamin L Mallajosyula, Vamsee Chakraborty, Srijoni Dubey, Megha Ashraf, Usama Cheng, Bowie Yik-Ling Kathale, Nimish Tran, Kim Quyen Thi Scallan, Courtney Sinnott, Aanika Cassidy, Arianna Chen, Steven T Gelbart, Terri Gao, Fei Golan, Yarden Ji, Xuhuai Kim-Schulze, Seunghee Prahl, Mary Gaw, Stephanie L Gnjatic, Sacha Marron, Thomas U Merad, Miriam Arunachalam, Prabhu S Boyd, Scott D Davis, Mark M Holubar, Marisa Khosla, Chaitan Maecker, Holden T Maldonado, Yvonne Mellins, Elizabeth D Nadeau, Kari C Pulendran, Bali Singh, Upinder Subramanian, Aruna Utz, Paul J

Sherwood, Robert Zhang, Sheng Jagannathan, Prasanna Tan, Gene S Wang, Taia T 2022/1/19.

[76] S. Chakraborty, J. Gonzalez, K. Edwards, V. Mallajosyula, A. S. Buzzanco, R. Sherwood, C. Buffone, N. Kathale, S. Providenza, M. M. Xie, J. R. Andrews, C. A. Blish, U. Singh, H. Dugan, P. C. Wilson, T. D. Pham, S. D. Boyd, K. C. Nadeau, B. A. Pinsky, S. Zhang, M. J. Memoli, J. K. Taubenberger, T. Morales, J. M. Schapiro, G. S. Tan, P. Jagannathan, and T. T. Wang. Proinflammatory igg fc structures in patients with severe covid-19. *Nat Immunol*, 2020.

[77] R. Kapur, I. Kustiawan, A. Vestrheim, C. A. Koeleman, R. Visser, H. K. Einarsdottir, L. Porcelijn, D. Jackson, B. Kumpel, A. M. Deelder, D. Blank, B. Skogen, M. K. Killie, T. E. Michaelsen, M. de Haas, T. Rispens, C. E. van der Schoot, M. Wuhrer, and G. Vidarsson. A prominent lack of igg1-fc fucosylation of platelet alloantibodies in pregnancy. *Blood*, 123(4):471–80, 2014.

[78] A. Dance. Refining the toolkit for sugar analysis. *Nature*, 599(7883):168–169, 2021. Dance, Amber 2021/11/3.

[79] V. Marx. Tools to cut the sweet layer-cake that is glycoproteomics. *Nat Methods*, 18(9):991–995, 2021. Marx, Vivien 2021/8/19.

[80] M. E. Griffin and L. C. Hsieh-Wilson. Tools for mammalian glycoscience research. *Cell*, 2022.

[81] Joshy Jacob, Garnett Kelsoe, Klaus Rajewsky, and Ursula Weiss. Intraclonal generation of antibody mutants in germinal centres. *Nature*, 354(6352):389–392, 1991.

[82] Klaus Rajewsky. Clonal selection and learning in the antibody system. *Nature*, 381(6585):751–758, 1996.

[83] Gabriel D Victora and Michel C Nussenzweig. Germinal centers. *Annual Review of Immunology*, 40:413–442, 2022.

[84] C Berek, A Berger, and M Apel. Maturation of the immune response in germinal centers. *Cell*, 67(6):1121–1129, 1991.

[85] Luka Mesin, Jonatan Ersching, and Gabriel D Victora. Germinal center b cell dynamics. *Immunity*, 45(3):471–482, 2016.

[86] Dahui Qin, Jiuhua Wu, Kalpit A Vora, Jeffrey V Ravetch, Andras K Szakal, Tim Manser, and John G Tew. Fcγ receptor iib on follicular dendritic cells regulates the b cell recall response. *The Journal of Immunology*, 164(12):6268–6275, 2000.

[87] Cees E van der Poel, Goran Bajic, Charles W Macaulay, Theo van den Broek, Christian D Ellson, Gerben Bouma, Gabriel D Victora, Søren E Degn, and Michael C Carroll. Follicular dendritic cells modulate germinal center b cell diversity through fcγriib. *Cell reports*, 29(9):2745–2755, 2019.

[88] Robert A Barrington, Olga Pozdnyakova, Mohammad R Zafari, Christopher D Benjamin, and Michael C Carroll. B lymphocyte memory: role of stromal cell complement and fcγriib receptors. *The Journal of experimental medicine*, 196(9):1189–1200, 2002.

[89] TE Mandels, RP Phippsi, A Abbot, and JG Tew. The follicular dendritic cell: long term antigen retention during immunity. *Immunological reviews*, 53(1):29–59, 1980.

[90] G. D. Victora, T. A. Schwickert, D. R. Fooksman, A. O. Kamphorst, M. Meyer-Hermann, M. L. Dustin, and M. C. Nussenzweig. Germinal center dynamics revealed by multiphoton microscopy with a photoactivatable fluorescent reporter. *Cell*, 143(4):592–605, 2010. Victora, Gabriel D Schwickert, Tanja A Fooksman, David

R Kamphorst, Alice O Meyer-Hermann, Michael Dustin, Michael L Nussenzweig, Michel C 2010/11/16.

[91] A. D. Gitlin, Z. Shulman, and M. C. Nussenzweig. Clonal selection in the germinal centre by regulated proliferation and hypermutation. *Nature*, 509(7502):637–40, 2014.

[92] GJV Nossal. Negative selection of lymphocytes. *cell*, 76(2):229–239, 1994.

[93] George W Chacko, Susheela Tridandapani, Jacqueline E Damen, Ling Liu, Gerald Krystal, and K Mark Coggeshall. Negative signaling in b lymphocytes induces tyrosine phosphorylation of the 145-kda inositol polyphosphate 5-phosphatase, ship. *The Journal of Immunology*, 157(6):2234–2238, 1996.

[94] Peter A Kiener, Mario N Lioubin, Larry R Rohrschneider, Jeffrey A Ledbetter, Steven G Nadler, and Michael L Diegel. Co-ligation of the antigen and fc receptors gives rise to the selective modulation of intracellular signaling in b cells: regulation of the association of phosphatidylinositol 3-kinase and inositol 5-phosphatase with the antigen receptor complex. *Journal of Biological Chemistry*, 272(6):3838–3844, 1997.

[95] Susheela Tridandapani, Todd Kelley, Madhura Pradhan, Damon Cooney, Louis B Justement, and K Mark Coggeshall. Recruitment and phosphorylation of sh2-containing inositol phosphatase and shc to the b-cell fc gamma immunoreceptor tyrosine-based inhibition motif peptide motif. *Molecular and cellular biology*, 17(8):4305–4311, 1997.

[96] Jacqueline E Damen, Ling Liu, Patricia Rosten, R Keith Humphries, Anne B Jefferson, Philip W Majerus, and Gerald Krystal. The 145-kda protein induced to associate with shc by multiple cytokines is an inositol tetraphosphate and phos-

phatidylinositol 3, 4, 5-triphosphate 5-phosphatase. *Proceedings of the National Academy of Sciences*, 93(4):1689–1693, 1996.

[97] Silvia Bolland, Roger N Pearse, Tomohiro Kurosaki, and Jeffrey V Ravetch. Ship modulates immune receptor responses by regulating membrane association of btk. *Immunity*, 8(4):509–516, 1998.

[98] Andrew M Scharenberg, Ousama El-Hillal, David A Fruman, Laurie O Beitz, Zuomei Li, Siqi Lin, Ivan Gout, Lewis C Cantley, David J Rawlings, and Jean-Pierre Kinet. Phosphatidylinositol-3, 4, 5-trisphosphate (ptdins-3, 4, 5-p3)/tec kinase-dependent calcium signaling pathway: a target for ship-mediated inhibitory signals. *The EMBO journal*, 17(7):1961–1972, 1998.

[99] S. Bolland and J. V. Ravetch. Spontaneous autoimmune disease in fc(gamma)riib-deficient mice results from strain-specific epistasis. *Immunity*, 13(2):277–85, 2000.

[100] Z. Xiang, A. J. Cutler, R. J. Brownlie, K. Fairfax, K. E. Lawlor, E. Severinson, E. U. Walker, R. A. Manz, D. M. Tarlinton, and K. G. Smith. Fcgammariib controls bone marrow plasma cell persistence and apoptosis. *Nat Immunol*, 8(4):419–29, 2007.

[101] E. Sterner, N. Flanagan, and J. C. Gildersleeve. Perspectives on anti-glycan antibodies gleaned from development of a community resource database. *ACS Chem Biol*, 11(7):1773–83, 2016. Sterner, Eric Flanagan, Natalie Gildersleeve, Jeffrey C 2016/5/26.

[102] Lars Nitschke and Takeshi Tsubata. Molecular interactions regulate bcr signal inhibition by cd22 and cd72. *Trends in immunology*, 25(10):543–550, 2004.

[103] Lars Nitschke. The role of cd22 and other inhibitory co-receptors in b-cell activation. *Current opinion in immunology*, 17(3):290–297, 2005.

[104] Takahiro Adachi, Chisato Wakabayashi, Toshinori Nakayama, Hidetaka Yakura, and Takeshi Tsubata. Cd72 negatively regulates signaling through the antigen receptor of b cells. *The Journal of Immunology*, 164(3):1223–1229, 2000.

[105] C. L. Law, A. Aruffo, K. A. Chandran, R. T. Doty, and E. A. Clark. Ig domains 1 and 2 of murine cd22 constitute the ligand-binding domain and bind multiple sialylated ligands expressed on b and t cells. *J Immunol*, 155(7):3368–76, 1995. Law, C L Aruffo, A Chandran, K A Doty, R T Clark, E A 1995/10/1.

[106] J. G. Cyster and C. C. Goodnow. Tuning antigen receptor signaling by cd22: integrating cues from antigens and the microenvironment. *Immunity*, 6(5):509–17, 1997. Cyster, J G Goodnow, C C 1997/5/1.

[107] K. Dang, W. Zhang, S. Jiang, X. Lin, and A. Qian. Application of lectin microarrays for biomarker discovery. *ChemistryOpen*, 9(3):285–300, 2020. Dang, Kai Zhang, Wenjuan Jiang, Shanfeng Lin, Xiao Qian, Airong 2020/3/11.

[108] L. Xia and J. C. Gildersleeve. The glycan array platform as a tool to identify carbohydrate antigens. *Methods Mol Biol*, 1331:27–40, 2015. Xia, Li Gildersleeve, Jeffrey C 2015/7/15.

[109] T. R. McKitrick, C. K. Goth, C. S. Rosenberg, H. Nakahara, J. Heimburg-Molinaro, A. M. McQuillan, R. Falco, N. J. Rivers, B. R. Herrin, M. D. Cooper, and R. D. Cummings. Development of smart anti-glycan reagents using immunized lampreys. *Commun Biol*, 3(1):91, 2020. McKitrick, Tanya R Goth, Christoffer K Rosenberg, Charles S Nakahara, Hirotomo Heimburg-Molinaro, Jamie McQuillan, Alyssa M Falco, Rosalia Rivers, Nicholas J Herrin, Brantley R Cooper, Max D Cummings, Richard D 2020/3/1.

[110] T. R. McKitrick, S. M. Bernard, A. J. Noll, B. C. Collins, C. K. Goth, A. M. McQuillan,

J. Heimburg-Molinaro, B. R. Herrin, I. A. Wilson, M. D. Cooper, and R. D. Cummings. Novel lamprey antibody recognizes terminal sulfated galactose epitopes on mammalian glycoproteins. *Commun Biol*, 4(1):674, 2021.

[111] C. L. Brooks, A. Schietinger, S. N. Borisova, P. Kufer, M. Okon, T. Hirama, C. R. Mackenzie, L. X. Wang, H. Schreiber, and S. V. Evans. Antibody recognition of a unique tumor-specific glycopeptide antigen. *Proc Natl Acad Sci U S A*, 107(22):10056–61, 2010. Brooks, Cory L Schietinger, Andrea Borisova, Svetlana N Kufer, Peter Okon, Mark Hirama, Tomoko Mackenzie, C Roger Wang, Lai-Xi Schreiber, Hans Evans, Stephen V 2010/5/19.

[112] D. Reusch, M. Haberger, D. Falck, B. Peter, B. Maier, J. Gassner, M. Hook, K. Wagner, L. Bonnington, P. Bulau, and M. Wuhrer. Comparison of methods for the analysis of therapeutic immunoglobulin g fc-glycosylation profiles-part 2: Mass spectrometric methods. *MAbs*, 7(4):732–42, 2015.

[113] L. Zhang, S. Luo, and B. Zhang. Glycan analysis of therapeutic glycoproteins. *MAbs*, 8(2):205–15, 2016. Zhang, Lei Luo, Shen Zhang, Baolin 2015/11/26.

[114] L. R. Ruhaak, G. Xu, Q. Li, E. Goonatilleke, and C. B. Lebrilla. Mass spectrometry approaches to glycomic and glycoproteomic analyses. *Chem Rev*, 118(17):7886–7930, 2018. Ruhaak, L Renee Xu, Gege Li, Qiongyu Goonatilleke, Elisha Lebrilla, Carlito B 2018/3/20.

[115] A. E. Mahan, J. Tedesco, K. Dionne, K. Baruah, H. D. Cheng, P. L. De Jager, D. H. Barouch, T. Suscovich, M. Ackerman, M. Crispin, and G. Alter. A method for high-throughput, sensitive analysis of igg fc and fab glycosylation by capillary electrophoresis. *J Immunol Methods*, 417:34–44, 2015. Mahan, Alison E Tedesco, Jacquelynne Dionne, Kendall Baruah, Kavitha Cheng, Hao D De Jager, Philip L Barouch, Dan H Suscovich, Todd Ackerman, Margaret Crispin, Max Alter, Galit 2014/12/20.

[116] D. Falck, B. C. Jansen, N. de Haan, and M. Wuhrer. High-throughput analysis of igg fc glycopeptides by lc-ms. *Methods Mol Biol*, 1503:31–47, 2017. Falck, David Jansen, Bas C de Haan, Noortje Wuhrer, Manfred 2016/10/16.

[117] M. P. Baković, M. H. Selman, M. Hoffmann, I. Rudan, H. Campbell, A. M. Deelder, G. Lauc, and M. Wuhrer. High-throughput igg fc n-glycosylation profiling by mass spectrometry of glycopeptides. *J Proteome Res*, 12(2):821–31, 2013. Baković, Maja Pučić Selman, Maurice H J Hoffmann, Marcus Rudan, Igor Campbell, Harry Deelder, André M Lauc, Gordan Wuhrer, Manfred 2013/1/10.

[118] M. Pucić, A. Knezević, J. Vidic, B. Adamczyk, M. Novokmet, O. Polasek, O. Gornik, S. Supraha-Goreta, M. R. Wormald, I. Redzić, H. Campbell, A. Wright, N. D. Hastie, J. F. Wilson, I. Rudan, M. Wuhrer, P. M. Rudd, D. Josić, and G. Lauc. High throughput isolation and glycosylation analysis of igg-variability and heritability of the igg glycome in three isolated human populations. *Mol Cell Proteomics*, 10(10):M111.010090, 2011. Pucić, Maja Knezević, Ana Vidic, Jana Adamczyk, Barbara Novokmet, Mislav Polasek, Ozren Gornik, Olga Supraha-Goreta, Sandra Wormald, Mark R Redzić, Irma Campbell, Harry Wright, Alan Hastie, Nicholas D Wilson, James F Rudan, Igor Wuhrer, Manfred Rudd, Pauline M Josić, Djuro Lauc, Gordan 2011/6/10.

[119] G. P. Subedi and A. W. Barb. The structural role of antibody n-glycosylation in receptor interactions. *Structure*, 23(9):1573–1583, 2015. Subedi, Ganesh P Barb, Adam W 2015/7/28.

[120] D. J. Falconer, G. P. Subedi, A. M. Marcella, and A. W. Barb. Antibody fucosylation lowers the fcriiia/cd16a affinity by limiting the conformations sampled by the n162-glycan. *ACS Chem Biol*, 13(8):2179–2189, 2018. Falconer, Daniel J Subedi, Ganesh P Marcella, Aaron M Barb, Adam W 2018/7/18.

[121] R. L. Shields, J. Lai, R. Keck, L. Y. O'Connell, K. Hong, Y. G. Meng, S. H. Weikert, and L. G. Presta. Lack of fucose on human igg1 n-linked oligosaccharide improves binding to human fcgamma riii and antibody-dependent cellular toxicity. *J Biol Chem*, 277(30):26733–40, 2002. Shields, Robert L Lai, Jadine Keck, Rodney O'Connell, Lori Y Hong, Kyu Meng, Y Gloria Weikert, Stefanie H A Presta, Leonard G 2002/5/3.

[122] L. Detalle, T. Stohr, C. Palomo, P. A. Piedra, B. E. Gilbert, V. Mas, A. Millar, U. F. Power, C. Stortelers, K. Allosery, J. A. Melero, and E. Depla. Generation and characterization of alx-0171, a potent novel therapeutic nanobody for the treatment of respiratory syncytial virus infection. *Antimicrob Agents Chemother*, 60(1):6–13, 2016.

[123] F. D. Mast, P. C. Fridy, N. E. Ketaren, J. Wang, E. Y. Jacobs, J. P. Olivier, T. Sanyal, K. R. Molloy, F. Schmidt, M. Rutkowska, Y. Weisblum, L. M. Rich, E. R. Vanderwall, N. Dambrauskas, V. Vigdorovich, S. Keegan, J. B. Jiler, M. E. Stein, P. D. B. Olinares, L. Herlands, T. Hatziioannou, D. N. Sather, J. S. Debley, D. Fenyö, A. Sali, P. D. Bieniasz, J. D. Aitchison, B. T. Chait, and M. P. Rout. Highly synergistic combinations of nanobodies that target sars-cov-2 and are resistant to escape. *Elife*, 10, 2021.

[124] P. Bannas, J. Hambach, and F. Koch-Nolte. Nanobodies and nanobody-based human heavy chain antibodies as antitumor therapeutics. *Front Immunol*, 8:1603, 2017. Bannas, Peter Hambach, Julia Koch-Nolte, Friedrich 2017/12/8.

[125] S. Jähnichen, C. Blanchetot, D. Maussang, M. Gonzalez-Pajuelo, K. Y. Chow, L. Bosch, S. De Vrieze, B. Serruys, H. Ulrichts, W. Vandevelde, M. Saunders, H. J. De Haard, D. Schols, R. Leurs, P. Vanlandschoot, T. Verrips, and M. J. Smit. Cxcr4 nanobodies (vhh-based single variable domains) potently inhibit chemotaxis and hiv-1 replication and mobilize stem cells. *Proc Natl Acad Sci U S A*, 107(47):20565–70, 2010. Jähnichen, Sven Blanchetot, Christophe Maussang, David Gonzalez-Pajuelo, Maria Chow, Ken Y Bosch, Leontien De Vrieze, Sindi Serruys, Benedikte Ulrichts,

Hans Vandevelde, Wesly Saunders, Michael De Haard, Hans J Schols, Dominique Leurs, Rob Vanlandschoot, Peter Verrips, Theo Smit, Martine J 2010/11/10.

[126] C. McMahon, A. S. Baier, R. Pascolutti, M. Wegrecki, S. Zheng, J. X. Ong, S. C. Erlandson, D. Hilger, S. G. F. Rasmussen, A. M. Ring, A. Manglik, and A. C. Kruse. Yeast surface display platform for rapid discovery of conformationally selective nanobodies. *Nat Struct Mol Biol*, 25(3):289–296, 2018.

[127] G. Dekkers, R. Plomp, C. A. Koeleman, R. Visser, H. H. von Horsten, V. Sandig, T. Rispens, M. Wuhrer, and G. Vidarsson. Multi-level glyco-engineering techniques to generate igg with defined fc-glycans. *Sci Rep*, 6:36964, 2016. Dekkers, Gillian Plomp, Rosina Koeleman, Carolien A M Visser, Remco von Horsten, Hans H Sandig, Volker Rispens, Theo Wuhrer, Manfred Vidarsson, Gestur 2016/11/23.

[128] W. Huang, J. Giddens, S. Q. Fan, C. Toonstra, and L. X. Wang. Chemoenzymatic glycoengineering of intact igg antibodies for gain of functions. *J Am Chem Soc*, 134(29):12308–18, 2012.

[129] T. Li, D. J. DiLillo, S. Bournazos, J. P. Giddens, J. V. Ravetch, and L. X. Wang. Modulating igg effector function by fc glycan engineering. *Proc Natl Acad Sci U S A*, 114(13):3485–3490, 2017.

[130] M. Schoof, B. Faust, R. A. Saunders, S. Sangwan, V. Rezelj, N. Hoppe, M. Boone, C. B. Billesbølle, C. Puchades, C. M. Azumaya, H. T. Kratochvil, M. Zimanyi, I. Deshpande, J. Liang, S. Dickinson, H. C. Nguyen, C. M. Chio, G. E. Merz, M. C. Thompson, D. Diwanji, K. Schaefer, A. A. Anand, N. Dobzinski, B. S. Zha, C. R. Simoneau, K. Leon, K. M. White, U. S. Chio, M. Gupta, M. Jin, F. Li, Y. Liu, K. Zhang, D. Bulkley, M. Sun, A. M. Smith, A. N. Rizo, F. Moss, A. F. Brilot, S. Pourmal, R. Trenker, T. Pospiech, S. Gupta, B. Barsi-Rhyne, V. Belyy, A. W. Barile-Hill,

S. Nock, N. J. Krogan, C. Y. Ralston, D. L. Swaney, A. García-Sastre, M. Ott, M. Vignuzzi, P. Walter, A. Manglik, and QCRG Structural Biology Consortium. An ultrapotent synthetic nanobody neutralizes sars-cov-2 by stabilizing inactive spike. *Science*, 370(6523):1473–1479, 2020.

[131] D. Wrapp, D. De Vlieger, K. S. Corbett, G. M. Torres, N. Wang, W. Van Breedam, K. Roose, L. van Schie, M. Hoffmann, S. Pöhlmann, B. S. Graham, N. Callewaert, B. Schepens, X. Saelens, J. S. McLellan, and VIB-CMB COVID-19 Response Team. Structural basis for potent neutralization of betacoronaviruses by single-domain camelid antibodies. *Cell*, 181(5):1004–1015.e15, 2020. Wrapp, Daniel De Vlieger, Dorien Corbett, Kizzmekia S Torres, Gretel M Wang, Nianshuang Van Breedam, Wander Roose, Kenny van Schie, Loes Hoffmann, Markus Pöhlmann, Stefan Graham, Barney S Callewaert, Nico Schepens, Bert Saelens, Xavier McLellan, Jason S 2020/5/7.

[132] A. W. Chung, M. Crispin, L. Pritchard, H. Robinson, M. K. Gorny, X. Yu, C. Bailey-Kellogg, M. E. Ackerman, C. Scanlan, S. Zolla-Pazner, and G. Alter. Identification of antibody glycosylation structures that predict monoclonal antibody fc-effector function. *AIDS*, 28(17):2523–30, 2014. Chung, Amy W Crispin, Max Pritchard, Laura Robinson, Hannah Gorny, Miroslaw K Yu, Xiaojie Bailey-Kellogg, Chris Ackerman, Margaret E Scanlan, Chris Zolla-Pazner, Susan Alter, Galit 2014/8/28.

[133] P. Smith, D. J. DiLillo, S. Bournazos, F. Li, and J. V. Ravetch. Mouse model recapitulating human fc receptor structural and functional diversity. *Proc Natl Acad Sci U S A*, 109(16):6181–6, 2012.

[134] John Jumper, Richard Evans, Alexander Pritzel, Tim Green, Michael Figurnov, Olaf Ronneberger, Kathryn Tunyasuvunakool, Russ Bates, Augustin Žídek, Anna

Potapenko, et al. Highly accurate protein structure prediction with alphafold. *Nature*, 596(7873):583–589, 2021.

[135] Francis Gaudreault, Christopher R Corbeil, Enrico O Purisima, and Traian Sulea. Coevolved canonical loops conformations of single-domain antibodies: A tale of three pockets playing musical chairs. *Frontiers in immunology*, 13, 2022.

[136] Abigail SL Sudol, John Butler, Dylan P Ivory, Ivo Tews, and Max Crispin. Extensive substrate recognition by the streptococcal antibody-degrading enzymes ides and endos. *bioRxiv*, 2022.

[137] S. B. Halstead and E. J. O'Rourke. Dengue viruses and mononuclear phagocytes. i. infection enhancement by non-neutralizing antibody. *J Exp Med*, 146(1):201–17, 1977.

[138] L. C. Katzelnick, L. Gresh, M. E. Halloran, J. C. Mercado, G. Kuan, A. Gordon, A. Balmaseda, and E. Harris. Antibody-dependent enhancement of severe dengue disease in humans. *Science*, 358(6365):929–932, 2017.

[139] S. N. Mohsin, S. Mahmood, A. Amar, F. Ghafoor, S. M. Raza, and M. Saleem. Association of fcgammariia polymorphism with clinical outcome of dengue infection: First insight from pakistan. *Am J Trop Med Hyg*, 93(4):691–6, 2015.

[140] K. R. Chan, S. L. Zhang, H. C. Tan, Y. K. Chan, A. Chow, A. P. Lim, S. G. Vasudevan, B. J. Hanson, and E. E. Ooi. Ligation of fc gamma receptor iib inhibits antibody-dependent enhancement of dengue virus infection. *Proc Natl Acad Sci U S A*, 108(30):12479–84, 2011.

[141] N. K. Thulin, R. C. Brewer, R. Sherwood, S. Bournazos, K. G. Edwards, N. S. Ramadoss, J. K. Taubenberger, M. Memoli, A. J. Gentles, P. Jagannathan, S. Zhang, D. H.

Libraty, and T. T. Wang. Maternal anti-dengue igg fucosylation predicts susceptibility to dengue disease in infants. *Cell Rep*, 31(6):107642, 2020.

[142] A. K. Pinto, J. D. Brien, C. Y. Lam, S. Johnson, C. Chiang, J. Hiscott, V. V. Sarathy, A. D. Barrett, S. Shresta, and M. S. Diamond. Defining new therapeutics using a more immunocompetent mouse model of antibody-enhanced dengue virus infection. *MBio*, 6(5):e01316–15, 2015.

[143] S. Orozco, M. A. Schmid, P. Parameswaran, R. Lachica, M. R. Henn, R. Beatty, and E. Harris. Characterization of a model of lethal dengue virus 2 infection in c57bl/6 mice deficient in the alpha/beta interferon receptor. *J Gen Virol*, 93(Pt 10):2152–7, 2012.

[144] R. M. Zellweger, T. R. Prestwood, and S. Shresta. Enhanced infection of liver sinusoidal endothelial cells in a mouse model of antibody-induced severe dengue disease. *Cell Host Microbe*, 7(2):128–39, 2010.

[145] S. J. Balsitis, K. L. Williams, R. Lachica, D. Flores, J. L. Kyle, E. Mehlhop, S. Johnson, M. S. Diamond, P. R. Beatty, and E. Harris. Lethal antibody enhancement of dengue disease in mice is prevented by fc modification. *PLoS Pathog*, 6(2):e1000790, 2010.

[146] A. P. Goncalvez, R. E. Engle, M. St Claire, R. H. Purcell, and C. J. Lai. Monoclonal antibody-mediated enhancement of dengue virus infection in vitro and in vivo and strategies for prevention. *Proc Natl Acad Sci U S A*, 104(22):9422–7, 2007.

[147] S. B. Halstead. In vivo enhancement of dengue virus infection in rhesus monkeys by passively transferred antibody. *J Infect Dis*, 140(4):527–33, 1979.

[148] D. F. Robbiani, C. Gaebler, F. Muecksch, J. C. C. Lorenzi, Z. Wang, A. Cho, M. Agudelo, C. O. Barnes, A. Gazumyan, S. Finkin, T. Hägglöf, T. Y. Oliveira,

C. Viant, A. Hurley, H. H. Hoffmann, K. G. Millard, R. G. Kost, M. Cipolla, K. Gordon, F. Bianchini, S. T. Chen, V. Ramos, R. Patel, J. Dizon, I. Shimeliovich, P. Mendoza, H. Hartweger, L. Nogueira, M. Pack, J. Horowitz, F. Schmidt, Y. Weisblum, E. Michailidis, A. W. Ashbrook, E. Waltari, J. E. Pak, K. E. Huey-Tubman, N. Koranda, P. R. Hoffman, A. P. West, C. M. Rice, T. Hatziioannou, P. J. Bjorkman, P. D. Bieniasz, M. Caskey, and M. C. Nussenzweig. Convergent antibody responses to sars-cov-2 in convalescent individuals. *Nature*, 584(7821):437–442, 2020. Robbiani, Davide F Gaebler, Christian Muecksch, Frauke Lorenzi, Julio C C Wang, Zijun Cho, Alice Agudelo, Marianna Barnes, Christopher O Gazumyan, Anna Finkin, Shlomo Hägglöf, Thomas Oliveira, Thiago Y Viant, Charlotte Hurley, Arlene Hoffmann, Hans-Heinrich Millard, Katrina G Kost, Rhonda G Cipolla, Melissa Gordon, Kristie Bianchini, Filippo Chen, Spencer T Ramos, Victor Patel, Roshni Dizon, Juan Shimeliovich, Irina Mendoza, Pilar Hartweger, Harald Nogueira, Lilian Pack, Maggi Horowitz, Jill Schmidt, Fabian Weisblum, Yiska Michailidis, Eleftherios Ashbrook, Alison W Waltari, Eric Pak, John E Huey-Tubman, Kathryn E Koranda, Nicholas Hoffman, Pauline R West, Anthony P Rice, Charles M Hatziioannou, Theodora Bjorkman, Pamela J Bieniasz, Paul D Caskey, Marina Nussenzweig, Michel C 2020/6/20.

[149] WHO Working Group on the Clinical Characterisation infection and Management of COVID-19. A minimal common outcome measure set for covid-19 clinical research. *Lancet Infect Dis*, 20(8):e192–e197, 2020. 2020/6/17.

[150] W. Li, Q. Liu, Y. Pang, J. Jin, H. Wang, H. Cao, Z. Li, X. Wang, B. Ma, Y. Chi, R. Wang, A. Kondo, J. Gu, and N. Taniguchi. Core fucosylation of heavy chains regulates assembly and intracellular signaling of precursor b cell receptors. *J Biol Chem*, 287(4):2500–8, 2012.

[151] W. Li, R. Yu, B. Ma, Y. Yang, X. Jiao, Y. Liu, H. Cao, W. Dong, L. Liu, K. Ma, T. Fukuda, Q. Liu, T. Ma, Z. Wang, J. Gu, J. Zhang, and N. Taniguchi. Core fucosylation of igg b cell receptor is required for antigen recognition and antibody production. *J Immunol*, 194(6):2596–606, 2015.

[152] J. Pae, J. Ersching, T. B. R. Castro, M. Schips, L. Mesin, S. J. Allon, J. Ordovas-Montanes, C. Mlynarczyk, A. Melnick, A. Efeyan, A. K. Shalek, M. Meyer-Hermann, and G. D. Victora. Cyclin d3 drives inertial cell cycling in dark zone germinal center b cells. *J Exp Med*, 218(4), 2021.

[153] J. Rip, M. J. W. de Bruijn, A. Kaptein, R. W. Hendriks, and O. B. J. Corneth. Phosphoflow protocol for signaling studies in human and murine b cell subpopulations. *J Immunol*, 204(10):2852–2863, 2020. Rip, Jasper de Bruijn, Marjolein J W Kaptein, Allard Hendriks, Rudi W Corneth, Odilia B J 2020/4/8.

[154] K. P. Lam, R. Kühn, and K. Rajewsky. In vivo ablation of surface immunoglobulin on mature b cells by inducible gene targeting results in rapid cell death. *Cell*, 90(6):1073–83, 1997. Lam, K P Kühn, R Rajewsky, K 1997/10/10.

[155] E. Sonoda, Y. Pewzner-Jung, S. Schwers, S. Taki, S. Jung, D. Eilat, and K. Rajewsky. B cell development under the condition of allelic inclusion. *Immunity*, 6(3):225–33, 1997.

[156] A. Roghanian, I. Teige, L. Mrtensson, K. L. Cox, M. Kovacek, A. Ljungars, J. Mattson, A. Sundberg, A. T. Vaughan, V. Shah, N. R. Smyth, B. Sheth, H. T. Chan, Z. C. Li, E. L. Williams, G. Manfredi, R. J. Oldham, C. I. Mockridge, S. A. James, L. N. Dahal, K. Hussain, B. Nilsson, J. S. Verbeek, G. Juliusson, M. Hansson, M. Jerkeman, P. W. Johnson, A. Davies, S. A. Beers, M. J. Glennie, B. Frendéus, and M. S. Cragg. Antagonistic human fcriib (cd32b) antibodies have anti-tumor activity and overcome resistance to antibody therapy in vivo. *Cancer Cell*, 27(4):473–88, 2015.

[157] L. Sordé, S. Spindeldreher, E. Palmer, and A. Karle. Massive immune response against ivig interferes with response against other antigens in mice: A new mode of action? *PLoS One*, 12(10):e0186046, 2017. Sordé, Laetitia Spindeldreher, Sebastian Palmer, Ed Karle, Anette 2017/10/13.

[158] C. C. Baniel, E. G. Sumiec, J. A. Hank, A. M. Bates, A. K. Erbe, A. A. Pieper, A. G. Hoefges, R. B. Patel, A. L. Rakhmilevich, Z. S. Morris, and P. M. Sondel. Intratumoral injection reduces toxicity and antibody-mediated neutralization of immunocytokine in a mouse melanoma model. *J Immunother Cancer*, 8(2), 2020. Baniel, Claire C Sumiec, Elizabeth G Hank, Jacquelyn A Bates, Amber M Erbe, Amy K Pieper, Alexander A Hoefges, Anna G Patel, Ravi B Rakhmilevich, Alexander L Morris, Zachary S Sondel, Paul M 2020/10/30.

[159] W. Luo, X. P. Wang, C. E. Kashtan, and D. B. Borza. Alport alloantibodies but not goodpasture autoantibodies induce murine glomerulonephritis: protection by quinary crosslinks locking cryptic 3(iv) collagen autoepitopes in vivo. *J Immunol*, 185(6):3520–8, 2010.

[160] C. S. Garris, J. L. Wong, J. V. Ravetch, and D. A. Knorr. Dendritic cell targeting with fc-enhanced cd40 antibody agonists induces durable antitumor immunity in humanized mouse models of bladder cancer. *Sci Transl Med*, 13(594), 2021. Garris, Christopher S Wong, Jeffrey L Ravetch, Jeffrey V Knorr, David A 2021/5/21.

[161] I. Ibarlucea-Benitez, P. Weitzenfeld, P. Smith, and J. V. Ravetch. Siglecs-7/9 function as inhibitory immune checkpoints in vivo and can be targeted to enhance therapeutic antitumor immunity. *Proc Natl Acad Sci U S A*, 118(26), 2021. Ibarlucea-Benitez, Itziar Weitzenfeld, Polina Smith, Patrick Ravetch, Jeffrey V 2021/6/23.

[162] P. Weitzenfeld, S. Bournazos, and J. V. Ravetch. Antibodies targeting sialyl lewis

a mediate tumor clearance through distinct effector pathways. *J Clin Invest*, 129(9):3952–3962, 2019.

[163] I. FULBERI, M. BACHER, R. DODEU, and S. ROSKAM. Evaluating the murine anti-human antibody response and assessment of general activity and cognition after treatment with human intravenous immunoglobulins in healthy adult c57/b6j mice, 2014.

[164] C. Hess, A. Winkler, A. K. Lorenz, V. Holecska, V. Blanchard, S. Eiglmeier, A. L. Schoen, J. Bitterling, A. D. Stoehr, D. Petzold, T. Schommartz, M. M. Mertes, C. T. Schoen, B. Tiburzy, A. Herrmann, J. Köhl, R. A. Manz, M. P. Madaio, M. Berger, H. Wardemann, and M. Ehlers. T cell-independent b cell activation induces immunosuppressive sialylated igg antibodies. *J Clin Invest*, 123(9):3788–96, 2013. Hess, Constanze Winkler, André Lorenz, Alexandra K Holecska, Vivien Blanchard, Véronique Eiglmeier, Susanne Schoen, Anna-Lena Bitterling, Josephine Stoehr, Alexander D Petzold, Dominique Schommartz, Tim Mertes, Maria M M Schoen, Carolin T Tiburzy, Ben Herrmann, Anne Köhl, Jörg Manz, Rudolf A Madaio, Michael P Berger, Markus Wardemann, Hedda Ehlers, Marc 2013/8/28.

[165] P. K. Mongini, K. E. Stein, and W. E. Paul. T cell regulation of igg subclass antibody production in response to t-independent antigens. *J Exp Med*, 153(1):1–12, 1981. Mongini, P K Stein, K E Paul, W E 1981/1/1.

[166] J. F. Scheid, J. A. Horwitz, Y. Bar-On, E. F. Kreider, C. L. Lu, J. C. Lorenzi, A. Feldmann, M. Braunschweig, L. Nogueira, T. Oliveira, I. Shimeliovich, R. Patel, L. Burke, Y. Z. Cohen, S. Hadrigan, A. Settler, M. Witmer-Pack, A. P. West, B. Juelg, T. Keler, T. Hawthorne, B. Zingman, R. M. Gulick, N. Pfeifer, G. H. Learn, M. S. Seaman, P. J. Bjorkman, F. Klein, S. J. Schlesinger, B. D. Walker, B. H. Hahn, and M. C.

Nussenzweig. Hiv-1 antibody 3bnc117 suppresses viral rebound in humans during treatment interruption. *Nature*, 535(7613):556–60, 2016.

[167] F. Nimmerjahn, R. M. Anthony, and J. V. Ravetch. Agalactosylated igg antibodies depend on cellular fc receptors for in vivo activity. *Proc Natl Acad Sci U S A*, 104(20):8433–7, 2007. Nimmerjahn, Falk Anthony, Robert M Ravetch, Jeffrey V 2007/5/9.

[168] F. Nimmerjahn and J. V. Ravetch. Divergent immunoglobulin g subclass activity through selective fc receptor binding. *Science*, 310(5753):1510–2, 2005. Nimmerjahn, Falk Ravetch, Jeffrey V 2005/12/3.

[169] I. Schwab, A. Lux, and F. Nimmerjahn. Pathways responsible for human autoantibody and therapeutic intravenous igg activity in humanized mice. *Cell Rep*, 13(3):610–620, 2015. Schwab, Inessa Lux, Anja Nimmerjahn, Falk 2015/10/13.

[170] W. W. Overwijk and N. P. Restifo. B16 as a mouse model for human melanoma. *Curr Protoc Immunol*, Chapter 20:Unit 20.1, 2001. Overwijk, W W Restifo, N P 2008/4/25.

[171] S. Bournazos, D. Corti, H. W. Virgin, and J. V. Ravetch. Fc-optimized antibodies elicit cd8 immunity to viral respiratory infection. *Nature*, 588(7838):485–490, 2020. Bournazos, Stylianos Corti, Davide Virgin, Herbert W Ravetch, Jeffrey V 2020/10/9.

[172] Johann DEISENHOFER, Peter M COLMAN, Robert HUBER, Heinz HAUPT, and Gerhard SCHWICK. Crystallographic structural studies of a human fc-fragment. i. an electron-density map at 4 resolution and a partial model. 1976.

[173] Robert Huber, Johann Deisenhofer, Peter M Colman, Masaaki Matsushima, and Walter Palm. Crystallographic structure studies of an igg molecule and an fc fragment. *Nature*, 264(5585):415–420, 1976.

[174] M. F. Jennewein, I. Goldfarb, S. Dolatshahi, C. Cosgrove, F. J. Noelette, M. Krykbaeva, J. Das, A. Sarkar, M. J. Gorman, S. Fischinger, C. M. Boudreau, J. Brown, J. H. Cooperrider, J. Aneja, T. J. Suscovich, B. S. Graham, G. M. Lauer, T. Goetghebuer, A. Marchant, D. Lauffenburger, A. Y. Kim, L. E. Riley, and G. Alter. Fc glycan-mediated regulation of placental antibody transfer. *Cell*, 178(1):202–215.e14, 2019.

[175] T. T. Wang, J. Maamary, G. S. Tan, S. Bournazos, C. W. Davis, F. Krammer, S. J. Schlesinger, P. Palese, R. Ahmed, and J. V. Ravetch. Anti-ha glycoforms drive b cell affinity selection and determine influenza vaccine efficacy. *Cell*, 162(1):160–9, 2015.

[176] R. Pfeifle, T. Rothe, N. Ipseiz, H. U. Scherer, S. Culemann, U. Harre, J. A. Ackermann, M. Seefried, A. Kleyer, S. Uderhardt, B. Haugg, A. J. Hueber, P. Daum, G. F. Heidkamp, C. Ge, S. Böhm, A. Lux, W. Schuh, I. Magorivska, K. S. Nandakumar, E. Lönnblom, C. Becker, D. Dudziak, M. Wuhrer, Y. Rombouts, C. A. Koeleman, R. Toes, T. H. Winkler, R. Holmdahl, M. Herrmann, S. Blüml, F. Nimmerjahn, G. Schett, and G. Krönke. Regulation of autoantibody activity by the il-23-t. *Nat Immunol*, 18(1):104–113, 2017.

[177] Y. Ohmi, W. Ise, A. Harazono, D. Takakura, H. Fukuyama, Y. Baba, M. Narazaki, H. Shoda, N. Takahashi, Y. Ohkawa, S. Ji, F. Sugiyama, K. Fujio, A. Kumanogoh, K. Yamamoto, N. Kawasaki, T. Kurosaki, Y. Takahashi, and K. Furukawa. Sialylation converts arthritogenic igg into inhibitors of collagen-induced arthritis. *Nat Commun*, 7:11205, 2016.

[178] M. J. Price, S. L. Hicks, J. E. Bradley, T. D. Randall, J. M. Boss, and C. D. Scharer. Igm, igg, and iga influenza-specific plasma cells express divergent transcriptomes. *J Immunol*, 203(8):2121–2129, 2019.

[179] S. Reynaud, L. Delpy, L. Fleury, H. L. Dougier, C. Sirac, and M. Cogné. Interallelic

class switch recombination contributes significantly to class switching in mouse b cells. *J Immunol*, 174(10):6176–83, 2005.

[180] C. H. Lee, T. H. Kang, O. Godon, M. Watanabe, G. Delidakis, C. M. Gillis, D. Sterlin, D. Hardy, M. Cogné, L. E. Macdonald, A. J. Murphy, N. Tu, J. Lee, J. R. McDaniel, E. Makowski, P. M. Tessier, A. S. Meyer, P. Bruhns, and G. Georgiou. An engineered human fc domain that behaves like a ph-toggle switch for ultra-long circulation persistence. *Nat Commun*, 10(1):5031, 2019. Lee, Chang-Han Kang, Tae Hyun Godon, Ophélie Watanabe, Makiko Delidakis, George Gillis, Caitlin M Sterlin, Delphine Hardy, David Cogné, Michel Macdonald, Lynn E Murphy, Andrew J Tu, Naxin Lee, Jiwon McDaniel, Jonathan R Makowski, Emily Tessier, Peter M Meyer, Aaron S Bruhns, Pierre Georgiou, George 2019/11/7.

[181] B. E. Low, G. J. Christianson, E. Lowell, W. Qin, and M. V. Wiles. Functional humanization of immunoglobulin heavy constant gamma 1 fc domain human. *MAbs*, 12(1):1829334, 2020. Low, Benjamin E Christianson, Gregory J Lowell, Emily Qin, Wenning Wiles, Michael V 2020/10/8.

[182] C. McMahon, D. P. Staus, L. M. Wingler, J. Wang, M. A. Skiba, M. Elgeti, W. L. Hubbell, H. A. Rockman, A. C. Kruse, and R. J. Lefkowitz. Synthetic nanobodies as angiotensin receptor blockers. *Proc Natl Acad Sci U S A*, 117(33):20284–20291, 2020. McMahon, Conor Staus, Dean P Wingler, Laura M Wang, Jialu Skiba, Meredith A Elgeti, Matthias Hubbell, Wayne L Rockman, Howard A Kruse, Andrew C Lefkowitz, Robert J 2020/8/6.

[183] E. K. Brinkman, T. Chen, M. Amendola, and B. van Steensel. Easy quantitative assessment of genome editing by sequence trace decomposition. *Nucleic Acids Res*, 42(22):e168, 2014. Brinkman, Eva K Chen, Tao Amendola, Mario van Steensel, Bas 2014/10/11.

[184] Hiromi Miura, Rolen M Quadros, Channabasavaiah B Gurumurthy, and Masato Ohtsuka. Easi-crispr for creating knock-in and conditional knockout mouse models using long ssdna donors. *Nature protocols*, 13(1):195–215, 2018.